Tampere University

Risto Toivola

VALORIZATION OF SHORT-CHAIN FATTY ACIDS IN MICROBIAL HOSTS

Production host screening and scale-up assessment

Master's Thesis
Faculty of Engineering and Natural Sciences
Examiners: Professor Ville Santala
Academy Research Fellow Suvi Santala
August 2025

ABSTRACT

Risto Toivola: Valorization of short-chain fatty acids in microbial hosts
Master's Thesis
Tampere University
Master's Degree Program in Environmental and Energy Engineering
August 2025

Short-chain fatty acids (SCFAs) can be produced from several existing industrial streams, such as organic waste and CO_2, through acid fermentation or microbial electrosynthesis. As the more traditional extraction methods for short-chain fatty acids require high energy inputs and specialized equipment, utilizing these compounds as substrates for biological conversion processes can offer an alternative. Toxic effects, low growth, and poor yield of reducing agents, however, make SCFAs challenging substrates for long chain products requiring reductive steps.

The purpose of this study was to compare acetate-consuming microbes to evaluate how well they could be utilized as part of the value chain to convert SCFAs into long-chain fatty acids, alcohols, and alkanes. Production pathways, tolerances, and genetic tractability were the main interests of the screening based on the literature and metabolic models. Small-scale cultivations were done to determine the acetate uptake rates. The goal of the large-scale simulations was to estimate what kind of productivities would be achievable through the co-feeding of glucose and acetate, as these methods have only been validated in laboratory.

After the initial screening, six strains were selected for further studies. Cultivations carried out in liquid Lysogeny broth revealed that only *Acinetobacter baylyi* ADP1, *Pseudomonas putida* KT2440, and *Cutaneotrichosporon oleaginosus* from the selected species can grow efficiently in undefined media supplemented with 100 mM acetate. *C. oleaginosus* reached the highest biomass while *P. putida* and ADP1 achieved higher specific uptake rates of acetate. *Corynebacterium glutamicum* also had efficient acetate uptake at the beginning of the cultivations, but the uptake and growth halted quickly. These results, combined with the ones obtained from screening, suggest that *C. oleaginosus* and ADP1 are the only microbes meeting the goal of this work since *P. putida* only accumulates storage compounds with medium-chain fatty acids.

With carbon catabolic repression and acetate inhibition included in the models based on laboratory experiments and previous studies, the disproportion of the ideal substrate uptake ratio in the reactor for *E. coli* increased by 41% when increasing the glucose feeding rate from 0.75 to 1.25 g L^{-1} h^{-1}. With similar change, the increase for *Y. lipolytica* was 27%. Slow uptake rates had a more negative effect on the oxygen heterogeneity than a higher degree of inhibition. Productivity at the reactor bottom relative to the top was 80–89% for ADP1 and 76–78% for *C. oleaginosus*, depending on product. Engineering uptake and feeding strategies appear to be necessary for uniform productivity from large-scale co-feeding.

C. oleaginosus and ADP1 were shown to be suitable candidates for converting acetate into higher-value long-chain products, and the simulations highlighted the potential of co-feeding at large scale. However, further studies are needed to determine the actual transformation rates, and to identify the modes of toxicity of inhibitory compounds present in real feed streams.

Keywords: short-chain fatty acids, acetate utilization, co-feeding

TIIVISTELMÄ

Risto Toivola: Lyhytketjuisten rasvahappojen jalostaminen mikrobien avulla
Diplomityö
Tampereen yliopisto
Ympäristö- ja energiatekniikan diplomi-insinöörin tutkinto-ohjelma
Elokuu 2025

Lyhytketjuisia rasvahappoja voidaan happokäymisellä tai mikrobielektrosynteesillä tuottaa useista tärkeistä teollisuuden sivuvirroista, kuten orgaanisesta jätteestä ja hiilidioksidista. Koska lyhytketjuisten rasvahappojen perinteisemmät erotusmenetelmät vaativat suuria energiamääriä ja kalliita laitteita, näiden yhdisteiden hyödyntäminen substraatteina biologisissa prosesseissa voi tarjota vaihtoehdon. Toksisuus, alhainen kasvu ja pelkistimien huono saanto tekevät lyhytketjuisista rasvahapoista kuitenkin haastavia substraatteja etenkin, kun halutut tuotteet vaativat useita syklejä rasvahapposynteesissä.

Tämän tutkimuksen tarkoituksena oli vertailla asetaattia hyödyntäviä mikrobeja sen arvioimiseksi, kuinka hyvin niitä voitaisiin soveltaa osana arvoketjua, jossa lyhytketjuiset rasvahapot muunnetaan pitkäketjuisiksi rasvahapoiksi, alkoholeiksi ja alkaaneiksi. Tuotantoreitit, inhiboivien aineiden sieto ja geneettinen muokattavuus olivat kirjallisuus- ja mallipohjaisen seulonnan kohteena. Asetaatin sisäänottonopeudet määritettiin laboratoriomittakaavan viljelyillä. Suuren tuotantomittakaavan simulaatioiden tavoitteena oli arvioida, millaisia tuottavuuksia on saavutettavissa glukoosin ja asetaatin yhteissyötöllä.

LB-liuoksessa suoritetut viljelyt paljastivat, että valituista lajeista vain *Pseudomonas putida* KT2440, *Acinetobacter baylyi* ADP1 ja *Cutaneotrichosporon oleaginosus* pystyvät kasvamaan tehokkaasti kompleksisessa kasvualustassa, johon on lisätty 100 mM asetaattia. *C. oleaginosus* saavutti korkeimman biomassan, kun taas *P. putida* ja ADP1 saavuttivat korkeammat spesifisen sisäänoton nopeudet asetaatille. *Corynebacterium glutamicum* hyödynsi myös tehokkaasti asetaattia kasvatusten alussa, mutta kasvu pysähtyi nopeasti. Nämä tulokset yhdistettynä seulonnasta saatuihin tuloksiin viittaavat siihen, että *C. oleaginosus* ja ADP1 ovat ainoat mikrobit, jotka täyttävät työssä määritellyt tavoitteet, sillä *P. putida* tuottaa vain varastorasvoja, jotka sisältävät keskipitkiä rasvahappoja.

Reaktorimalleissa, joissa oli huomioitu katabolinen repressio ja asetaatin aiheuttama inhibitio, epäsuhde substraattien ideaaliin sisäänottoon nähden reaktorissa *E. colilla* kasvoi 41 %, kun glukoosin syöttönopeutta nostettiin arvosta 0,75 arvoon 1,25 g L^{-1} h^{-1}. Samalla muutoksella *Y. lipolytican* simulaatioissa epäsuhteen kasvu oli 27 %. Hitailla substraattien ottonopeuksilla oli negatiivisempi vaikutus liuenneen hapen heterogeenisuuteen kuin substraatti-inhibitioilla. Tuottavuus reaktorin alaosassa suhteessa yläosaan oli tuotteesta riippuen ADP1:llä 80–89 % ja *C. oleaginosuksen* tapauksessa 76–78 %. Ottonopeuden muokkaus ja syöttöstrategioiden optimointi näyttävät olevan välttämättömiä tasaisen tuottavuuden saavuttamiseksi yhteissyötöllä.

C. oleaginosus ja ADP1 osoittautuivat sopiviksi kandidaateiksi asetaatin muuntamiseen arvokkaammiksi pitkäketjuisiksi tuotteiksi, ja simulaatiot korostivat yhteissyötön potentiaalia teollisessa mittakaavassa. Lisätutkimuksia tarvitaan kuitenkin todellisten konversionopeuksien määrittämiseksi sekä syötteissä esiintyvien inhiboivien yhdisteiden toksisuuksien selvittämiseksi.

Avainsanat: lyhytketjuiset rasvahapot, asetaatin hyödyntäminen, yhteissyöttö

USE OF ARTIFICIAL INTELLIGENCE IN THIS WORK

Artificial intelligence (AI) has been used in generating this work:

☐ No
☒ Yes

I hereby declare, that the AI-based applications used in generating this work are as follows:

Application	Version
ChatGPT	GPT-4o
Writefull	2025.45.0

Purpose of the use of AI

ChatGPT was used to proofread the code that was designed for modelling and figure generation. In text, Writefull was used to revise and refine the sentence structure and formulation.

Parts of this work, where AI was used

ChatGPT was used in chapters 2, 4, and 5. Writefull was used throughout the thesis.

Acknowledgement of risks

I hereby acknowledge, that as the author of this work, I am fully responsible for the contents presented in this thesis. This includes the parts that were generated by an AI, in part or in their entirety. I therefore also acknowledge my responsibility in the case, where use of AI has resulted in ethical guidelines being breached.

PREFACE

This work was done as part of the isoSUS research project, which aims to identify ecologically and economically feasible value chains for converting industrial waste and side streams into valuable products. Exploring such a broad area of research and being able to give my own contribution to an important matter was a rewarding way to finish my journey at Tampere University.

I would like to show my gratitude to Ville Santala for guiding me through this work. I am especially thankful for trusting me to explore the thesis in a direction that interested me, and to apply and refine the skills and knowledge I wanted to strengthen. I also want to thank Suvi Santala for giving me insightful recommendations considering the lab work and the thesis structure. In addition, I am grateful to Sara Sohkanen for teaching me to carry out my work independently in the laboratory, to Pauli Losoi for providing valuable tips on the modelling aspect, and to the entire SynBio group for always offering help if needed. Finally, I want to thank everyone who has been part of my life during these past years, filling my free time with unforgettable experiences.

Tampere, 29th August 2025

Risto Toivola

CONTENTS

ABBREVATIONS AND SYMBOLS

CCR	Carbon catabolic repression
DCW	Dry cell weight
OD_{600}	Optical density at 600 nm
PHA	Polyhydroxyalkanoate
SCFA	Short-chain fatty acid
TAG	Triacylglycerol
WE	Wax ester

α	Proportion of long-chain fatty acids
D	Impeller diameter
ϵ	Axial flow coefficient
Γ	Diffusivity
H	Reactor height
h	Net prdocuction
K_i	Inhibition constant
$k_L A$	Oxygen transfer coefficient
K_p	Impeller discharge coefficient
K_S	Substrate affinity constant
L	Lipid content
μ	Specific growth rate
N	Stirrer speed
n	Number density
O	Dissolved oxygen concentration
O^*	Oxygen solubility
$\mathbf{P}$	Indicator matrix
Q	Volumetric flow
q	Specific uptake rate or decay rate

R	Reactor diameter
r	Reaction rate
S	Substrate concentration
$\mathbf{\Sigma}$	Diagonal matrix with singular values
T	Adaptation time constant
t	Time
$\mathbf{U}$	$k \times k$ unitary matrix of a singular value decomposition of $k \times l$ matrix.
$\mathbf{V}$	$l \times l$ unitary matrix of a singular value decomposition of $k \times l$ matrix.
$\overline{\varsigma}$	Internal variable vector
X	Biomass concentration
$\overline{x}$	Spatial coordinate vector
Y	Yield coefficient
ζ	Transfer velocity in internal space

1. INTRODUCTION

Currently, most of the biological processes used on industrial scale are dependent on feeds with high sugar content. As these often directly compete with food production, other options are constantly being investigated. Short-chain fatty acids (SCFAs), due to their abundance in industrial streams, can offer an alternative substrate source for biotechnical processes. Short-chain fatty acids include all fatty acids with fewer than six carbons. Usually, short-chain fatty acids are extracted from industrial streams through various means such as adsorption, ion exchange, electrodialysis, or liquid-liquid extraction (Polat et al. 2025). Although they can be used in this form, the low concentrations and mixed nature of the solutions present difficulties. Many of the extraction methods are expensive due to the energy requirements and can be challenging to implement for varying pH and concentrations. With microbial systems, higher-value end-products could be achieved without these energy-intensive purification steps.

The problem of the SCFAs as substrates is usually the poor growth of them, as well as the low yield of the reducing agents necessary for several production routes. For that, there are multiple proposed reasons. In particular, the free energy generated from the metabolic reactions has been shown to be linearly correlated with microbial growth (Roden et al. 2011). Although, for example, propionate as the sole carbon source can lead to higher yields than ethanol or lactate, in the majority of microbes, glucose still vastly outperforms all SCFAs under aerobic conditions. Another obstacle to tackle is the inhibitory and toxic effects of the SCFAs. For example, in most microbial hosts, acetate accumulation can cause cytotoxicity (L. Chen et al. 2021). Common preservative propionate expresses even more toxic effects and requires specific metabolic pathways in order to be utilized (Brock et al. 2004; Muñoz-Elías et al. 2006). Longer chain SCFAs pose even more challenges for the majority of the microbes. In addition to SCFAs, the streams from industry can also include toxic degradation products of lignocellulosic biomass, other weak acids, or alcohols.

The aim of this study is to find optimal microbial hosts to be utilized in the biological conversion of SCFA-rich side streams into more valuable products. The most important task is to determine how effectively a certain microbial host can use acetate as a substrate. Other SCFAs are also discussed, but acetate is chosen for further studies because it is the most abundant in the studied streams. Other criteria for the suitability of the hosts

include tolerance to other inhibitors and the possibilities for further engineering of the microbes to meet the performance parameters such as high yield titer and productivity. In this thesis, long-chain fatty acids and their derivatives are the products of main interest. The productivity potential is studied to investigate how well the conversion of SCFAs could be integrated into large-scale processes. The research questions addressed in this study are: (i) which microbes are most suitable for converting SCFAs derived from industrial streams into higher-value long-chain products, (ii) how efficiently these microbes utilize acetate, and (iii) whether acetate can serve as a suitable substrate for larger-scale processes.

In the second chapter, the relevant theory behind SCFA utilization is explained. Also, the different production routes for lipid products, the composition of the SCFA-rich industry effluents, along with the inhibitory effects, are discussed. Mechanical modelling of the microbial growth and processes, as well as statistical tools relevant for the study, are investigated. Chapter 3 goes through the set of potential microbial hosts and explains their current state in six key categories to be suitable for the conversion of SCFA-rich feeds. Chapter 4 consists of a three-step approach to answer the research questions. Firstly, a comparision between the selected microbes is made based on the narrative literature review and existing genome-scale models. Next, small-scale cultivations for the most prominent hosts are performed using model media to investigate the acetate utilization. Based on existing knowledge and laboratory experiments, mechanistic models for the selected hosts growing on acetate are built and integrated into large-scale reactor simulations for the evaluation of the productivity potential. In Chapter 5, the findings from the literature are compiled, and the results of the cultivations and large-scale simulations are presented. The results are supported by tables and figures. Chapter 6 consists of an analysis of the results, their reliability, and suggestions for the most suitable hosts based on the results. In the final chapter, the major findings are concluded with suggestions for future work regarding the studied topic.

2. BACKGROUND

2.1 Microbial utilization of short-chain fatty acids

When microbes grow solely on fatty acids (FAs), the route to convert acetyl-CoA into oxaloacetate must bypass the decarboxylation steps when the carbon is directed toward gluconeogenesis. Instead of the tricarboxylic acid (TCA) cycle, the glyoxylate cycle or an analogous route is required. Metabolic routes for acetate and propionate are presented in the following subsections, as they form the backbone for the utilization of both even- and odd-chain SCFAs. Although the glyoxylate cycle is similar to the TCA cycle, having most of the same reactions as shown in Figure 2.1, two different reactions and therefore enzymes are used: isocitrate is converted into succinate and glyoxylate by isocitrate lyase (ICL), and glyoxylate is condensed with acetyl-CoA to form malate by malate synthase (MS) (Muñoz-Elías et al. 2006). To tackle the limits of SCFAs, co-feeding can be implemented. As can be seen in Figure 2.1, acetate enters the metabolism as acetyl-CoA, so the reducing agents produced are NADH and $FADH_2$ during the TCA cycle. However, these carry electrons mainly for electron transport chain, whereas NADPH is required for anabolic lipid synthesis. If other substrates such as hexose or pentose sugars are used for the cofactor and biomass production, SCFAs that do not go through decarboxylation can be directed to product synthesis.

2.1.1 Growth on acetate

The lipid bilayers are more permeable for small molecules that associate weakly with water. Therefore, due to being a small molecule, acetic acid in its undissociated form can diffuse through the cell membrane (Mutyala et al. 2023). This may increase the uptake rate, but as mentioned before, the accumulation of acetate has inhibitory and, in high concentrations, toxic effects on most species. Active transport occurs via specific acetate permeases or monocarboxylate transporters (Hosmer et al. 2023; Giannattasio et al. 2013). Similar monocarboxylic transporters are found for other SCFAs. In addition to the reaction where acetyl-CoA synthetase catalyzes the conversion of acetate into acetyl-CoA, at least one other way utilizing two steps is possible. Acetate may first undergo phosphorylation by acetokinase, after which phosphate acetyltransferase facilitates its transfer to coenzyme A (Salcedo-Vite et al. 2019). After acetate is converted to isocitrate

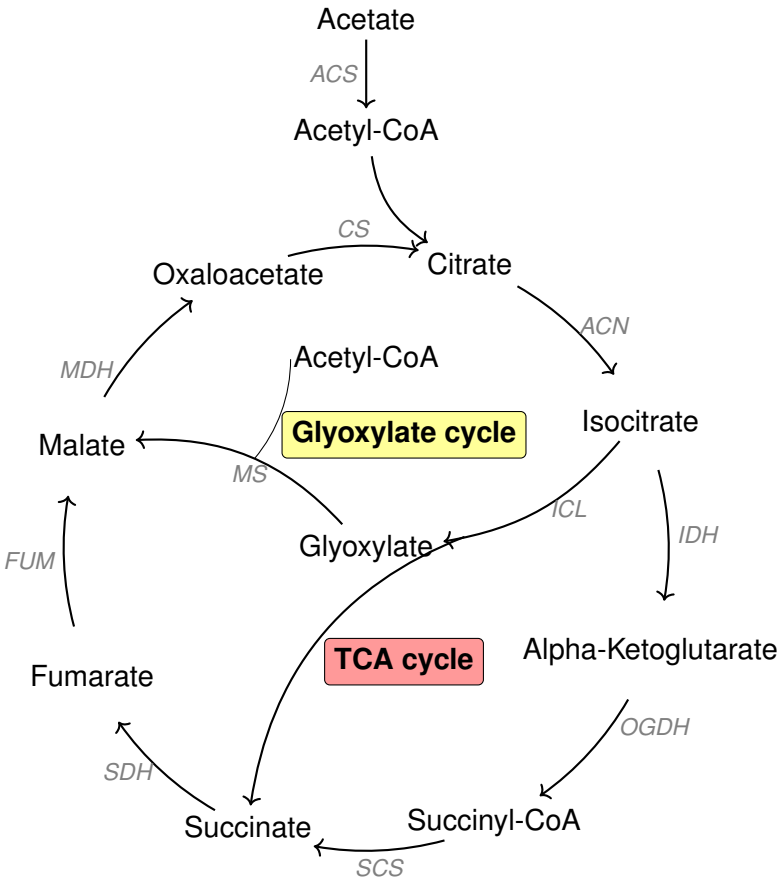

Figure 2.1. *Glyoxylate cycle and the TCA cycle with the corresponding enzymes. ACS, acetyl-CoA synthetase; CS, citrate synthase; ACN, aconitase; IDH, isocitrate dehydrogenase; OGDH, 2-oxoglutarate dehydrogenase; SCS, succinyl coenzyme A synthetase; SDH, succinate dehydrogenase; FUM, fumarase; MDH, malate dehydrogenase; ICL, isocitrate lyase; MS, malate synthase.*

in the first steps of the TCA cycle, depending on the host and the conditions, isocitrate can be directed into the glyoxylate cycle, be oxidized by regular TCA enzymes, or fluxes to both routes can be simultaneous (Schmollack et al. 2022).

As can be seen, the glyoxylate cycle does not include reactions from isocitrate to succinate, where a lot of the cofactors for the oxidative phosphorylation are produced. Therefore, the energy yield is low compared to the TCA cycle, but also the decarboxylation steps that produce CO_2 are excluded. With all carbon atoms preserved, oxaloacetate can be directed to gluconeogenesis (Chew et al. 2019). Roden et al. (2011) showed that there is a linear correlation between growth yield and estimated free energy from catabolic reactions. For acetate in aerobic conditions, the estimated free energy of -847.1 kJ rxn^{-1} based on this correlation would result in 19.95 g cells mol^{-1} substrate. For comparison, the free energy of glucose, -2883.3 kJ rxn^{-1}, would result in 62.92 g cells mol^{-1} substrate. Estimated free energies alone do not explain the inferiority of the acetate as a substrate, but toxic effects are also a major factor. Even microbial hosts that can utilize acetate start to show longer lag phases at elevated acetate concentrations.

2.1.2 Growth on propionate

Propionate is similar to acetate in a way that it can be converted directly to propionyl-CoA by a synthetase. There are several ways for microbes to metabolize propionate. Based on current knowledge, these include the 2-Methylcitrate cycle (2-MC cycle), methylmalonyl pathway, and the incorporation of propionyl moieties into cell wall lipids (Dolan et al. 2018). In prokaryotes, the 2-Methylcitrate cycle is the most common one. The reactions in this pathway are analogous to the glyoxylate cycle, and the schematic is shown in Figure 2.2. The pathway is initiated when propionyl-CoA and oxaloacetate are combined to form 2-methylcitrate, a reaction catalyzed by 2-methylcitrate synthase (MCS). Subsequently, 2-methylcitrate is dehydrated to 2-methyl-cis-aconitate by 2-methylcitrate dehydratase (MCD) and then converted to 2-methylisocitrate through the action of aconitase (ACN). In the final step, 2-methylisocitrate is broken down into pyruvate and succinate by 2-methylisocitrate lyase (MCL). (Huang et al. 2023)

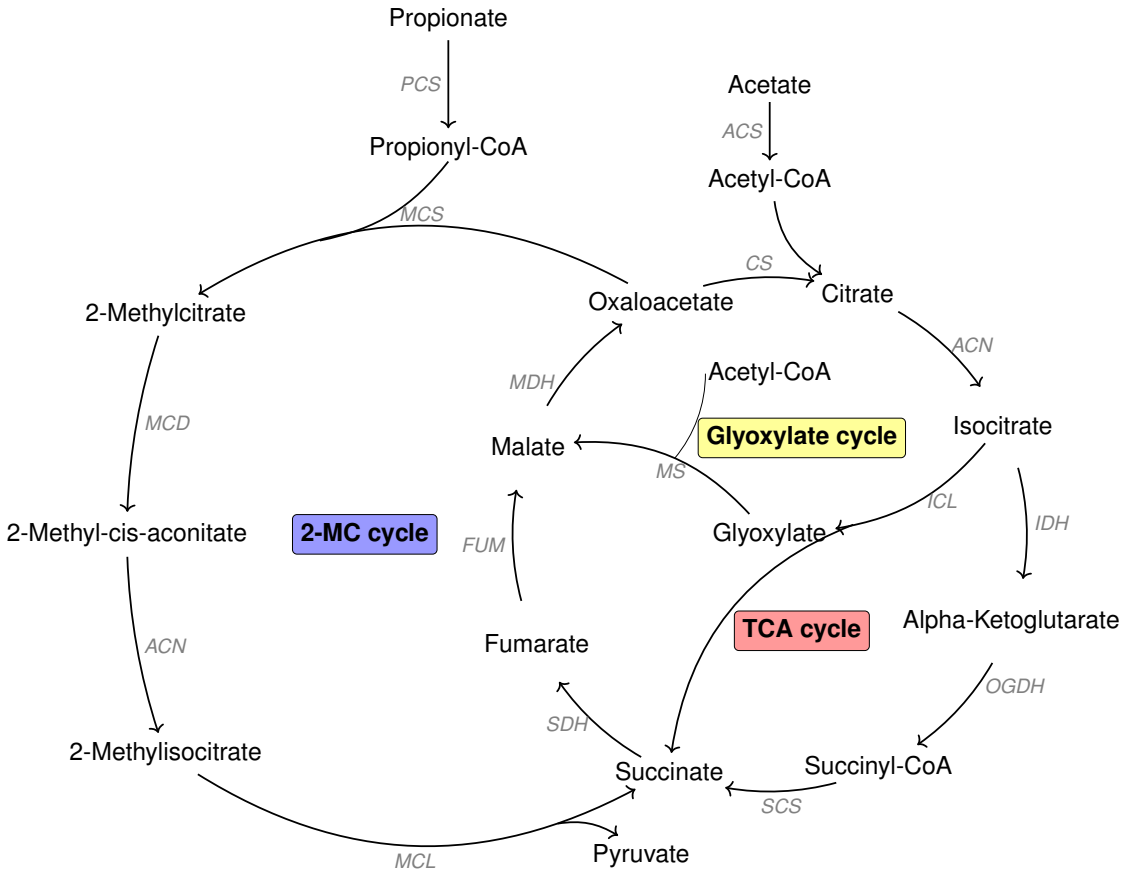

Figure 2.2. *2-Methylcitrate cycle, intervening with the glyoxylate and the TCA cycles. PCS, propionate-CoA synthetase; ACS, acetyl-CoA synthetase; CS, citrate synthase; ACN, aconitase; IDH, isocitrate dehydrogenase; OGDH, 2-oxoglutarate dehydrogenase; SCS, succinyl coenzyme A synthetase; SDH, succinate dehydrogenase; FUM, fumarase; MDH, malate dehydrogenase; ICL, isocitrate lyase; MS, malate synthase; MCD, 2-methylcitrate dehydratase; MCS, 2-methylcitrate synthase; MCL, 2-methylisocitrate lyase.*

The aerobic growth observed with propionate also aligns quite well with the linear correlation with free energy, and therefore the calculated biomass yield based on the correlation would be 33.46 g cells mol^{-1} substrate (Roden et al. 2011). The estimated free energy of propionate catabolism is -1487.2 kJ rxn^{-1}. Similarly to acetate, propionate also affects the intracellular pH. The accumulation of propionyl-CoA has also been shown to inhibit the function of CoA-dependent enzymes such as pyruvate dehydrogenase and succinyl coenzyme dehydrogenase (Brock et al. 2004).

2.1.3 Utilization of other SCFAs

Fatty acids with four or more carbons are not as common substrates as acetate or propionate, but there are still microbes that can utilize them. However, in industrial streams, other SCFAs, especially butyrate, can be abundant (Raes et al. 2017). One difference between longer chained SCFAs with acetate and propionate is that FAs with four or more carbons need to go through beta oxidation to yield acetyl-CoA, and in case of odd-chained FAs, also propionyl-CoA (Muñoz-Elías et al. 2006; Mutyala et al. 2023; Dolan et al. 2018). Since beta oxidation of even chain fatty acids produces only acetyl-CoA, they can be used in the glyoxylate cycle (Muñoz-Elías et al. 2006). This has been validated by deletion of the genes required for the 2-MC cycle in *Mycobacterium tuberculosis*, which was still able to grow in butyrate (Muñoz-Elías et al. 2006). However, in another study using *Trichoderma atroviride* with the deletion of MCL, a 80% reduction in growth was observed with butyrate as a sole carbon source (Dubey et al. 2013). This indicates that some hosts might still direct the intermediates of even-chained fatty acids toward the methylcitrate cycle. Valerate utilization closely recalls that of propionate. It is first converted into valeryl-CoA, which can in beta oxidation produce acetyl-CoA and propionyl-CoA. In addtion, it can be converted to 3-hydroxyvaleryl-CoA, which is a precursor for polyhydroxyalkanoates (PHA. (Alvarez et al. 1997) *Cupriavidus necator* is well known for its ability to use both butyrate and valerate as sole carbon sources for PHA production (Cai et al. 2023).

2.1.4 Substrate co-feeding

Because SCFAs are not very energy-efficient substrates and in many organisms can not maintain growth, co-feeding of multiple substrates is a valid solution to maximize the production from SCFAs. As mentioned before, acetate does not undergo any decarboxylation steps and acetyl-CoA can be used directly for fatty acid synthesis (Salcedo-Vite et al. 2019). However, acetate usually leads to lower lipid yields than glucose (S. Santala, V. Santala, et al. 2021; J. O. Park et al. 2019). This is mainly due to the requirement of NADPH for fatty acid synthesis. Glucose, for example, can be decarboxylated in the oxidative pentose phosphate pathway to produce greater amounts of NADPH (M. H. Lee

et al. 2019).

With co-feeding it is important to find a good balance between the substrate feeding rates or amounts. If the microorganism has a strong catabolic repression system and exhibits diauxic growth, providing too much preferred carbon source at once may suppress the consumption of acetate or other SCFAs (J. O. Park et al. 2019). Fed-batch system where only small quantities of glucose are fed to a culture containing acetate has shown to be a valid answer. On the other hand, microbial hosts without catabolic repression will use both substrates mainly for central metabolism and growth (S. Santala, V. Santala, et al. 2021). This can be solved by genetically engineering the host, so certain pathways are blocked, or by limiting nitrogen and other nutrients, so growth is also limited and cells move to the lipogenic phase.

2.2 Industrial effluents

The substrates for the SCFA-consuming microbial hosts can be derived from various industrial waste and side streams. The pulp and paper side streams are broken chemically into smaller compounds, and these are converted into acids by anaerobic fermentation. In addition to this, carbon dioxide is an alternative source that can be converted to SCFAs by microbial electrosynthesis (MES). Both routes can generate SCFA-rich effluents, but the compositions have some dissimilarities.

2.2.1 Thermal treatment and acid fermentation of the industrial waste and side streams

Pulp and paper mills produce many different kinds of by-products, including black liquor, wood and bark residues, and various sludges (Haile et al. 2021). Many of these can be recycled or used for energy production, but especially wet sludges are harder to utilize in other processes (Mendoza Martinez et al. 2021).

The first step toward acidic substrates from forest industry effluents is thermochemical treatment. In hydrothermal carboxylation (HTC), wet biomass is converted to hydrochar, HTC liquor, and gaseous by-products (Mendoza Martinez et al. 2021). Hydrochar has applications, for example, as a fertilizer, and gasses, which mostly consist of carbon dioxide (CO_2), can be utilized by C1 using bacteria, which is discussed more in the next subsection. The liquid part can contain up to 15% of the initial carbon content and is rich in SCFAs, mostly acetic acid and formic acid, with additional compounds such as phenols and furfurals (Mendoza Martinez et al. 2021). Most inorganic elements bind to hydrochar, whereas possible proteins are mostly found in the liquid portion. Depending on the biomass composition, some glucose and lactate formation can also be expected. (Díez et al. 2024)

One versatile treatment method for side streams from the forest industry is pyrolysis. With high temperatures, long-chained complex molecules can be broken down. The depolymerization of hemicellulose can be achieved at 510 K, whereas cellulose requires a slightly higher temperature of around 570-660 K and at 700 K produces high amounts of levoglucosan with additional products such as furans (Senneca et al. 2020). If pyrolysis is followed by hydrolysis, levoglucosan can be further hydrolyzed to glucose. Commonly used sulfuric acid catalysts may however be difficult to neutralize, leaving the product to be excessively acidic. (Nomura et al. 2024).

Another hydrothermal treatment similar to HTC is hydrothermal liquefaction (HTL). Since the liquid fraction is higher in HTL than in HTC, it has the potential to be more suitable considering acid fermentation. However, the scaling and integration of the HTL method are still in the early stages. To maximize liquid production, temperatures between 200 and 350 °C at high pressure (12-18 MPa) are used (Hamaguchi et al. 2012). Common products of HTL from wood-based waste are syringol and phenol from the lignin, and glucose, aldehydes, and carboxylic acids from the cellulose and hemicellulose (Woerner et al. 2022).

After thermal treatment has converted the complex waste streams into sugars and other digestible compounds, acid fermentation (acidogenesis) can be performed. Acidogenesis is usually the second part of the anaerobic digestion process, which can be separated in four main stages. Depending on the feedstock, the first part is hydrolysis, which in this case is done with thermal treatments. The follow-up stages are acetogenesis and methanogenesis (Cremonez et al. 2021). Often, all the stages are performed in a single reactor, so methanogenesis produces SCFAs just as intermediates, and the process is utilized in biogas formation (Tampio et al. 2019). CO_2 can be further utilized in microbial electrosynthesis. Using mainly thermophilic acetogenic bacteria in the reactor is optimal when acetate is the main product of interest. From solid organic waste, an acetate concentration of over 85% has been achieved by doing the fermentation at 60 °C and at pH 6. (David et al. 2020) By dividing the entire anaerobic digestion process into two stages, higher yields are achieved due to easier process parameter control, and the product from the acidogenesis phase can also be collected (Cremonez et al. 2021). In addition to SCFAs, the acid fermentation mixture can have high concentrations of gases such as hydrogen and ammonium, as well as alcohols, especially ethanol (A. Zhang et al. 2015; Leitão et al. 2006).

2.2.2 Acetogenesis and microbial electrosynthesis

Acetogens are microorganisms capable of turning one carbon (C1) substates into more valuable chemical compounds. There are several known carbon fixation pathways for acetogens, including the Wood-Ljungdahl (WL) pathway, the reverse tricarboxylic acid

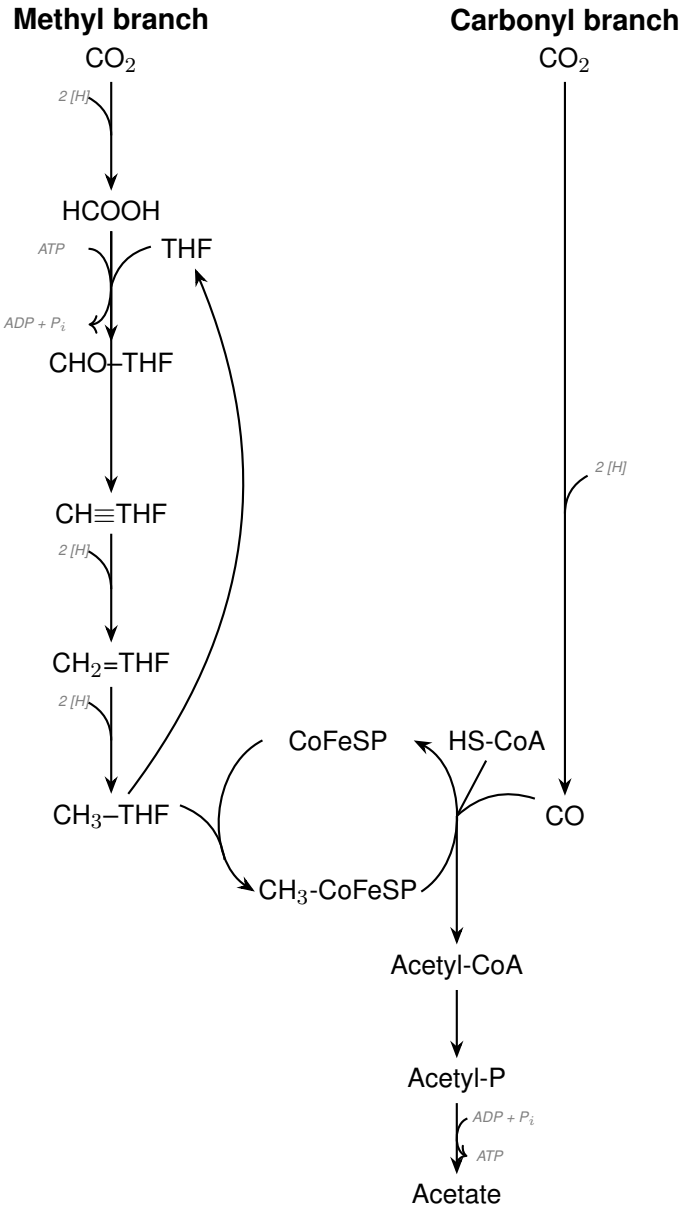

Figure 2.3. *Wood-Ljungdahl pathway in acetogens. Two molecules of carbon dioxide are reduced into acetyl-CoA. H_2 is the most common electron donor.*

cycle, the reductive pentose phosphate cycle, the 3-hydroxypropionate pathway, the 3-hydroxypropionate/4-hydroxybutyrate pathway and the dicarboxylate/4-hydroxybutyrate pathway (Fast et al. 2015). Out of these, by far the most energetically efficient route is the Wood-Ljungdahl pathway, which can be coupled with membrane-bound complexes to actually have net positive ATP yield when producing acetate (Schuchmann et al. 2014).

The simplified scheme of the Wood-Ljungdahl pathway is shown in Figure 2.3. The pathway is divided into carbonyl and methyl branches, and the first step of the methyl branch is the conversion of CO_2 and hydrogen to formate. Formate dehydrogenase (FDH) drives the reduction in all cases, but the electron delivery system differs between the organisms. These can be categorized by three model organisms. While *Acetobacterium woodii*

uses direct electron transfer from hydrogen, *Clostridium ljungdahlii* and *Moorella thermoacetica* utilize different cofactors, reduced ferredoxin (Fd_{red}) and NADPH, respectively, to facilitate the reduction process (H. Lee et al. 2022). Tetrahydrofolic acid (THF) attaches to the formate and via few steps is transformed into methyl-THF. Enzymes catalyzing these reactions, in the following order, are formyl-tetrahydrofolate synthase (FHS), formyl-cyclohydrolase (FCH), methylene-tetrahydrofolate dehydrogenase (MDH), and, for the final step, methylene-tetrahydrofolate reductase (MTHFR). (Ragsdale et al. 2008)

In the first reaction of the carbonyl branch, carbon dioxide is reduced to carbon monoxide (CO) by a bifunctional CO dehydrogenase/acetyl-CoA synthase (CODH/ACS) (Fast et al. 2015). The methyl group of the methyl branch is transferred to the corrinoid iron-sulfur protein (CoFeSP) by methyltansferase (MT), while the THF is released. The formation of the acetyl-CoA from methyl-CoFeSP and CO is facilitated by the acetyl-CoA synthase. From there, the final product, acetate, is achieved in two steps, facilitated by phosphotransacetylase (PTA) and acetate kinase (ACK), respectively. (Ragsdale et al. 2008)

Microbial electrosynthesis is a system that combines electrochemical cells with microbial cell culture. Water is oxidized at the anode, and the electrons and protons formed are used for the Wood-Ljungdahl pathway in the biofilm covering the cathode. (Dessì et al. 2021) MES is usually performed by mixture cultures and little is known about the specific functions of each microbial genus. Genera *Eubacterium* and *Proteiniphilum* have at least been shown to play some role in the production of acetate from carbon dioxide. (Vassilev et al. 2024) If the mixture culture has bacteria capable of chain elongation, other SCFAs can be formed. Butyrate is often the second most abundant fatty acid produced in MES. The pathways for butyrate formation are still only speculated, but a proposed way is that acetate is converted into ethanol and lactate, which then act as electron donors (Raes et al. 2017). By adjusting the feeding rates of H_2 and CO_2, the pH can be shifted to acidic, which favors the ethanol production and the chain elongation to achieve higher butyrate yields (Batlle-Vilanova et al. 2017). Another way to increase butyrate production is to feed methanol to the cathode (Yao et al. 2025). Even with this method, the butyrate yields are still highly affected by pH.

2.2.3 Inhibitory effects of the feeds

As mentioned in previous subsections, the hydrolytic steps, acid fermentation, and acetogenesis produce many side products that can stay in the effluent in small concentrations. Many of them are harmless, but others can be toxic to cells, even in small doses. Especially harmful are the furan derivatives produced during thermal treatment (Mills et al. 2009; Konzock et al. 2021; W. Wang et al. 2014; Xia Wang et al. 2018). From these compounds, furfural is extensively studied and has been shown to inhibit glycolytic pathways and harm cell membranes (Konzock et al. 2021). Because of inhibited glycolysis,

the growth rate usually slows down significantly and the lag phases are longer. This can be due to direct enzymatic inhibition or damage caused to DNA or the cell membrane, which leads to the depletion of ATP and NADPH reserves (Almeida et al. 2009). Damage is typically done by reactive oxygen species (ROS), and their concentration tends to rise in response to elevated furfural and HMF levels. The ROS can then cause lipid peroxidation, protein misfolding, or DNA strand breaking. (Almeida et al. 2009) Although the membrane is highly sensitive to hydrophobic compounds, intracellular effects seem to be affected more by furfural and HMF (Mills et al. 2009).

Phenolic compounds include a variety of chemicals with an aromatic ring, including hydroxy groups, as a unifying characteristic. The aromatic and phenolic compounds are usually not as toxic as furan derivatives and can even be used as substrates by some microbial strains. However, phenolic compounds are still hydrophobic and in most species have inhibiting effects. Aromatic acids can cause membrane leakage and vanillin is a bacteriostat that disrupts potassium gradients. (Mills et al. 2009) Just like the furan derivatives, phenolic compounds can induce the formation of the ROS and therefore can have an effect on protein structures and lipids or break DNA (Sui et al. 2024; Almeida et al. 2009). Recent discoveries have also shown that a phenolic compound phloroglucinol can form a complex with iron inside the cell and therefore generate hydroxy radicals. These radicals cause lipid peroxidation and deplete the microbes' reducing power, leading to ferroptosis-like death (Sui et al. 2024).

The third major inhibitory group that forms during the hydrothermal processes is weak acids. They are also the main product of interest during the MES and acid fermentation. Despite their use as a sustainable substrate, most of them are inhibitory, especially at high concentrations. The toxicity of weak aids is largely due to their ability to diffuse through the cell membrane in an undissociated form. Once inside, they dissociate, releasing a proton, lowering the intracellular pH by anion accumulation. (Mills et al. 2009) Formic acid has a lower pKa value than acetic acid, making it more toxic. As a smaller molecule, it also diffuses more easily in the cells (Konzock et al. 2021). If mixed with a more preferred substrate, such as glucose, propionic acid in certain hosts has shown to also inhibit the function of many key enzymes due to the intracellular rise in propionyl-CoA. These enzymes include pyruvate dehydrogenase, ATP citrate lyase, and succinyl-CoA synthetase, which all play a role in central metabolism. (Brock et al. 2004) The longer chained weak acids, butyric acid and valeric acid, show modes of toxicity similar to acetate, propionate, and formiate (Kovanda et al. 2019). However, because of their larger size, these cannot permeate the membrane as easily but on the other hand are not used as widely as substrates, which would deplete the accumulation.

2.3 Production of acetyl-CoA products

Acetyl-CoA acts as a building block for fatty acid synthesis and reverse beta-oxidation. The products of these cyclic routes can vary based on the length, degree of unsaturation, and branching. Inside the cells, these compounds can be stored as part of several different lipid products. Alternatively, they can be secreted in the medium as extracellular fatty acids (Stahl et al. 2001; Gildemyn et al. 2017).

2.3.1 Fatty acid synthesis

The rate and composition of the lipid products are largely determined by the fatty acid synthesis. In bacteria, fatty acids are synthesized by type II fatty acid synthase (FAS II), which consists of multiple monofunctional polypeptides, each catalyzing a single step (Cronan Jr et al. 2002). This allows the formation of a variety of different types of FAs, such as unsaturated or branched ones. In yeasts, on the other hand, type I fatty acid synthase (FAS I) is mainly used, which consist of multifuntional polypeptides encoded by only two genes (Cronan Jr et al. 2002). The products of FAS I consist mainly of palmitic acid, but since all enzymatic activities are fused into a few polypeptides and the intermediates do not diffuse from the complex, FAS I allows more efficient productivity, which explains the high lipid productivities of many yeast species.

The fatty acid synthesis scheme in the *E. coli* is shown in Figure 2.4. The first phase is the initiation, where ACC catalyzes the carboxylation of acetyl-CoA to form malonyl-CoA, and after this, FabD transfers the malonyl group to ACP (Magnuson et al. 1992). The first step requires ATP. The final initiation step is the condensation of malonyl-CoA with acetyl-CoA, which is catalyzed by FadH (Jackowski et al. 1987; Rawlings et al. 1992).

After the intiation, the elongation cycles start. β-Ketoacyl-ACP is reduced to β-Hydroxyacyl-ACP by FabG (Lai et al. 2004). This step requires NADPH in both FAS I and FAS II (Van Rossum et al. 2016). Next, the β-Hydroxyacyl-ACP is dehydrated by FabA or FabZ to form trans-2-enoyl-ACP (Bloch 1971). In some bacteria, FabA can also catalyze the formation of cis-3-decenoyl-ACP, which leads to unsaturated fatty acids (Bloch 1971; White et al. 2005). FabI or the corresponding enzyme catalyzes the reduction of enoyl-ACP to acyl-ACP. Acyl-ACP can be terminated from the cycle and be used as a precursor for products or go through another elongation cycle. Multiple possible synthases may catalyze the acyl-ACP and malonyl-ACP condensation, depending on the current acyl-ACP chain. If, for example, previously cis-3-decenoyl-ACP was formed, FabB is used (Clark et al. 1983). In yeasts, different but homologue enzymes are used for the reactions. To produce odd-chain fatty acids, propionyl-CoA must be used in the initiation step to be condensed with malonyl-CoA. In wild-type microorganisms, this is however very rare and only a small number of produced FAs are odd-chained (Y.-k. Park et al. 2020).

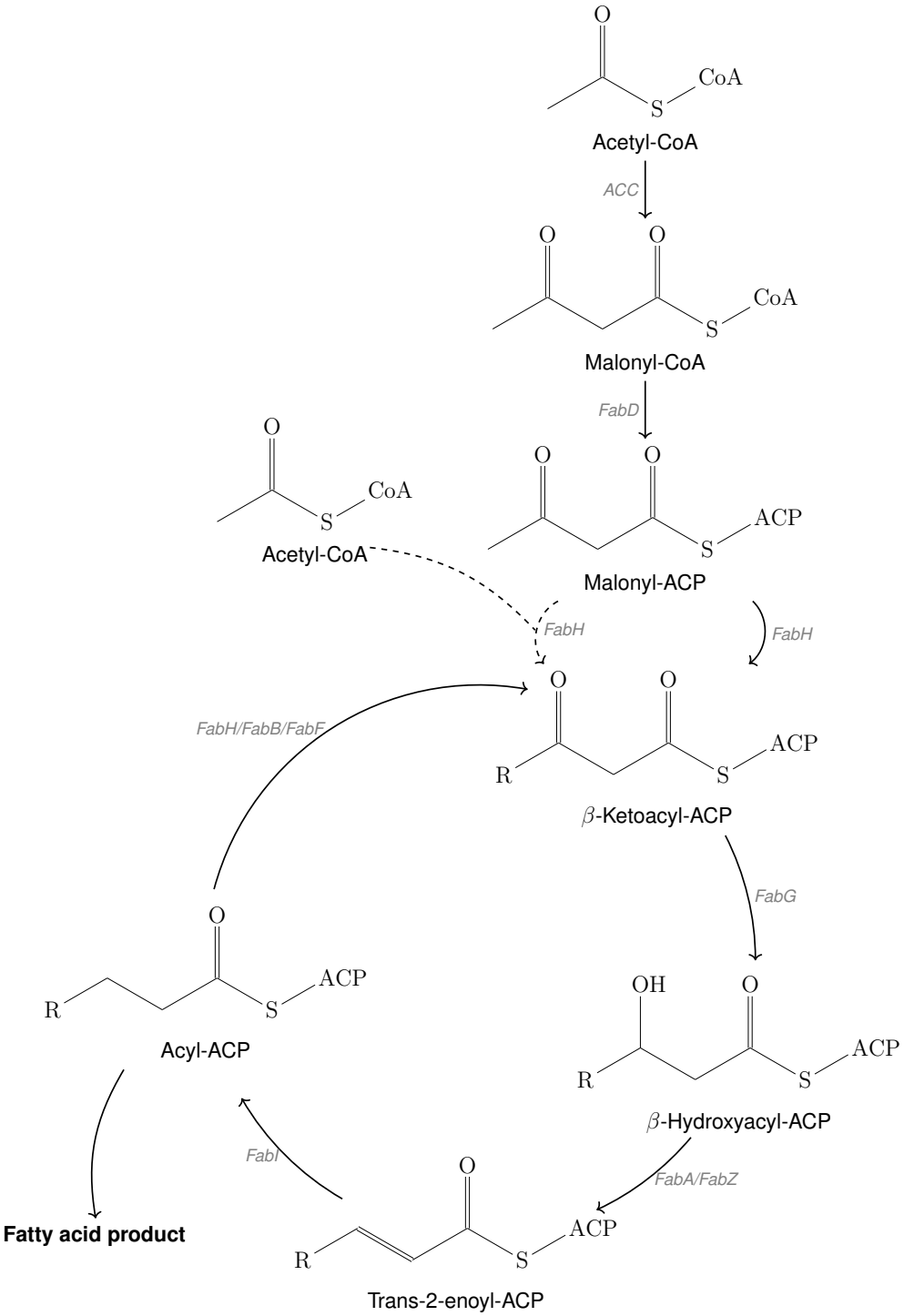

Figure 2.4. *Type II fatty acid synthesis pathway. Dashed lines mean that acetyl-CoA is condensed with malonyl-CoA only during the initialization cycle. Otherwise, malonyl-CoA is condensed with the growing acyl-ACP chain. In the dehydration step, FabA can also isomerize the product to form cis-3-decenoyl-ACP. Elongation of this is then done by FabB. ACC, acetyl-CoA carboxylase; FabD, malonyl-CoA:ACP transacylase; FabH, β-ketoacyl-ACP synthase III; FabB, β-ketoacyl-ACP synthase I; FabF, β-ketoacyl-ACP synthase II; FabG, β-ketoacyl-ACP reductase; FabA/FabZ, β-hydroxyacyl-ACP dehydratases; FabI, enoyl-ACP reductase (White et al. 2005; Cronan et al. 2009).*

2.3.2 Reverse beta-oxidation

An alternative route to produce longer-chain acyl-CoA molecules is the reverse β-oxidation. It is also a cyclic route with steps similar to the fatty acid synthesis, but instead of NADPH, it utilizes NADH as the reducing power and does not require any ATP (Garces Daza et al. 2023).

In reverse beta-oxidation, the initiation begins with the condensation of 2 acetyl-CoA molecules to form acetoacetyl-CoA (Teixeira et al. 2017). The step is catalyzed by the thiolase enzyme. In elongation, the intermediates are corresponding to the ones in the fatty acid synthesis, but instead of ACP, CoA is used as the carrier (Garces Daza et al. 2023). Enzymes are also similar to the ones in fatty acid synthesis, but, as mentioned before both of the reduction steps use NADH.

Propionyl-CoA can also be used for chain elongation in some bacteria like *C. kluyveri* (Parera Olm et al. 2023). Like in fatty acid synthesis, this produces odd-chained fatty acids. In reverse β-oxidation enzymes that participate in odd-numbered elongation still seem to have lower affinity than those in even chain elongation, usually resulting a greater portion of even-chained products (Parera Olm et al. 2023).

2.3.3 Free fatty acids, fatty alcohols, alkanes and wax ester synthesis

From the acyl-ACPs/acyl-CoAs, free fatty acids can be generated by thiosterases such as TesA (Steen et al. 2010). Free fatty acids have multiple usages and can be further transformed into fatty alcohols and alkenes or form membrane molecules such as glycerolipids or phospholipids. The biosynthetic path from acyl-CoA/acyl-ACP to wax ester is shown in Figure 2.5. Acyl-CoAs/acyl-ACPs can be reduced into fatty alcohols by one- or two-step reactions. In some hosts, fatty acyl-CoA reductases can reduce the acyl-CoAs/acyl-ACPs directly to fatty alcohols (A. Liu et al. 2013). Another path is for fatty acyl-ACP reductase to first catalyze the reduction to aldehyde and then reduce it to fatty alcohol by aldehyde reductase. In *Marinobacter aquaeolei*, the same enzymes have been shown to produce aldehydes and fatty alcohols (A. Liu et al. 2013). Reduction reactions require NADPH.

Alkanes can also be produced from acyl-CoA/acyl-ACP by a two-step reaction. The first step to form an aldehyde is a similar reduction reaction as when producing fatty alcohols. The second step is the decarbonylation of an aldehyde leading into an alkane, or in the case of unsaturated fatty acids, alkene (Schirmer et al. 2010). In addition to plant and animal cells, the decarbonylation of aldehyde in microbes is mainly found in cyanobacteria, and the function of similar enzymes in bacteria or yeast species is largely unknown (Marsh et al. 2013).

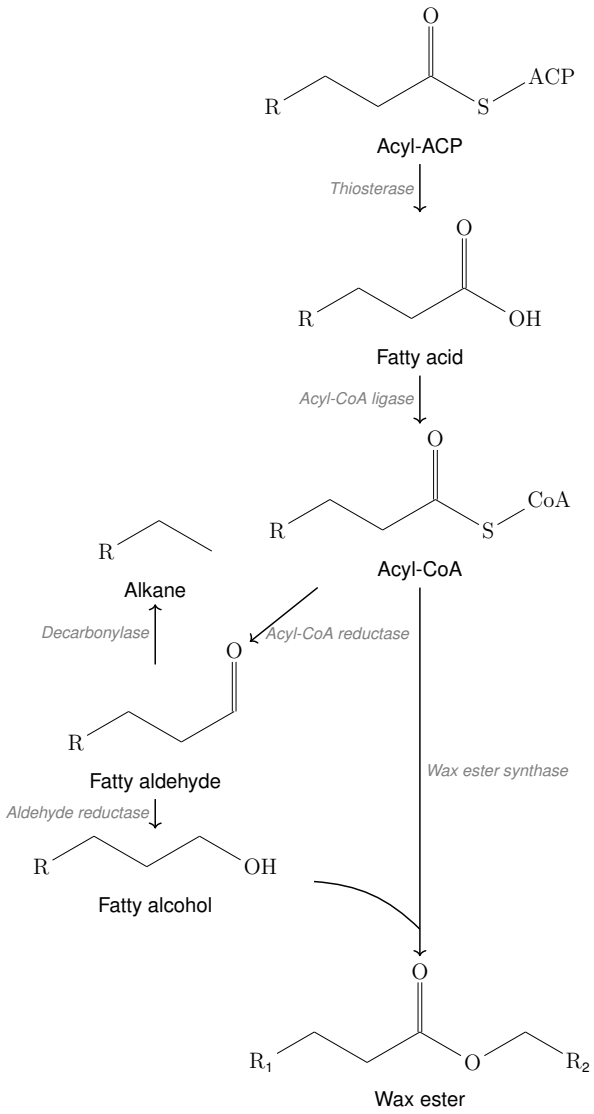

Figure 2.5. *Synthesis of fatty acids, fatty alcohols, alkanes, and wax esters from acyl-ACP.*

Wax esters are formed from long-chain fatty acids and fatty alcohols. Chemically, they resemble compounds like whale oil, and as microbial storage compounds, can offer a sustainable alternative. In the WE model organism *Acinetobacter baylyi* ADP1, the wax ester synthesis includes the two reduction steps to aldehyde and further to fatty alcohol that were described earlier. After this, the fatty alcohol and another fatty acyl-CoA are esterified by ester synthase/diacylglycerol acyltransferase (WS/DGAT) (Kalscheuer et al. 2003; Stöveken et al. 2005). In the wild-type strain, the fatty acid composition consists mainly of palmitic (C16) and stearic (C18) acids.

2.3.4 Polyhydroxyalkanoate synthesis

Polyhydroxyalkanoates (PHAs) are a group of diverse polyesters with more than 150 known possible monomers (Choi et al. 2020). These are common storage compounds

found in bacteria and are usually produced when there is an abundance of carbon sources and a limited amount of nitrogen or phosphorus. The length of the side chains usually determines the functionality of the compounds. PHA with many possible applications as a replacement for chemically synthesized plastics is poly-3-hydroxybutyrate (PHB) (Vicente et al. 2023).

PHB synthesis can be divided into two major parts: generation of hydroxyacyl-CoA and polymerization of hydroxyacyl-CoA to PHA. Hydroxyacyl-CoA can be generated from fatty acid synthesis or by simpler acetoacetyl-CoA synthesis as shown in Figure 2.6 (Vicente et al. 2023). The first step in the latter pathway is the condensation of two acetyl-CoAs to form acetoacetyl-CoA by acetyl-CoA acetyltransferase (PhaA). After this, acetoacetyl-CoA is reduced to (R)-3-hydroxybutyryl-CoA by acetoacetyl-CoA reductase (PhaB). The reduction requires NADPH as a cofactor (Sagong et al. 2018). Polymerization is catalyzed by PHA synthase (PhaC), which is also the key enzyme if the (R)-3-hydroxybutyryl-CoA is generated by fatty acid synthesis (Vicente et al. 2023).

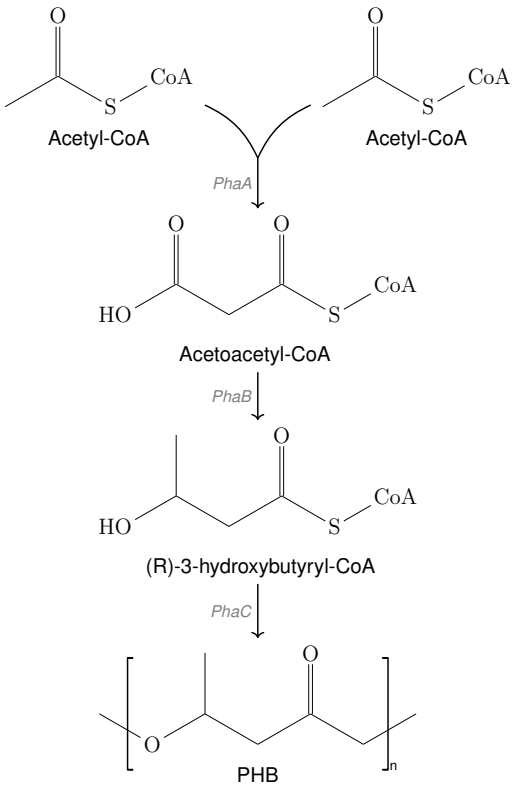

Figure 2.6. *PHB synthesis via acetoacetyl-CoA synthesis route. PhaA, acetyl-CoA acetyltransferase; PhaB, acetoacetyl-CoA reductase; PhaC, PHA synthase.*

2.3.5 Triacylglycerol synthesis

Triacylglycerols (TAG) are lipid molecules that are commonly found in algae but also in oleaginous microbes, especially yeasts (J. Xu et al. 2017). TAGs are prominent for

biodiesel production. They are trisubstituted glycerols with fatty acid chains. The starting point for glycerolipid synthesis is glycerol-3-phosphate, which can be generated from glycerol or glycolysis intermediates. Therefore, co-feeding sugar substrate would also provide a more efficient way for backbone generation in addition to the reducing agents that are required in all lipid biosynthesis pathways. The formation of triacylglycerols is illustrated in Figure 2.7.

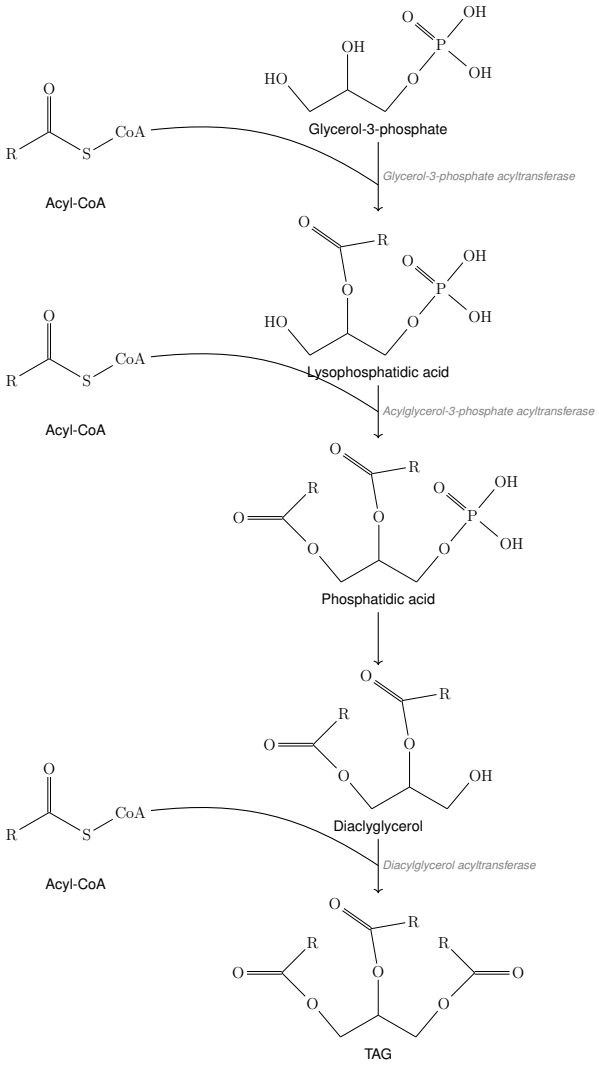

Figure 2.7. *Synthesis of triacylglycerol.*

During TAG synthesis, three acylation steps occur in which acyltransferases add fatty acids from acyl-CoA to the different positions of glycerol (Tai et al. 2013). The first glycerol-3-phosphate acyltransferase catalyzes the production of lysophosphatidic acid (LPA). In the second acylation, acylglycerol-3-phosphate acyltransferase forms phosphatidic acid (PA). This is then dephosphorylated to form diacylglycerol (DAG), and with diacylglycerol acyltransferase (DGA), the third acylation is catalyzed to produce TAG (Tai et al. 2013). TAGs can form a large amount of cellular dry matter in oleaginous species, with more than 80% in yeasts like *Yarrowia lipolytica* and even in some bacteria like *Rhodococ-*

cus opacus over 75% (Tai et al. 2013; Wältermann et al. 2000)

2.4 Models and data management tools

One crucial tool of the design–build–test–learn cycle in synthetic biology and genetic engineering is the usage of computational and metabolic models during the design phase. Based on the experimental results and mathematical equations, novel functions and pathways can be modeled, and later validated by new experiments. Modeling the metabolism and growth of microbes becomes especially important when moving to larger-scale processes. With substrates such as acetate, which are known to be toxic, results obtained under controlled laboratory conditions are unlikely to scale directly to large-scale processes, where heterogeneity is a major challenge. Based on the models, optimized and predictive control of process variables can be done, which again gives more data to validate the process parameters for more accurate models, and so the cycle continues. This way, the productivity can be increased by for example finding the optimal acetate feeding rates.

2.4.1 Metabolic flux models

Metabolic flux models allow for the estimation of multiple extracellular or intracellular reaction rates on the basis of a few experimentally determined extracellular rates. In flux balance analysis (FBA) metabolism is represented by a diagram that links the anabolic and catabolic reactions through common carbon skeletons or other intermediates. If pseudosteady-state is assumed, metabolite accumulation does not occur, and the basic equation for FBA is obtained

$$0 = \frac{d\mathbf{C}_{met}}{dt} = \mathbf{S}_m \cdot \mathbf{v}_m + \mathbf{S}_c \cdot \mathbf{v}_c. \tag{2.1}$$

In Equation 2.1 $\mathbf{S}$ is the matrix containing the stoichiometric coefficients and $\mathbf{v}$ is the vector of reaction rates. Subscript *m* refers to measured values and *c* to calculated values. Therefore, by multiplying left by the inverse of $\mathbf{S}_c$, the desired fluxes can be calculated.

Flux balance analysis can be simplified by lumping multiple reactions, or it can be expanded to take into account thousands of various gene products. These genome-scale models (GEMs) exist for most of the industrially relevant microbes and can be used to predict environmental impacts and to help visualize metabolic regulations (Reed et al. 2003; Nogales et al. 2020). However, as stoichiometric models, GEMs tend to show an unrealistic linear increase in yields when carbon source amounts are increased, and these models usually have an over-representation of central metabolic pathways compared to secondary pathways that would be relevant when screening for the specific and unique

production capabilities (Niu et al. 2022; Monk et al. 2014). As improvement, different constraint based models have been implemented with integrating enzyme kinetics or various omic datasets to the stoichiometric models (Niu et al. 2022; Duman-Özdamar et al. 2025).

2.4.2 Large-scale reactor models

In larger volumes, the idel reactor assumption is not justified due to gradients caused by long mixing times. The mixing time describes how long it takes to reach homogenity in the reactor and depends on the reactor dimensions, stirrer configurations, and the mean specific energy dissipitation rate (Peter Vrábel et al. 2000).

In compartment modelling, the reactor volume is divided into smaller cells, where local concentrations can be taken into account, and the compartments are connected via fluid flows. The concept is similar to computational fluid dynamics (CFD) where conservation of momentum, mass, and energy, among other variables, are described by the Navier-Stokes equations. Solving CFD systems with bioreactions is however computationally expensive. That is why in compartment models the flows are often determined by experimentally calculated patterns (Pigou et al. 2015; Vrábel et al. 1999). Circulation flow rates produced by mechanical stirrers can be estimated by the discharge flow

$$Q_L = K_p N D^3, \tag{2.2}$$

where K_p is the dimensioless impeller discharge coefficient, *N* is the stirrer speed (s^{-1}) and *D* is the impeller diameter (m) (Vrábel et al. 1999). Vertical transport can be modeled with exchange flows that are also dependent on the stirrer speed and diameter, and also on the gas hold-up and pneumatic power if aeration is included (Vrábel et al. 1999; Peter Vrábel et al. 2000).

The effect of the fluctuations between the local concentrations on cell growth can not be expressed by single environmetally restricted kinetic values (Morchain et al. 2013). To acknwoledge the constant flows from one compartment to another, population balance models can be used. In the population balance equation (PBE), the transport between the physical and internal variable space are described by the number density *n* according to following equation

$$\frac{\partial n(\overline{\varsigma}, \overline{x}, t)}{\partial t} + u_i \frac{\partial n(\overline{\varsigma}, \overline{x}, t)}{\partial x_i} + \frac{\partial}{\partial x_i}\left(\Gamma \frac{\partial n(\overline{\varsigma}, \overline{x}, t)}{\partial x_i}\right) = -\frac{\partial}{\partial \varsigma_j}(n(\overline{\varsigma}, t).\zeta) + h(\overline{\varsigma}, t) \tag{2.3}$$

(Morchain et al. 2013).In the equation $\overline{\varsigma}$ is the vector of the internal variable coordinate, $\overline{x}$ is the vector of spatial coordinates, Γ is the diffusivity, ζ is the velocity of the transfer

in iternal space and *t* represnts the time (Morchain et al. 2013). First term on the right is the transport in the internal space and *h* indicates the net production (Pigou et al. 2015; Morchain et al. 2013). In case of substrate consumption the rates are usually calculated with Monod equation

$$r_S = q_{Smax}\frac{S}{S+K_S}X, \tag{2.4}$$

where q_{Smax} is the maximum specific uptake rate (h^{-1}), *S* is the local substrate concentration (g L^{-1}), K_S is the substrate affinity constant (g L^{-1}) and *X* is the biomass concentration (g L^{-1}). The biomass production rate can be calculated from the substrate consumption by multiplying with the yield coefficient Y_{XS} (g g^{-1}) and subtracting the cell deaths caused by q_d (h^{-1}). If the change in spatial coordinates is handled by predetermined flow rates, and biomass *X* is number density divided into *i* classes, the PBE can be simplified into

$$\frac{\partial X(\overline{\varsigma},t)}{\partial t} = -\frac{\partial}{\partial \varsigma_j}(X(\overline{\varsigma},t).\zeta) + h(\overline{\varsigma},t). \tag{2.5}$$

The internal variable ς can be, for example, the growth rate, the uptake rate for substrate, or the oxygen uptake, and should be selected based on the phenomenom studied. The common characteristic is that biomass always transfers towards classes close to the environmental equilibrium, but the transfer rate depends on the adaptation time constant (Losoi et al. 2022).

2.4.3 Multiple correspondence analysis

Multiple correspondence analysis (MCA) is a method to reduce the dimensions of categorical datasets. MCA is similar to principal component analysis (PCA), where orthogonal vectors are built as linear combinations of original quantitative variables to explain the total variance (inertia) in fewer dimensions. In MCA, from the original data matrix $\mathbf{M}$ with *k* rows and *l* columns, an indicator matrix $\mathbf{P} = [\mathbf{P}^1\ \mathbf{P}^2\ ...\ \mathbf{P}^l]$ is formed, where $\mathbf{P}^j \in \{0,1\}^{k\times R_j}$ with row *i* is equivalent to the one-hot encoded x_{ij} (Fithian et al. 2017). This means that the original variables are assigned binary values: 1 on their corresponding level and 0 on all the other levels. After obtaining the indicator matrix, the singular value decomposition can be solved like in the case of PCA or two-variable correspondence analysis from the matrix $\mathbf{Z}$ of the standarized residuals

$$\mathbf{Z} = \mathbf{U}\mathbf{\Sigma}\mathbf{V}^{\mathbf{T}}. \tag{2.6}$$

Here $\mathbf{U}$ and $\mathbf{V}$ are unitary matrices and $\mathbf{\Sigma}$ is the diagonal matrix with singular values in descending order (Khangar et al. 2017). The total inertia is then the sum of the squares of

the singular values. The precise procedure for acquiring the singular value decomposition for correspondence analysis is presented in the article by Khangar et al. (Khangar et al. 2017).

In principal component analysis, a threshold for the required number of principal components is often between a total inertia of 70% and 90% explained. One common procedure is to choose only the principal components with eigenvalues higher than the mean of all eigenvalues (Abdi and Williams 2010). For multiple correspondence analysis, a lower total inertia is acceptable, and the significance of the first dimensions is often underestimated due to the bloated total inertia caused by the one-hot encoding of the contingency table (Abdi and Valentin 2007). Due to its nature of dealing with categorical variables, MCA is mainly popular in the fields of social sciences, but multiple uses, for example in health and genetic studies, are reported (Sourial et al. 2010; Goes Job et al. 2025).

3. SELECTION CRITERIA FOR ACETATE-CONSUMING MICROORGANISMS

In this study, eight microbial species were selected for comparison based on their potential in the bioconversion of acetate-rich industry effluents. These microbes exhibit diverse metabolic capabilities, genetic accessibility, and industrial relevance. The selected species are: *Escherichia coli*, *Pseudomonas putida*, *Acinetobacter baylyi* ADP1, *Yarrowia lipolytica*, *Corynebacterium glutamicum*, *Cutaneotrichosporon oleaginosus*, *Clostridium kluyveri* and *Cupriavidus necator*. *E. coli* serves as the model for metabolic engineering, while *P. putida*, ADP1, and *C. necator* are known for their robustness and potential in PHA or WE production. *C. glutamicum* and *C. kluyveri* provide unique metabolic routes for acetate utilization and have high tolerance. The oleaginous yeasts *Y. lipolytica* and *C. oleaginosus* excel in lipid accumulation. The following sections provide a detailed comparison of these microbes in six key attributes.

3.1 Acetate utilization

The first requirement for microbial hosts to be suitable is the ability to utilize acetate. There are three major ways: using acetate as the sole carbon substrate, diauxic growth with another preferred or inferior substrate, and simultaneous utilization as a co-substrate.

Most of the selected microbes, including *E. coli*, ADP1, *P. putida*, *C. glutamicum*, *C. necator*, *Y. lipolytica* and *C. oleaginosus* can grow on acetate as the sole carbon source (Konzock et al. 2021; L. Chen et al. 2021; Narisetty et al. 2022; Salcedo-Vite et al. 2019; Yang et al. 2019; Kedia et al. 2014; Wolf et al. 2020; Gong et al. 2015). This is enabled by the glyoxylate cycle, which bypasses the carbon loss in the TCA cycle and allows the assimilation of C2 units. In contrast, an anaerobic bacterium *C. kluyveri* based on the current knowledge, lacks the glyoxylate cycle and cannot use acetate alone. Instead, it requires ethanol as a co-substrate and employs a chain elongation pathway (Reddy et al. 2018). Study by Reddy et al. (2018) showed some growth when no ethanol was added on the medium. However, ethanol consumption was still observed likely due to residuals from the preculture, so this does not debunk the hypothesis that ethanol is vital as an electron donor.

From the bacterial species, *E. coli* demonstrates clear diauxic growth, preferentially consuming sugars before switching to suboptimal metabolism (Enjalbert et al. 2015). In contrast, ADP1, *C. necator* and *C. glutamicum* similarly to *C. kluyveri* can co-utilize acetate with other carbon sources, giving them more metabolic flexibility (S. Santala, V. Santala, et al. 2021; Wendisch et al. 2000; Fereidouni et al. 2011). *P. putida* also does not have as strong a catabolic repression system as *E. coli*, and it uptakes acetate and glucose simultaneously (Wirth et al. 2022).

From yeast species *Yarrowia lipolytica* shows diauxic growth on multiple substrates. *Y. lipolytica* does not consume acetate until glycerol is depleted (L. Chen et al. 2021) and with glucose, only a small portion of acetate is consumed even with an evolved strain (Narisetty et al. 2022). *C. oleaginosus* on the other hand, can co-utilize acetate and glucose (Zhou et al. 2019). Both of these strains direct acetate metabolism toward lipid accumulation rather than energy generation, making them popular candidates for biotechnological applications.

3.2 Acetate tolerance

Since all of the selected microbes can utilize acetate, it already means that they have some tolerance to it. A faster consumption rate means less accumulation inside the cell, leading to a drop in pH. Absolute thresholds are still difficult to determine since tolerance can be greatly improved by controlling pH and gradual adaptation. *E. coli* has the lowest acetate tolerance of the bacterial species, and with 85 mM concentrations, the wild type is severely impaired (Gu et al. 2024). In 50 mM growth still happens. The infromation about the tolerance of wild-type *Y. lipolytica* strains without major optimizations is scarce, but at 75 mM of acetic acid, growth can not happen for the lipid-accumulating strain OKYL049 (Konzock et al. 2021). It has to be noted, that this is in the presence of another substrate, glucose, and in an undissociated form, so at an adjusted pH, the tolerance will be higher. Strain *Y. lipolytica* W29 has been shown to completely metabolize 5 g L^{-1} of acetate in a batch cultivation. (Pereira et al. 2021). *Y. lipolytica* is still often used as an example of being highly tolerant against SCFAs, but experiments are not performed on a wild-type strain. However, multiple engineered strains have been able to tolerate notably high acetate concentrations (J. Xu et al. 2017; Koh et al. 2024). With slight modifications to *Y. lipolytica*, by expressing the acs as well as subjecting the strain to adaptive laboratory evolution, tolerance of up to 500 mM acetate has been reported (Narisetty et al. 2022). This is a good implication that naturally low tolerance is not an insurmountable obstacle.

When comparing the wild-type strains, *C. oleaginosus* exceeds *Y. lipolyticas* acetate tolerance, and utilization. Effective lipid production has been reported to take place in all the way up to 270 mM of acetate, and in pH 5.5 growth still occurs in up to 500 mM (Gong et al. 2015). *C.necator* has been shown to accumulate PHAs between 350 and 500 mM

of acetic acid concentrations, but in these cases the addition was made after cultures had reached the stationary phase (Kedia et al. 2014). This is therefore not comparable as such with the other results. When cultivating with acetate as the main carbon source from the beginning, concentrations between 100 and 200 mM can be tolerated but with a notably prolonged lag phase (Jawed et al. 2022; Amer et al. 2023).

Other microbes settle somewhere between these low-tolerant and very-high-tolerant microbes. ADP1 can grow in 250 mM of acetate and *C. glutamicum* in 200 mM (Salcedo-Vite et al. 2019; Wolf et al. 2020). These are still not necessarily the absolute highest concentrations that these strains can handle. *C. kluyveri* is also still relatively little studied, so it is difficult to say at what acetate amounts the growth stops, but concentrations from 100 to 200 mM has not shown any inhibitory effects (Reddy et al. 2018; Otten et al. 2022). Lastly, *P. putida* can tolerate acetate atleast up to 170 mM (Yang et al. 2019). This was achieved with strain KT2440, which is commonly used in a laboratory environment.

3.3 Model availability

E. coli is by far the most well-modeled bacterium and has several genome-scale metabolic models (GEMs) and constraint-based models (CBMs), as well as kinetic models for countless different production paths (Jahan et al. 2016; Weaver et al. 2014). Another model organism from the selected ones is *P. putida*, with also multiple GEMs, CBMs and kinetic models (Tokic et al. 2020; Nogales et al. 2020). *C. glutamicum* is not yet studied on the same level as the previous two species, but due to its ability to produce amino acids, several GEMs and kinetic models have been built for it (Gayen et al. 2007; Y. Zhang et al. 2017). In addition, CBMs where enzyme kinetics has been integrated with the genomic data, have been implemented (Niu et al. 2022).

Y. lipolytica has been the go-to strain of the oleaginous yeasts for many studies, so there is a large library of different models. There are GEMs/CBMs available, and a lot of the kinetic models and dynamic flux balances are aimed to support the optimal conditions for the lipid accumulation (Kavšček et al. 2015; Carlos E Robles-Rodríguez et al. 2018; Carlos Eduardo Robles-Rodríguez et al. 2015). The parameter estimations from these models can also be used as guidelines for the *C. oleaginosus*, which is better at utilizing acetate but has only a small number of models. There is a GEM for *C. oleaginosus* and this has also recently been integrated with proteomics data to identify gene targets and media for enhanced lipid production (Pham et al. 2021; Duman-Özdamar et al. 2025). The limited specific models can also be replaced with response surface models (RSMs) to predict impacts of carbon sources (Pham et al. 2021). These kinds of design of experiment (DoE) approaches are viable for screening and optimization, but also require a lot of experimental data if reliable mechanistic links are not available.

ADP1 and *C. necator* both have available GEMs (Durot et al. 2008; Pearcy et al. 2022).

There is another older GEM built for *C. necator* but it is not publicly available online (J. M. Park et al. 2011). Since both of these bacteria have been gathering interest due to their ability to metabolize a variety of substrates, some kinetic models have also emerged (Baei et al. 2011). The equations are still not too specific and are mainly used for parameter estimation. They both can also be considered model organisms for relevant lipid production pathways, ADP1 for wax esters and *C. necator* for PHAs. *C. kluyveri* has a similar level of model availability compared to *C. oleaginosus*. Because there are not too many model organisms for medium chain fatty acid production, *C. kluyveri* is often used and has an available GEM as well as some kinetic models that can be used to estimate the growth parameters (Candry et al. 2018; Zou et al. 2018).

3.4 Genetic engineering possibilities

Same as for the model availability, *E. coli* has also the largest amount of tools for genetic manipulation. Multiple CRISPR/Cas systems have been successfully used for *E. coli* to modify the genome, regulate transcription, or for base editing. CRISPRi has proven to be useful for repressing competing pathways, for example to prevent malonyl-CoA depletion. (Z. Liu et al. 2020) CRISPR/Cas-mediated editing has been utilized for the majority of the other selected microbes, except for *C. kluyveri* (Schwartz et al. 2018; J. Liu et al. 2017; Z. Wang et al. 2024; Stellner et al. 2023). One beneficial factor for genetic modifications is the natural transformation efficiency. From the selected microbes, ADP1 is known to be highly competent for natural transformation (S. Santala and V. Santala 2021). The rest of the selected bacteria, on the other hand, are not naturally competent (Carlson et al. 1983; Komiyama et al. 2020; Weldon et al. 2025; Lobanova et al. 2022). For the yeast species, only a scarce set of tools for introducing foreign DNA is available (A.-Q. Yu et al. 2016; Stellner et al. 2023).

P. putida, *C. necator* and *Y. lipolytica* have also been the subjects of many engineering studies. In *C. necator* by expressing *pncB* and *nadE*, a higher NADPH pool can be achieved to increase PHB production (S. M. Lee et al. 2022). This has been shown to improve the tolerance towards furfural, vanillin, 5-HMF, and acetate by depleting the intracellular accumulation. In *P. putida*, the *acs* gene encoding acetyl-CoA synthase has been successfully overexpressed, whereas in *Y. lipolytica*, *acs* has been heterologously expressed to enable the ligation of acetate and coenzyme A in cytosol (Yang et al. 2019; Narisetty et al. 2022). Because in oleaginous yeasts the majority of acetyl-CoA is generated by ATP:citrate lyase from the citrate that is transported from the mitochondria, *acs* expression could significantly enhance the fatty acid synthesis (Fakas 2017).

In *C. glutamicum* deleting the *ramB* gene, which encodes a transcriptional regulator of glyoxylate shunt enzymes, is viable for increasing itaconic acid yield from acetate (Schmollack et al. 2022). Similarly, in ADP1, carbon flux from acetate has been directed towards

the WE synthesis pathway by overexpressing fatty acyl-CoA reductase *acr1* and deleting the *aceA* to block isocitrate lyase (Luo et al. 2020). For *C. oleaginosus* mitochondrial pyruvate dehydrogenase (PDH) bypass has been implemented, so citrate from the mitochondria is not needed for the acetyl-CoA generation (Koivuranta et al. 2018). This resulted in a higher TAG yield. As this was done using sugar substrates, three new genes were introduced: *pdc1*, *ald6*, and *acs2* (Koivuranta et al. 2018). If acetate is used, introducing *acs* gene is enough, like in the case of *Y. lipolytica*, but may not result in that much higher lipid yield because NADPH in the bypass was generated by the reaction catalyzed by acetaldehyde dehydrogenase (ALD).

C. kluyveri is a strict anaerobe, and applying genetic engineering tools to it is challenging. Creating an oxygen-free environment requires chambers where other gases like nitrogen replace oxygen, or cultivation must be done in vials or jars where oxygen is exhausted (Börner 2016).

3.5 Production pathways and major product composition

Most of the selected species utilize fatty acid synthesis. *E. coli*, *P. putida* and ADP1 have the bacterial type II FA synthase (Lennen et al. 2012; Yang et al. 2019). The eukaryotic type I FA synthase is found in *Y. lipolytica*, *C. oleaginosus* and exceptionally in the bacterium *C. glutamicum* (Ikeda et al. 2017). In wild-type *E. coli* storage lipid or PHB accumulation is insignificant and the acetyl-CoA is directed into the TCA cycle or fermentation products (Gu et al. 2024). *P. putida* KT2440 on the other hand is shown to produce mcl-PHAs even without any modifications (Yang et al. 2019). ADP1 accumulates both WEs and TAGs, but the wax ester proportion is noticeably higher (S. Santala, Efimova, et al. 2014). Since the wax ester production pathway can also produce fatty alcohols and alkanes, with genetic modifications of shutting down catalytic enzymes, a variety of products could be extracted.

Y. lipolytica, like other oleaginous yeasts, directs a good portion of the acetyl-CoA to TAG synthesis (J. Xu et al. 2017). The current assumption is that acetyl-CoA in oleaginous yeasts comes mainly from the cleavage of citrate that is exported from the mitochondria to the cytosol (Pham et al. 2021). *C. oleaginosus* has the highest lipid content from acetate produced up to 73.4% of the cell dry mass, and efficient lipid production can be reached even without limiting the nitrogen supply (Gong et al. 2015). Over 95 percent of the fatty acid chains in the products consist of palmitic acid, stearic acid, and oleic acid (Gong et al. 2015). Uniformity in the product helps with downstream processing.

Only a few studies have been done for fatty acid production in *C. glutamicum* but it is an interesting chassis for acetate-based protein synthesis (Takeno et al. 2013). As one of the most well studied organisms for large-scale L-glutamate and L-lysine production, the ability to produce recombinant proteins on acetate as a sole carbon source makes

C. glutamicum one of the more noteworthy candidates for biotransformation of acetate effluents (Schmollack et al. 2022; Kiefer et al. 2022). With a unique FAS system and the ability to grow on acetate, extending genetic engineering efforts to improve FA synthesis is a promising prospect.

C. necator does not utilize fatty acid synthase but instead produces acetoacetyl-CoA for the PHA pathway by condensation of two acetyl-CoA molecules (Cai et al. 2023). When grown solely on acetate or butyrate, only PHB is produced. The addition of odd-chained SCFAs will also yield other PHAs such as poly(3-hydroxybutyrate-co-3-hydroxvalerate) (PHBV) (Cai et al. 2023). *C. kluyveri* also does not utilize the traditional FA synthesis but relies on beta-oxidation. (Gildemyn et al. 2017). The main products of fermentation on ethanol and acetate are butyrate, caproate, and caprylate (Reddy et al. 2018; Gildemyn et al. 2017). Higher acetate/ethanol ratios lead to more efficient chain elongation, but also lower the proportional yield of longer-chained products (Gildemyn et al. 2017).

3.6 Robustness to inhibitory effluents

In addition to tolerating acetate, small residuals of compounds from the pretreatment steps should not completely halt metabolism. Furan derivatives, especially furfural, are highly toxic for most of the selected microbes already in small concentrations (Xuan Wang et al. 2013; W. Wang et al. 2014; X. Yu et al. 2014; Konzock et al. 2021; Xia Wang et al. 2018). The exceptions are *P. putida*, in which small amounts of furfural do not have a major effect on growth, and ADP1 and *C. necator*, as they both can biotransform furfural with high rates, although it still negatively affects growth (Pedrino et al. 2025; Arteaga et al. 2021).

C. oleaginosus, ADP1 and *P. putida* are all able to metabolize aromatic substrates and have a great tolerance to phenolic compounds (Salcedo-Vite et al. 2019; Pedrino et al. 2025; X. Yu et al. 2014). Other microbes that are able to grow without major inhibition by these compounds are *Y. lipolytica*, *C. glutamicum* and *C. necator* (Xia Wang et al. 2018; W. Wang et al. 2014; Konzock et al. 2021). *E. coli* does not have as high a tolerance to aromatics and its cell membrane is sensitive to phenols (Mills et al. 2009). It has to be noted that even when growth is not impaired, some of these compounds, especially if uptake happens, may shift the carbon flux toward undesirable pathways. For *C. kluyveri* the effects of inhibitory hydrolysate products are not widely studied. Thriving in ethanol-rich cultures gives it some flexibility when it comes to growth media acquired from industrial effluents since acid fermentation can lead to the ethanol formation (Reddy et al. 2018).

4. MATERIALS AND METHODS

4.1 Literature- and model-based screening

All relevant attributes were simultaneously screened to narrow the strains for cultivation studies and to identify all-round microbial hosts. Flux balance analysis was used to gain comparable numerical data before cultivations. The categorization of the literature data and the software used are described below.

4.1.1 Table construction and multiple correspondence analysis

Based on information gathered from the literature and previous studies, a table was built in which categorical values were set for each attribute. The categorization was performed in a way that microbes with clearly distinct performances would not be in the same class. However, the number of different classes was kept as small as possible, since too narrow value ranges would be influenced too much by the varying experimental set-ups and errors. The acetate tolerance levels in the table were categorized based on reported acetate concentrations at which the microbes maintain efficient function, with distinctions made in 100 mM increments. In the robustness category, a microbe was classified as highly robust if it tolerates furfural and can metabolize aromatic compounds. Model availability was considered high for microbes with more than one publicly available GEM. The high genetic engineering potential was assigned to microbes with well-established tools and documented successful modifications of the acetate utilization pathways. The main product listed was the predominant compound produced when the microbe is grown on acetate.

To visualize all variables at once as well as to find similarities between the microbes, FactoMineR (version 2.11) R package was used to perform multiple correspondence analysis (MCA) on the categorical table (Lê et al. 2008). The three-dimensional visualization was done using Plotly (version 4.10.4) (Sievert 2020).

4.1.2 Flux balance analysis

Flux balance analysis (FBA) was performed on all selected microbes with the Python package COBRApy (version 0.29.1) (Ebrahim et al. 2013). The following genome-scale models were used: *E. coli* (Reed et al. 2003), *P. putida* (Nogales et al. 2020),*A. baylyi* (Durot et al. 2008), *Y. lipolytica* (Kerkhoven et al. 2016), *C. oleaginosus* (Pham et al. 2021), *C. glutamicum* (Feierabend et al. 2021), *C. necator* (Pearcy et al. 2022) and *C. kluyveri* (Zou et al. 2018). The models with the number of reactions and metabolites are listed in Table 4.1. The palmitic acid exchange reaction was added to the models for ADP1, *C. kluyveri*, *C. necator*, *C. glutamicum* and *P. putida*. Theoretical maximal growth rates on acetate as the sole carbon source were calculated, as well as theoretical palmitic acid yields. The acetate intake flux was set to 1 g gCDW^{-1} h^{-1}, and other settings were kept at the default values.

Table 4.1. *Genome-scale metabolic models (GEMs) used in this study. Number of reactions listed does not include the palmitic acid exchange reaction that was later added to some of the models.*

Organism	Model name	Reactions	Metabolites	Reference
E. coli	iJR904	1075	761	(Reed et al. 2003)
A. baylyi	iAbaylyi^{v4}	875	701	(Durot et al. 2008)
P. putida	iJN1462	2929	2155	(Nogales et al. 2020)
Y. lipolytica	iYali4	1985	1683	(Kerkhoven et al. 2016)
C. necator	iCN1361	1292	1263	(Pearcy et al. 2022)
C. oleaginosus	iNP636	1553	1373	(Pham et al. 2021)
C. kluyveri	iCKL708	994	708	(Zou et al. 2018)
C. glutamicum	iCGB21FR	1539	1042	(Feierabend et al. 2021)

4.2 Small scale cultivations

Of the eight microbes studied, six were further investigated in batch cultivations. Outliers from MCA results were left out, except for *E. coli*, which was kept mainly for comparison. The following subsections describe the strains used, the growth conditions, and the analytical methods.

4.2.1 Strains

For this study, mainly wild-type strains were used. *P. putida* KT2440 (DSM 6125, DSMZ, Germany), *A. baylyi* ADP1 (DSM 24193, DSMZ, Germany) and *C. necator* (DSM 13513, DSMZ, Germany) were obtained from previously made glycerol stocks at Tampere Uni-

versity. *E. coli* XL1-Blue (Stratagene, USA) was used instead of the wild-type due to its availability. *C. glutamicum* (DSM 20300, DSMZ, Germany) and *C. oleaginosus* (DSM 11815, DSMZ, Germany) were ordered from DSMZ as freeze-dried cells and revived by cultivating in Lysogeny-broth. All the used strains are compiled in Table 4.2.

Table 4.2. *Microbial strains used in this study.*

Strain	Description	Reference
E. coli XL1-Blue	Cloning host	Lab stock (Stratagene)
P. putida KT2440 (DSM 6125)	Wild-type	Lab stock (DSMZ)
A. baylyi ADP1 (DSM 24193)	Wild-type	Lab stock (DSMZ)
C. necator (DSM 13513)	Wild-type	Lab stock (DSMZ)
C. glutamicum (DSM 20300)	Wild-type	DSMZ
C. oleaginosus (DSM 11815)	Wild-type	DSMZ

4.2.2 Culture media and growth conditions

Lysogeny-broth-agar (LA) plates were used for plating the strains stored in -80 ℃ glycerol stocks. LA media was prepared with 10 g L^{-1} tryptone, 5 g L^{-1} yeast extract, 5 g L^{-1} NaCl and 15 g L^{-1} agar. No antibiotics were added as only wild-type strains or well-established laboratory strains were used. 20 g L^{-1} glucose was added to plates used for *C. oleaginosus* to ensure clear colonies in sufficient time periods. All plates were incubated at 30 ℃ or room temperature.

The precultivations and the first round of final cultivations were performed in Lysogeny-broth (LB) liquid medium with 10 g L^{-1} tryptone, 5 g L^{-1} yeast extract, and 1 g L^{-1} NaCl. Precultivations were done as 5 mL cultures in 14 mL tubes. For *C. oleaginosus* 10 g L^{-1} glucose was again added. From precultivations, optical density at 600 nm (OD_{600}) was measured using Ultrospec 500 pro (Amersham Biosciences, UK).

The batch experiments were carried out in 50 mL LB cultures in 250 mL flasks with 100 mM of Na-acetate added. The preculture inoculants were added in volumes that resulted in a starting OD_{600} of 0.05. Similar incubation conditions were used for all the strains, with temperature being 30 ℃ and shaking of 300 rpm.

4.2.3 Optical density, substrate uptake and biomass measurements

Similarly, as from the preculture, the OD_{600} was measured at each sampling point from 1:10 dilutes using Ultrospec 500 pro. The dilution was done with pure LB medium, as it was also used as the blank.

At each sampling point, separate aliquots were also taken and centrifuged at 14 750 g for

3.5 minutes to separate the supernatant from the cells. The supernatants were stored at -20 ℃ and thawed right before the analysis. The acetate concentrations from the samples were determined with high-performance liquid chromatography (HPLC). Chromatographic analysis was performed with a Shimadzu UFLC HPLC system equipped with a Rezex RHM-Monosaccharide H^+ (8%) column (300 × 7.8 mm, Phenomenex). The temperature was kept at 40 ℃. The mobile phase consisted of 5 mM H_2SO_4. The flow rate was 0.5 mL min $^{-1}$.

The final dry mass of the cells was estimated by centrifuging the remaining aliquot after the sampling and separating the supernatant from the pellets. After this, the pellets were frozen before freeze-drying for 24 hours. The freeze drying was performed with Christ Alpha 1-4 LD lyophilizer (Martin Christ Gefriertrocknungsanlagen GmbH, Germany).

4.3 Model set-up and simulation

The feasibility of co-feeding acetate and glucose for the production of long-chain lipid products in large-scale bioreactors was evaluated using numerical simulations. The first simulations were performed to investigate the effects of carbon catabolic repression and substrate inhibition on the ideal ratio of substrate uptake rates. The second set of simulations assessed the volumetric productivities in different regions of the reactor. The equations and parameters used for the modeling are provided in the following subsections.

4.3.1 Growth rate and substrate uptake kinetics

Unstructured models were used for the kinetic equations. The ubstrate uptake rates for glucose (r_G) and acetate (r_A) were calculated with equation 2.4, and biomass growth was taken as the sum of the two uptake rates multiplied by the respective yield coefficients

$$r_X = Y_{XG} r_G + Y_{XA} r_A - q_d X, \tag{4.1}$$

where Y_{XG} is the yield from glucose and Y_{XA} is the yield from acetate. The cell death is modeled with a decay rate q_d (h^{-1}). Carbon catabolic repression of acetate uptake by glucose was modeled with two different methods: non-competitive inhibition $K_i/(K_i + S)$ where K_i is the inhibition constant, and based on affinity of the preferred susbtrate (S_p) as $(1 - \alpha)$ where $\alpha = S_p/(K_{sp} + S_p)$. Non-competitive enzyme kinetics are commonly used, but due to the complexity of regulatory systems, estimation of a single K_i value is difficult (Pigou et al. 2015; Kremling et al. 2018; Cecilia et al. 2019). The second method, on the other hand, assumes that uptake of the inferior substrate is halved when the concentration of the preferred substrate equals its affinity constant (Jahan et al. 2016). The non-competitive inhibition was also used for modeling the acetate toxicity.

4.3.2 Adaptation rates

The total biomass was divided into classes based on the specific growth rate, the specific glucose uptake rate, and the specific acetate uptake rate according to the following equations

$$\mu_i = \frac{(Y_{XG}q_{Gmax} + Y_{XA}q_{Amax})(2i-1)}{20}, \tag{4.2}$$

$$q_{Gi} = \frac{q_{Gmax}(2i-1)}{20} \tag{4.3}$$

$$q_{Ai} = \frac{q_{Amax}(2i-1)}{20}, \tag{4.4}$$

where q_{Gmax} is the maximum specific glucose uptake rate, q_{Amax} is the maximum specific acetate uptake rate and *i*=1,2,...,10 (Losoi et al. 2022). The transfer rate between the specific growth rate classes was expressed with a formula

$$\zeta(\mu) = \left(\frac{1}{T_\mu} + \mu_i\right)(\mu_{env} - \mu_i) \tag{4.5}$$

(Pigou et al. 2015). T_μ is the time constant for the growth rate adaptation, and μ_{env} is the environmentally limited growth rate. The used parameters are compiled in Table 4.3.

The transfer rates for the biomass in the specific uptake classes were calculated similarly, but the adaptation term differs. For example, the adaptation time for glucose uptake is approximately one percent of the magnitude of the adaptation time scale for growth (Morchain et al. 2014).

With the transfer rate equations, the first term on the right side of the population balance equation 2.5 can be discretized to form

$$-\frac{\partial}{\partial\varsigma}(X_i\zeta(\varsigma)) = \frac{\zeta(\varsigma_{i-1})X_{i-1} - \zeta(\varsigma_i)X_i}{\Delta\varsigma} + \frac{\zeta(\varsigma_i)X_i - \zeta(\varsigma_{i+1})X_{i+1}}{\Delta\varsigma}, \tag{4.6}$$

which was used to determine the class distributions (Morchain et al. 2013). In the equation, $\Delta\varsigma$ is the value of the internal variable interval between two classes. If the environmental rates defined by local concentrations are higher than the class value ς_i, transfer to the class above happens, and if the rates are lower, transfer happens to the class below.

Table 4.3. *Kinetic parameters used for E. coli and Y. lipolytica. Acetate uptake rates and glucose uptake rate for Y. lipolytica were estimated from specific growth rates and biomass yields. Biomass yield from glucose for Y. lipolytica was estimated from the carbon yield reported.*

Parameter	*E. coli*	*Y. lipolytica*	Reference
q_G (h^{-1})	1	0.49	(Losoi et al. 2022; L. Chen et al. 2021)
q_A (h^{-1})	0.85	0.4729	(Kotte et al. 2014; Gao et al. 2020)
Y_{XG} (g g^{-1})	0.5	0.49	(Losoi et al. 2022; Ochoa-Estopier et al. 2014)
Y_{XA} (g g^{-1})	0.4	0.37	(B. Xu et al. 1999; Gao et al. 2020)
q_d (g g^{-1} h^{-1})	0.025	0.025	(Losoi et al. 2022)
k_La (h^{-1})	180	180	(Losoi et al. 2022)
Y_{OG} (g g^{-1})	1.067	1.067	Stoichiometry
Y_{OA} (g g^{-1})	1.066	1.066	Stoichiometry
T_x (h)	2.5	2.5	(Morchain et al. 2013; Losoi et al. 2022)
T_s (h)	0.025	0.025	(Morchain et al. 2014; Losoi et al. 2022)
O^* (mg L^{-1})	12.69	12.69	(Losoi et al. 2022)
K_{sG} (g L^{-1})	0.025	0.115-3.6	(Losoi et al. 2022; Robak et al. 2002)
K_{sA} (g L^{-1})	0.5	0.01	(Kotte et al. 2014; Béligon et al. 2015)
K_{iA} (g L^{-1})	0.47	0.79	(Pinhal et al. 2019; Konzock et al. 2021)
K_{iG} (g L^{-1})	0.1	–	(Pigou et al. 2015)
K_O (mg L^{-1})	0.1	0.1	(Morchain et al. 2013)

4.3.3 Compartment model basis

The physical parameters for the model are adapted from the reactor used by Cui et al. (1996) with a total effective volume of the vessel being 22 m^3 and are shown in Table 4.4.

Table 4.4. *Hydrodynamic parameters for the stirred-tank reactor. T, reactor diameter; V, volume; H, reactor height; D, impeller diameter; N, stirrer speed; K_p, impeller discharge coefficient; N_E, axial flow coefficient.*

R (m)	V (m^3)	H (m)	D (m)	B (rpm)	K_p	ϵ	Reference
2.09	23.8	6.96	0.70	115	1.5	0.539	(Cui et al. 1996; Losoi et al. 2022)

Mechanical impellers create upward and downward circulation flow loops with the rates of the Equation 2.2 (Vrábel et al. 1999; Cui et al. 1996). In this model, nested loops similar to the work by Losoi et al. (2022) were used. The flow equations and magnitudes also follow the ones provided in the mentioned article. The total circulation flow was divided by the number of nested loops. The same circular flow was set across the tangential layers and divided by the number of nested tangential loops. The stagnant zone on top was

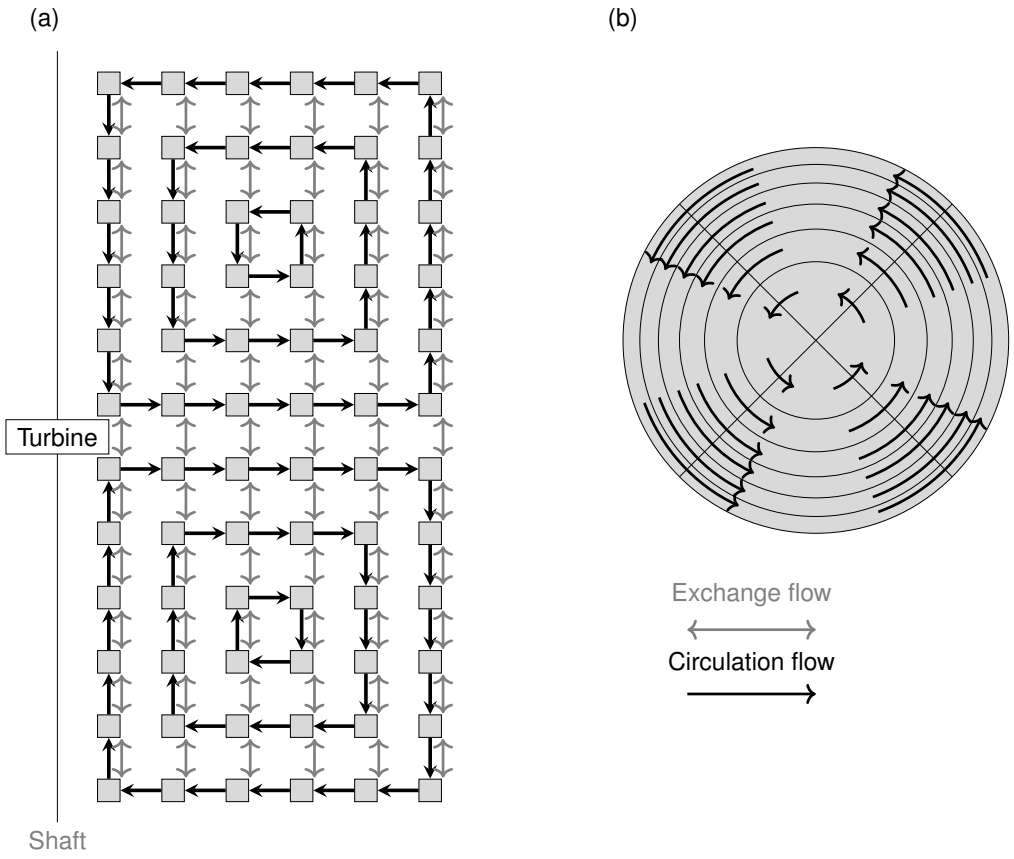

Figure 4.1. *Configuration of the compartment model with flow patterns. (a) One block of two nested loop networks around the turbine. A similar pattern is replicated four times around each turbine, with a single network at the stagnant zone on the top. In total, there are 324 compartments in one tangential layer. (b) Cross-section of the compartment model from the top. The reactor was divided into 4 tangential layers.*

modeled with a single nested loop network, and all the circulation flows were assumed to be one-eighth of the rest of the reactor's circulation flow rates. Exchange flows were modeled with an equation

$$Q_L = \epsilon N D^3, \tag{4.7}$$

where the exchange flow constant ϵ was fitted to match the reactor mixing times by Losoi et al (2022). The exchange flow was divided within the cross-sections of the model. The model consists of 54 axial, 6 radial, and 6 tangential dimensions, yielding a total of 1296 compartments. The patterns of exchange and circulation flows are shown in Figure 4.1. The feeding point was set into a single compartment at the top of the reactor.

The reactor was modeled as a single-phase system as the aeration only has a low influence on the mixing in a multi-impeller system (Vrábel et al. 1999). The assumption of sufficient oxygen in the liquid phase to enable aerobic growth was used, and the transfer

equation

$$\frac{dO}{dt} = k_L a(O^* - O) \tag{4.8}$$

determined the oxygen supply rate. $k_L a$ (h^{-1}) is the transfer coefficient depending on the mass coefficient and the sizes of gas bubbles, *O* is the local dissolved oxygen (g L^{-1}) and O^* is the oxygen solubility (g L^{-1}) (Garcia-Ochoa et al. 2009). The oxygen demand ratios for aerobic growth on glucose and acetate were estimated from the stoichiometric energy-generating equations

$$\mathrm{C_6H_{12}O_6} + 6\mathrm{O_2} \rightarrow 6\mathrm{HCO_3^-} + 6\mathrm{H^+}, \tag{4.9}$$

$$\mathrm{CH_3COOH} + 2\mathrm{O_2} \rightarrow 2\mathrm{HCO_3^-} + 2\mathrm{H^+}. \tag{4.10}$$

The coefficients for oxygen usage (g g^{-1}), Y_{OG} and Y_{OA}, obtained from the stoichiometric equations, were then integrated with the oxygen uptake rate to get the consumption

$$r_O = Y_{OG}\frac{O}{O + K_O}r_G + Y_{OA}\frac{O}{O + K_O}r_A, \tag{4.11}$$

where K_O is the oxygen affinity constant (g L^{-1}).

4.3.4 Palmitic acid, cetyl alcohol, and pentadecane productivities

The production of fatty acids, fatty alcohols, and alkanes was determined by yield coefficients extracted from the stoichiometric equations. The simplified net reaction for palmitic acid production is

$$8\mathrm{Acetyl} - \mathrm{CoA} + 7\mathrm{ATP} + 14\mathrm{NADPH} \rightarrow \mathrm{C_{16}H_{32}O_2} + 6\mathrm{H_2O}. \tag{4.12}$$

All the acetate is assumed to be directed towards ATP and acetyl-CoA production for the fatty acid synthesis, and the glucose is used for NADPH in oxidative pentose phosphate pathway (oxPPP), similarly to experiments by Park et al. (2019). This way the the carbon loss is minimized by limiting the formation of $\mathrm{CO_2}$. The equation for producing palmitic acid from glucose and acetate with these restrictions is

$$11.04\mathrm{CH_3COOH} + 1.17\mathrm{C_6H_{12}O_6} + 6.04\mathrm{O_2} \rightarrow \mathrm{C_{16}H_{32}O_2} + 13.04\mathrm{CO_2} + 13.04\mathrm{H_2O}. \tag{4.13}$$

The stoichiometry analysis is shown in A.1.1 and the calculated requirement for glucose

based on the Equation 4.13 is 0.24 g glucose g^{-1} substrates. Similarly to palmitic acid production, the cetyl alcohol and pentadecane productions were calculated

$$11.17\mathrm{CH_3COOH} + 1.33\mathrm{C_6H_{12}O_6} + 6.33\mathrm{O_2} \rightarrow \mathrm{C_{16}H_{34}O} + 14.33\mathrm{CO_2} + 13.33\mathrm{H_2O}, \tag{4.14}$$

$$11.17\mathrm{CH_3COOH} + 1.33\mathrm{C_6H_{12}O_6} + 6.83\mathrm{O_2} \rightarrow \mathrm{C_{15}H_{32}} + 14.33\mathrm{CO_2} + \mathrm{CO} + 14.33\mathrm{H_2O}. \tag{4.15}$$

Since the certain pathways used for alkane decarbonylation in bacteria and yeasts are largely unknown, an assumption was made that the step released carbon monoxide and required NADPH. The precise procedure to get these equations is again described in A.1.1. For both cetyl alcohol and pentadecane, the ideal ratio of substrates was 0.26 g glucose g^{-1} substrates. These stoichiometric equations were also used to get the maximal theoretical product yields. The maximum amount of lipids that are free fatty acids or storage lipids like WEs, PHAs, or TAGs were taken from the literature and compiled in table A.1. Also, the percentages for long-chain fatty acids were estimated based on existing studies.

The product synthesis was simulated on ADP1 and *C. oleaginosus* fermentations as these are the only microbes from the selection producing a significant amount of long-chained storage compounds. In the models, all of the long-chain FAs were treated as palmitic acid. In reality, longer-chained products would require more NADPH due to the fatty acid synthesis cycles, and the yield of these products from acetate and glucose would be slightly lower compared to the one presented in Equation 4.13. To obtain the actual palmitic acid yield from the acetate, the non-lipid biomass yields were determined. For the elemental formula of *C. oleaginosus*, the average yeast composition was used, and the average bacterial composition was used for ADP1 (Von Stockar et al. 1999). The stoichiometric equation for non-lipid biomass of bacteria species, with the ideal substrate ratio presented in the Equation 4.13, is

$$11.04\mathrm{CH_3COOH} + 1.17\mathrm{C_6H_{12}O_6} \rightarrow 10.52\mathrm{CH_{1.66}O_{0.41}N_{0.21}} + 18.58\mathrm{CO_2}. \tag{4.16}$$

Reaction was built based on the estimation that the biomass yield per available electron is 3.14 g DCW, and the ATP usage of 105 mmol $\mathrm{g^{-1}\,DCW}$, which has been calculated for yeasts, was used (Shuler 1992; Verduyn 1992; DeLisa et al. 2017; Bansal-Mutalik et al. 2011). As the yields in the reaction depend solely on the available electrons, only carbon

balance is fulfilled, and the intermediates or other by-products are not considered. With similar methods, the non-lipid yield for oleaginous yeasts was calculated

$$11.04\mathrm{CH_3COOH} + 1.17\mathrm{C_6H_{12}O_6} \rightarrow 10.36\mathrm{CH_{1.65}O_{0.54}N_{0.14}} + 18.74\mathrm{CO_2}. \quad (4.17)$$

Therefore, the non-lipid biomass yield on acetate while supplied alongside glucose for bacteria was 0.415 g g^{-1} acetate used and for the yeasts, 0.410 g g^{-1} acetate used. The energy yields from acetate and glucose were assumed to be similar for both yeasts and bacteria (Hu et al. 2016). It has to be noted that even as these values are presented as biomass produced per acetate, they are not actual conversion efficiencies for acetate. The values were extracted in these forms to fit the volumetric productivity simulations. The precise procedure to acquire the equations for non-lipid biomass is given in A.1.2. The actual palmitic acid yield on acetate (g g^{-1}) for each microbial process was then calculated as

$$Y_{PA} = \alpha \frac{L}{\frac{L}{Y_{PA}^{\max}} + \frac{100-L}{Y_{NA}^{\max}}}, \quad (4.18)$$

where α is the proportion of long-chained FAs, L is the extractable lipid content, $Y_{PA}^{\max}$ is the theoretical maximum of lipid yield from acetate and $Y_{NA}^{\max}$ is the theoretical maximum of non-lipid biomass yield from acetate. For the productivity simulations, inhibition constants were set to zero. Since both ADP1 and *C. oleaginosus* can tolerate very high acetate concentrations, the effect of inhibition in the continuous phase of the fed-batch process would be negligible in most parts of the reactor. The affinity constants and adaptation rates were assumed to be the same as for *E. coli*. The rest of the parameters used are compiled in Table 4.5.

The largest theoretical instantaneous production rate of palmitic acid was then determined as

$$r_{Pmax} = Y_{PA} min(r_A, \frac{r_G}{0.32}). \quad (4.19)$$

Dividing r_G by 0.32 was due to the necessary glucose, which allowed acetate to be used solely for the palmitic acid carbon skeleton. The minimum was taken to determine if the NADPH production or the carbon skeleton and energy production was the limiting factor. Analogous steps were replicated for the productivities of fatty alcohol and alkane. Here, it was assumed that after one substrate limits the optimal fatty acid synthesis, the rest of the substrate was not used for the production pathway.

Table 4.5. *Uptake rates, yields, and growth parameters of A. baylyi ADP1 and C. oleaginosus.*

Parameter	ADP1	*C. oleaginosus*	Reference
q_A (g g^{-1} h^{-1})	0.33	0.14	This study
q_G (g g^{-1} h^{-1})	0.514	0.302	(M. Kannisto et al. 2014; Seo et al. 2013)
Y_{XA} (g g^{-1})	0.34	0.20	This study
Y_{XG} (g g^{-1})	0.35	0.43	(M. Kannisto et al. 2014; Christophe et al. 2012)
$Y_{NA}^{\max}$ (g g^{-1})	0.415	0.410	Stoichiometry
$Y_{PA}^{\max}$ (g g^{-1})	0.39	0.39	Stoichiometry
$Y_{CA}^{\max}$ (g g^{-1})	0.36	0.36	Stoichiometry
$Y_{DA}^{\max}$ (g g^{-1})	0.32	0.32	Stoichiometry
L (%)	10	73	(M. S. Kannisto et al. 2015; Gong et al. 2015)
α (%)	95	95	(Barney et al. 2012; Gong et al. 2015)

4.3.5 Numerical simulations

All reactor simulations were performed with Python 3.11 language. Numpy version 2.2.1 (Harris et al. 2020) and Scipy version 1.15.0 (Virtanen et al. 2020) were used for the calculations. Matplotlib version 3.9.1 (Hunter 2007) was used for the visualization of the results.

The fed-batches were simulated during the phase of constant feeding rates. Substrate concentrations were solved from a system of nonlinear equations. Biomass was initially distributed evenly between all the growth and uptake classes. Total biomass was chosen based on the microbial host used. After the uptake class distributions were solved, oxygen uptake and volumetric productivities of palmitic acid, cetyl alcohol, and pentadecane were calculated from the substrate uptake class averages in each compartment.

5. RESULTS

5.1 Findings from literature, FBA results and the theoretical yields

The information compiled from the literature and previous studies in Chapter 4 is summarized in Table 5.3. Since only microbes relevant to the target objective were selected, their comparative attributes are defined relative to each other. Notably, majority of the microbes meet several of the requirements. The acetate tolerance is high for every host, excluding *E. coli*. The genetic tractability defined based on models and engineering, is on the highest level for *E. coli*, *P. putida* and due to recent advancements also for *Y. lipolytica*. ADP1 and *P. putida* have the greatest tolerance to the inhibitors found in industrial streams, since the rest of the species are either sensitive to high shifts in pH or do not possess the capability to metabolize diverse carbon compounds. Even though wax esters, polyhydroxyalkanoates, and triacylglycerols are all acyl-CoA derivatives, only ADP1, *Y. lipolytica* and *C. oleaginosus* produces significant amounts of compounds with long-chain fatty acids.

Table 5.1. *Comparison of microbial traits based on literature review. WE, wax esters; PHA, polyhydroxyalkanoates; TAG, triacylglycerides; MCFA, medium-chain fatty acids; AA, amino acids.*

Microbe	Acetate Utilization	Acetate Tolerance	Model Availability	Engineering Potential	Product	Robustness
E. coli	Sole & Diauxic	Low	High	High	Mixture	Low
A. baylyi ADP1	Sole & Co-substrate	Very High	Moderate-High	Moderate-High	WE	High
P. putida	Sole & Co-substrate	High	High	High	PHA	High
Y. lipolytica	Sole & Diauxic	High	High	High	TAG	Moderate
C. glutamicum	Sole & Co-substrate	High	High	Moderate-High	AA	Moderate
C. oleaginosus	Sole & Co-substrate	Very High	Moderate	Moderate	TAG	Moderate-High
C. kluyveri	Co-substrate	High	Moderate	Low	MCFA	Moderate
C. necator	Sole & Co-substrate	High	Moderate-High	High	PHA	Moderate-High

The results presented with the first two dimensions of the MCA are shown in Figure 5.1. Dimension 1 explains 24.9% of the variance between microbes and dimension 2 explains 23.1% of the variance. The non-distinguishable product mixture, low robustness, and low acetate tolerance contribute mostly to positive values on the first dimension. The highest negative impact comes from low engineering potential, MCFA production, and moderate model availability. For the second dimension, positive values are affected mainly by the production of MCFAs, low engineering potential, and the ability to use acetate only as a co-substrate. Wax ester synthesis, moderately high model availability, as well as high acetate tolerance, contribute mostly to negative values. The further the microbes are from each other, the more distinct they are. These two dimensions create noticeable clusters of microbes on the basis of the acetate utilization mechanisms.

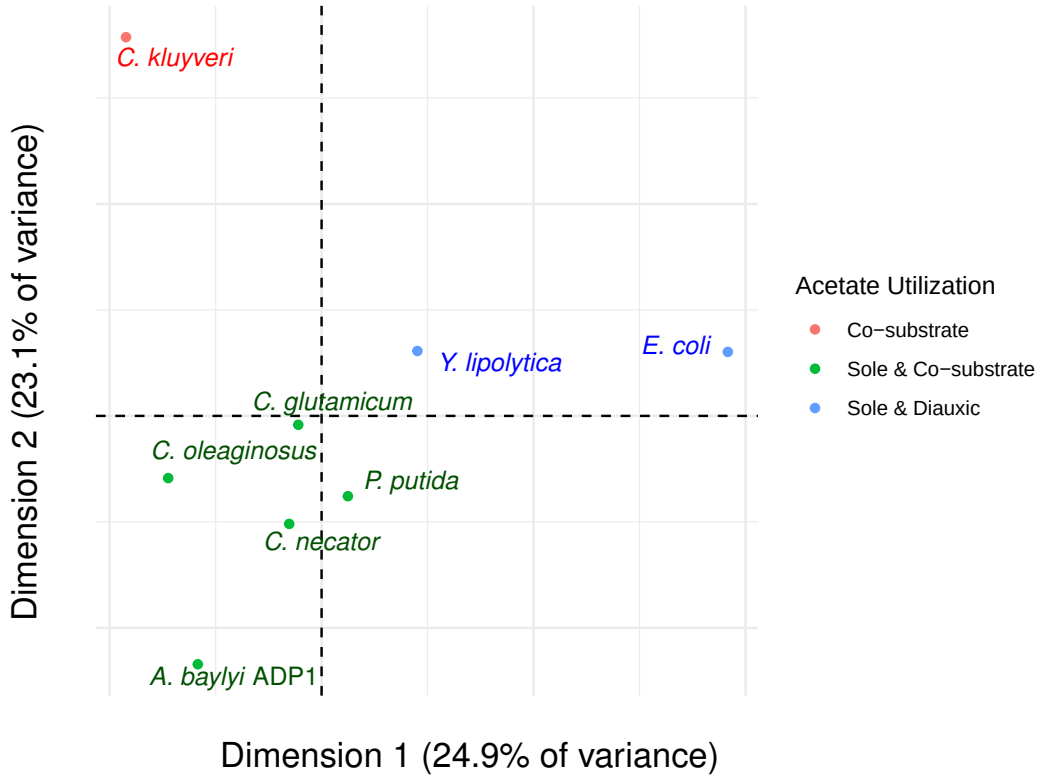

Figure 5.1. *MCA results presented by the first two dimensions. The combined effect of all six major attributes is presented. Together, they explain 48.0% of the variability. Microbes are colored based on the possible acetate utilization mechanisms.*

The third dimension of the MCA explains 16.4% of the variability, so plotting it against the first two dimensions lifts the total explained variability to 64.4%. Visualization is shown in Figure 5.2. The moderate engineering potential has the most significant effect on the

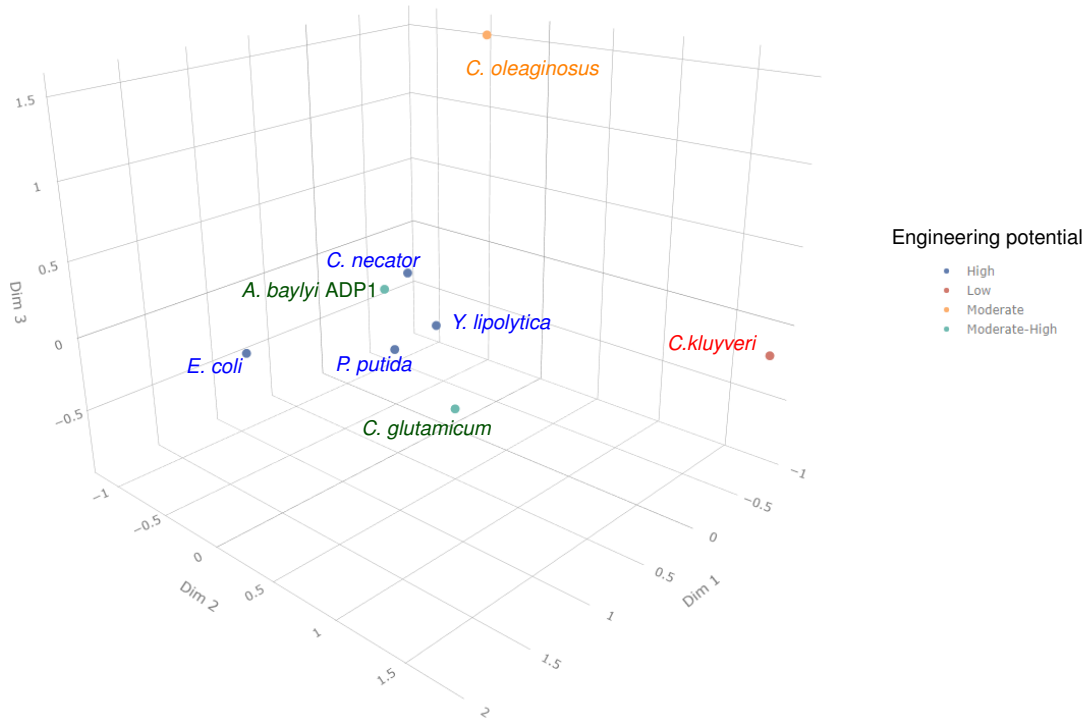

Figure 5.2. *MCA results presented by the first three dimensions. Together, they explain 64.4% of the variability. Each species is colored by its engineering potential level.*

positive values in dimension three. Amino-acid production and moderate-high engineering potential have the highest effect on the negative values. Adding the third dimension helps to distinguish the differences between microbes that are located near the origin in Figure 5.1.

Attributes that correlate strongly with each other are engineering potential and model availability. In addition, microbes that have high tolerance towards acetate tend to have higher tolerance towards other hydrolysate inhibitors. *E. coli* with low robustness has non-uniform product compositions, while free MCFA production is observed only in *C. kluyveri* with low engineering potential. However, since these traits were exhibited by only a single microbe each, it cannot be concluded that they are inherently linked. Rather, these production routes simply do not appear in microbes with higher robustness or greater engineering potential. The visual representation of the attribute correlations and the contributions to the MCA dimensions can be found in Figures A.1 and A.2. From the visualized results, it can be noted that the preferred production pathway and the carbon catabolic repression are the attributes that cause the major distinction between the microbes. The majority of the desired attributes are strongly exhibited at the bottom left corner of the two-dimensional representation.

The maximum theoretical yields for palmitic acid, cetyl alcohol, and pentadecane are shown in Table 5.2. The yields are relative to the combined amount of acetate and glucose in optimal ratios according to the stoichiometric equations in the Section 4.3.4. These

results assume that all of the substrate is directed into lipid production and the portion of non-lipid biomass is neglected.

Table 5.2. *Maximal theoretical yields from co-feeding acetate and glucose: Carbon and mass yield of palmitic acid, cetyl alcohol, and pentadecane.*

Product	**Carbon yield (C/C)**	**Mass yield (g g^{-1})**
Palmitic acid ($C_{16}H_{32}O_2$)	0.55	0.29
Cetyl alcohol ($C_{16}H_{34}O$)	0.53	0.27
Pentadecane ($C_{15}H_{32}$)	0.49	0.23

The theoretical palmitic acid yields and growth rates on acetate as sole carbon source, according to FBA, are shown in Table 5.3. ADP1 has the highest palmitic acid yield of 55% C/C-substrate and *P. putida* has the highest growth rate of 0.46 h^{-1}. Of the microbes that can grow on acetate and utilize fatty acid synthase, *C. glutamicum* performed the worst in both categories. Since *C. necator* does not utilize FA synthase and directs acetyl-CoA to the PHB pathway, the palmitic acid yield was 0. For comparison, the PHB yield from acetate was calculated, which was 0.60. *C. kluyveri* requires ethanol to grow and also does not possess the synthesis of long fatty acids.

Table 5.3. *Comparison of microbial traits based on the FBA: Carbon yield of palmitic acid from acetate and growth rate on acetate (1 g/gCDW/h^{-1}) as the sole carbon source. Model optimization for C. oleaginosus with acetate as the sole carbon source leads to an infeasible solution.*

Microbe	**C-yield (palmitate/acetate)**	**Specific growth rate (h^{-1})**
E. coli	0.41	0.36
P. putida	0.55	0.46
A. baylyi ADP1	0.56	0.41
Y. lipolytica	0.53	0.45
C. glutamicum	0.16	0.13
C. necator	0.00	0.39
C. kluyveri	0.00	0.00

C. oleaginous can utilize acetate as a sole carbon source, but the model with only acetate was infeasible. This might be due to missing reactions, so the steady-state requirement of all metabolites can not be satisfied. However, since the metabolic model was built using the *Y. lipolytica* model as a scaffold and considering the similarities between species, values close to those of *Y. lipolytica* could be expected.

5.2 Batch cultures

The results of microbial growth in 50 mL batch cultivations are shown in Figure 5.3. The highest measured OD_{600} was 6.4 achieved by *C. oleaginosus* followed by *P. putida* KT2440 and ADP1 reaching OD_{600} values of 4.7 and 3.7, respectively. *C. glutamicum* and *E. coli* XL1-blue showed only slight growth. However, *C. glutamicum* alongside *C. oleaginosus* was the only microbe that did not seem to exhibit any lag phase, while the other strains reached the highest exponential growth between 10 and 17 hours. The first 15 hours of growth for *P. putida*, *C. glutamicum* and *C. oleaginosus* is presented in Figure A.3. *C. necator* did not show any growth during the 42 hours.

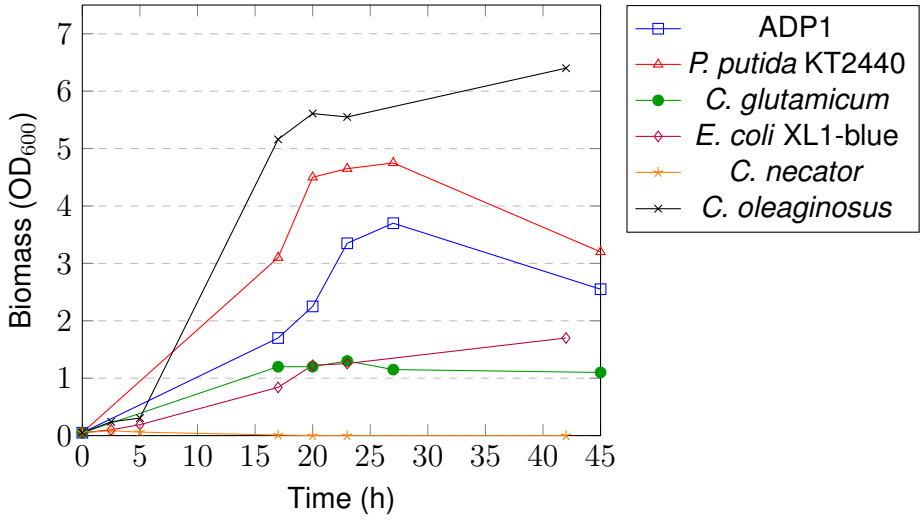

Figure 5.3. *Biomass production in batch cultivations. LB-media supplemented with 100 mM Na-acetate was used. The OD_{600} data is calculated as the average of two parallel replicates. Standard errors are not presented due to the clarity.*

The substrate consumptions measured by HPLC are presented in Figure 5.4. *P. putida* consumed acetate the fastest, and by 26 h there was no substrate left. ADP1 had used 92% of the available acetate during the 26 hours. *C. oleaginosus* was the third microbe that consumed all the available acetate in the time period of these cultivations. Compared to *P. putida* and ADP1, the uptake rate was slower and steadier, as there was no lag phase and the faster consumption began immediately. *E. coli* did not consume any acetate until 21 h, and there was still 24% of the acetate left at the end of the cultivation. As was seen also from the growth curves, *C. glutamicum* consumed part of the acetate at the beginning but then the uptake halted and the acetate concentration remained between 80 and 85 mM for the rest of the cultivation. *C. necator* did not exhibit any acetate uptake. As *C. necator* did not remove the weak acids from the medium, the pH at the end was slightly below neutral. In contrast, cultures of *E. coli*, *P. putida*, and *C. glutamicum* showed a moderate increase in pH to between 7 and 8, while the pH in cultures of ADP1 and *C. oleaginosus* rose more substantially, reaching values between 8 and 9.

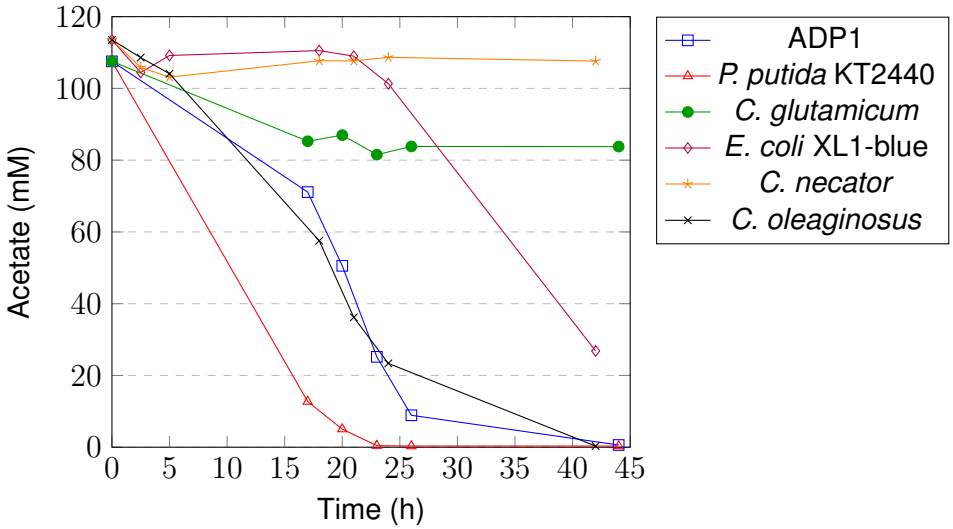

Figure 5.4. *Acetate consumption in batch cultivations. Acetate concentrations at different data points were measured using HPLC. LB-media supplemented with 100 mM Na-acetate was used. The concentrations are calculated as the averages of two parallel replicates. Standard errors are not presented due to the clarity.*

The maximum specific acetate uptake rates and instantaneous biomass yields are shown in Table 5.4. The biomass yields on the substrate were calculated from the exponential growth phases to diminish the effect of the adaptation phase and cell deaths. Other media components still affect the yield values. The highest uptake rate was 0.43 h^{-1} by *P. putida*. The highest instantaneous biomass yield on acetate was 0.62 g g^{-1} by *C. glutamicum*. All parallel measurements of OD_{600} and acetate concentrations followed the same pattern and there were no outliers.

Table 5.4. *Maximal specific acetate uptake rates during the batch cultivations, and instantaneous biomass yields calculated from the exponential growth phases. Values are taken as the averages from two independent replicates.*

Microbe	**Specific acetate uptake rate (h^{-1})**	**Biomass yield (g g^{-1})**
E. coli	0.21	0.07
P. putida	0.43	0.29
C. oleaginosus	0.14	0.20
A. baylyi ADP1	0.33	0.34
C. glutamicum	0.28	0.62
C. necator	0	0

5.3 Large-scale co-feeding simulations

The combined effects of carbon catabolic repression, acetate inhibition, mixing, and cell adaptation in large-scale fed-batch simulations are shown in Figures 5.5 and 5.6. *E. coli* culture has the highest uptake rates on top of the reactor for both substrates with all three feeding combinations. The difference between the uptake ratios of acetate and glucose in different parts of the reactor becomes more distinguishable with higher glucose feeding rates. At the top of the reactor, there is an abundance of glucose compared to acetate, and at the bottom, vice versa. When glucose is added in conjunction with 3 g L^{-1} h^{-1} of acetate with feeding rates 0.75, 1.0 or 1.25 g L^{-1} h^{-1}, the normalized deviation around the ideal uptake ratio (0.24 g glucose g^{-1} substrates) gets values 0.32, 0.41 and 0.45, respectively.

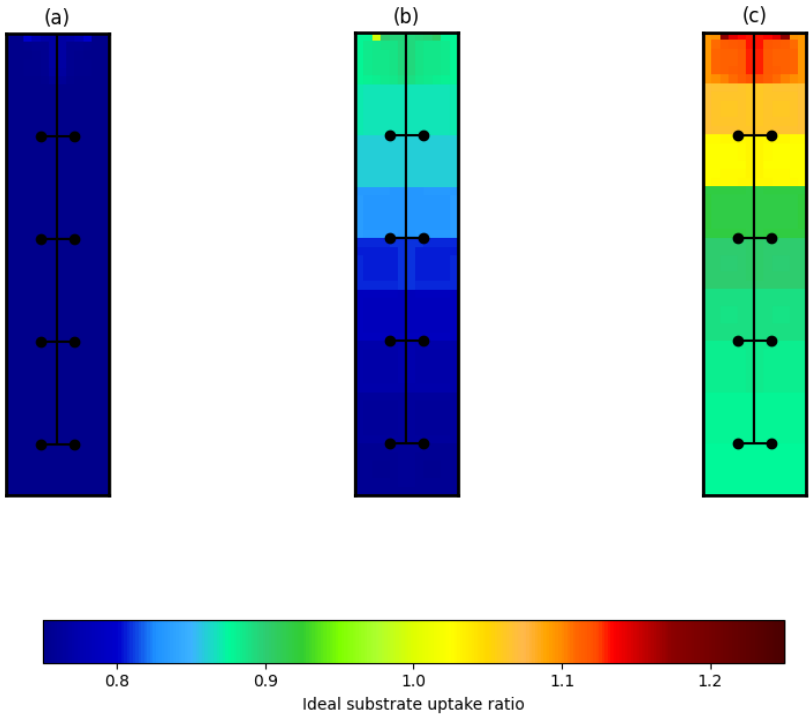

Figure 5.5. *Ratio of glucose and acetate uptake class averages for E. coli in large-scale fed-batch simulation. Biomass concentration was set to 20 g L^{-1}. Values are normalized around the optimal 0.24 g glucose g^{-1} substrates for palmitic acid production. Values greater than 1 indicate excess glucose and values less than 1 indicate excess acetate. Acetate feeding rate is fixed to 3.0 g L^{-1} h^{-1}. (a) Glucose feeding rate 0.75 g L^{-1} h^{-1}. (b) Glucose feeding rate 1.0 g L^{-1} h^{-1}. (c) Glucose feeding rate 1.25 g L^{-1} h^{-1}.*

For *Y. lipolytica* the difference between the ratios also increases with higher glucose feeding rates. Normalized deviations around the ideal uptake ratios, in order from the lowest glucose feeding rate to the highest, are 0.22, 0.24, and 0.28. In contrast to *E. coli*, there is a lack of glucose at the top of the reactor. Although the deviation between the uptake ratios is more modest than in the case of *E. coli*, the zones with either too high or too

low glucose are more discrete. In *E. coli* simulations, the change between the zones with different uptake combinations happens gradually.

The heterogeneity of the dissolved oxygen concentration in the *E. coli* and *Y. lipolytica* fed-batch simulations is shown in Figure 5.7. For both cases, oxygen is lowest at the top of the reactor, where the growth is the fastest due to the highest substrate concentrations. In *E. coli* simulation, the concentration gets gradually higher towards the bottom of the reactor, whereas in *Y. lipolytica* simulation, there are two distinct zones, with oxygen concentration staying close to constant in the bottom half. This means that the combined uptake of acetate and glucose for *E. coli* is more evenly distributed around the reactor.

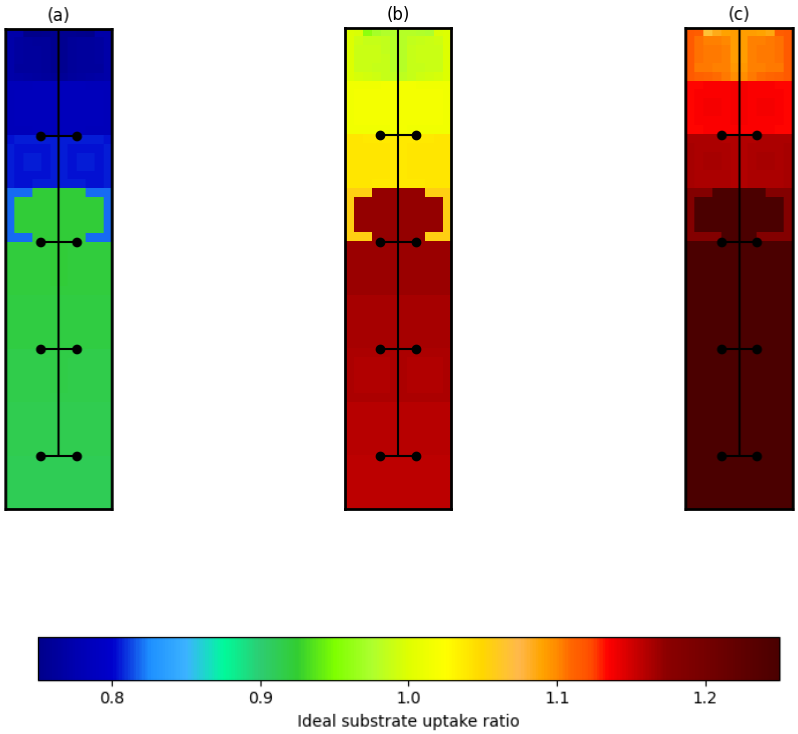

Figure 5.6. *Ratio of glucose and acetate uptake class averages for Y. lipolytica in large-scale fed-batch simulation. Biomass concentration of 20 g L^{-1} h^{-1} was used. Values are normalized around the optimal 0.24 g glucose g^{-1} substrates for palmitic acid production. Values greater than 1 indicate excess glucose and values less than 1 indicate excess acetate. Acetate feeding rate is fixed to 3.0 g L^{-1} h^{-1}. (a) Glucose feeding rate 0.75 g L^{-1} h^{-1}. (b) Glucose feeding rate 1.0 g L^{-1} h^{-1}. (c) Glucose feeding rate 1.25 g L^{-1} h^{-1}.*

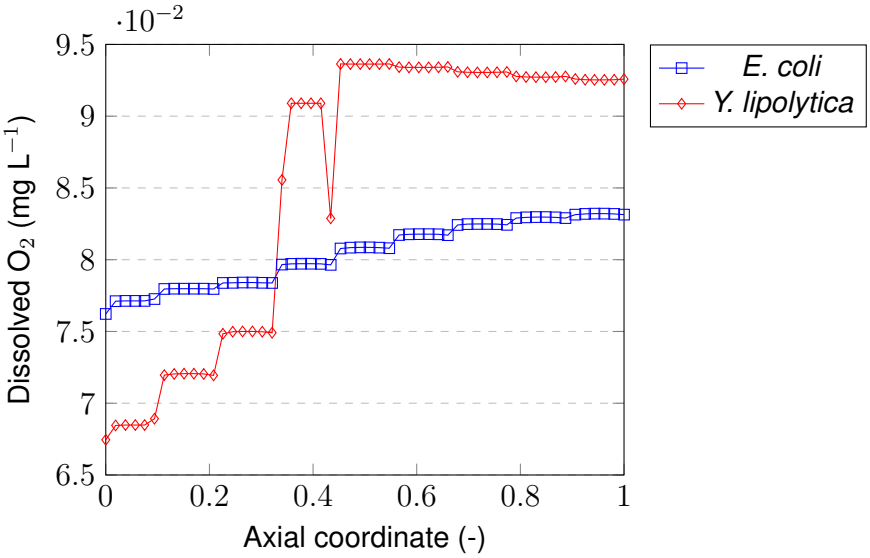

Figure 5.7. *Oxygen profile in large-scale fed-batch reactor simulations. Biomass concentration was set to 20 g L^{-1}. Values represent the average on an axial position, with 0 being at the top of the reactor. Acetate feeding rate of 3.0 g L^{-1} h^{-1} and glucose feeding rate of 1.0 g L^{-1} h^{-1} were used.*

The volumetric productivities for palmitic acid, cetyl alcohol, and pentadecane in ADP1 large-scale simulation are shown in Figure 5.8. For all of the compounds, the highest productivities are achieved at the top of the reactor, close to the feeding regime. The change in productivity is greater at the top, and the curves flatten toward the bottom. The productivity is at every part of the reactor highest for the palmitic acid with value at top being 0.081 g L^{-1} h^{-1}. The volumetric productivity at the bottom region is approximately 89% of the productivity at the top. For cetyl alcohol and pentadecane the productivities at the top are 0.080 g L^{-1} h^{-1} and 0.079 g L^{-1} h^{-1}, respectively. For both the values at the bottom drop down to 80% of the maximum.

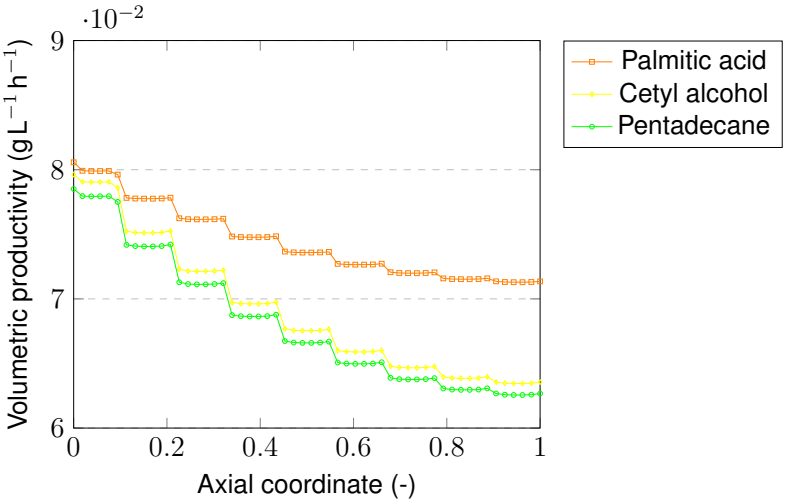

Figure 5.8. *Volumetric productivities in large-scale fed-batch reactor simulations for ADP1. Biomass concentration was set to 30 g L^{-1}. Values represent the average on an axial position, with 0 being at the top of the reactor. Acetate feeding rate of 1.5 g L^{-1} h^{-1} and glucose feeding rate of 0.5 g L^{-1} h^{-1} were used.*

For *C. oleaginosus*, the simulated results follow those of ADP1 in the sense that the highest productivities are reached at the top. However, for each compound, there is a more sudden drop in productivity followed by a small spike around the middle of the reactor's axial dimension. These results are shown in Figure 5.9. Cetyl alcohol production for *C. oleaginosus* at the bottom of the reactor reaches average values of 78% of 0.50 g L^{-1} h^{-1} at the top. Fatty acid and alkane productivities at the bottom of the reactor are equal to 76% of the productivities achieved at the top. For palmitic acid, the maximum productivity is 0.50 g L^{-1} h^{-1} and for pentadecane 0.47 g L^{-1} h^{-1}. Another difference between the compounds is that for palmitic acid, the change is gradual at the top, but then a sudden drop halfway through is more drastic. Cetyl alcohol and pentadecane productivities have more distinct zones already in the top region.

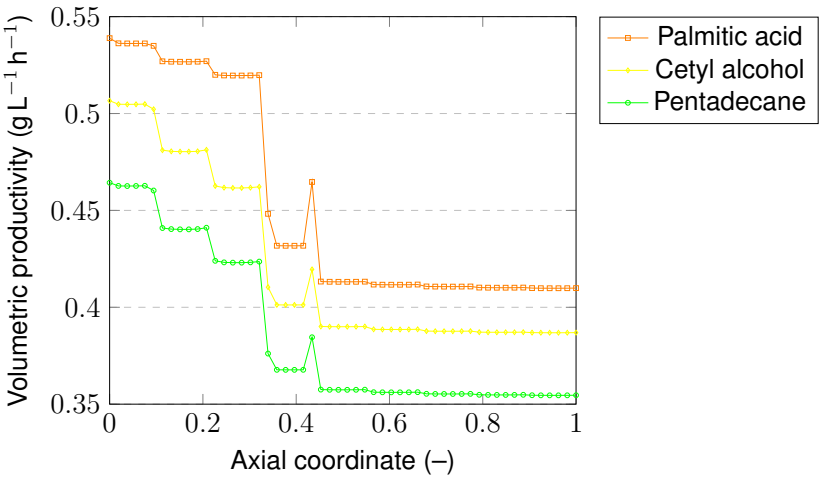

Figure 5.9. *Volumetric productivities in large-scale fed-batch reactor simulations for C. oleaginosus. Biomass concentration was set to 50 g L^{-1}. Values represent the average on an axial position, with 0 being at the top of the reactor. Acetate feeding rate of 1.5 g L^{-1} h^{-1} and glucose feeding rate of 0.5 g L^{-1} h^{-1} were used.*

6. DISCUSSION

6.1 Challenges with the media components and comparability with the real feeds

As LB is a rich medium, it can not be concluded how well each species uses acetate as a sole carbon source just based on the results from the batch cultivations. From Figures 5.3 it is clear that *E. coli* shows strong diauxia when other growth factors are present alongside acetate. For the other strains, it is difficult to make a precise distinction as to how much the growth was affected by LB components. *C. glutamicums* instantaneous yield value is likely highly bloated due to the co-utilization of the acetate with yeast extract. The FBA results suggest that with acetate as the sole carbon source, *C. glutamicum* should have a significantly lower growth rate compared to other used strains. ADP1 and *P. putida* both had similar growth patterns with each other. *P. putida* consumed acetate slightly faster and reached a higher total OD_{600}. The higher instantaneous biomass yield from acetate by ADP1 during the exponential growth can be explained by two factors. *P. putida* is presumably less efficient in utilizing tryptone and yeast extract at high acetate uptake rates. Another reason is that OD_{600} is not a fully compatible measurement between the different strains. Light refraction is affected by cell morphology and size, and does not linearly correlate with viable cell count (Fukuda 2023). Growth could have also been significantly affected by the precultures, particularly in the case of *C. oleaginosus*. The added glucose boosted growth, and it is known that the lag-phase in the new culture is generally shorter if the inoculum contains cells in exponential phase (Oehlenschläger et al. 2024; Sandoval-Espinola et al. 2015). On the other hand, in *S. cerevisiae* cultivations, the inoculants from the early stationary phase have been more tolerant towards inhibitory compounds at low pH (Narayanan et al. 2017). Since *C. oleaginosus* can tolerate much higher concentrations of acetate than 100 mM, the net effect of higher growth in precultivations was likely positive.

The effects of non-defined media lead to elevated pH in most of the cultures. Tryptone acted as the main nitrogen source and ammonia release caused the alkalinity, which explains the neutral pH in *C. necator* cultures. As *C. glutamicum* tolerates high acetate concentrations and can grow on LB supplemented with glucose (C. Chen et al. 2015), pH rising due to the lack of buffer might have been the cause for the sudden stop of acetate

consumption. Slightly higher pH of ADP1 and *C. oleaginosus* cultures compared to the *E. coli* can be due to the effects of acidic secretion. *E. coli* produces lactate and acetate, whereas ADP1 and *C. oleaginosus* accumulate high amounts of lipids (M. S. Kannisto et al. 2015; Gong et al. 2015). *P. putida* also accumulates a lot of PHAs (Yang et al. 2019). Therefore, the higher pH compared to ADP1 can simply be due to the higher growth and nitrogen requirement.

The lack of growth and acetate consumption in *C. necator* cultures indicate that the instant addition of 100 mM acetate at the start of the cultivation is toxic or that the lag-phase exceeds 42 hours. As seen in previous studies, *C. necator* tolerates higher acetate concentrations than 100 mM, and in minimal media, the final pH was 6 (Amer et al. 2023). This suggests that the lack of buffer in the LB medium is unlikely to be the cause of the problem. As OD_{600} increased slightly at the beginning of the cultivations, it can also be interpreted that the cells remained viable for a time. Therefore, longer cultivation times may be required to reliably make conclusions of *C. necators* acetate tolerance in undefined media.

The real SCFA-rich feeds from the industry would be complex, similarly to the LB, but the biomass yields would differ. First of all, the low amounts of phosphorus and nitrogen would limit the growth. Whereas LB is supplemented with tryptone, pretreatments such as MES and acid fermentation have depleted the majority of nutrients in industrial feeds. Nitrogen-depleted environments would probably enhance lipogenesis to some degree, but total productivity and titer would suffer if not enough biomass was produced. The second effect would come from the inhibitory compounds. The three best growing microbes have also shown strong tolerance, so the performance would depend on the source of the feeds. The high lignin content in the original side streams would lead to more aromatic and phenolic residuals, which *C. oleaginosus*, *P. putida* and ADP1 all can metabolize to some degree. If the original side streams, however, were rich in cellulose and hemicellulose, there would be a higher chance of furfural and HMF residuals. This could shift the higher yields in favor of *P. putida* and ADP1. In real feeds, SCFAs would also mainly be in the undissociated form, and diffusion through membranes would significantly lower the intracellular pH. Therefore, to maintain the tolerance in these real samples, active control of pH would be a prerequisite. In larger scales, an automated control loop with alkali and acid pumps is the typical solution. In addition to traditional acid and alkali pumps, control of pH by controlling the sparging of air and CO_2 is viable, at least in small-scale processes (Hoshan et al. 2019). As the goal is to use renewable raw materials from the industry, a sufficiently tolerant strain paired with a sparger pH control loop could reduce the need for chemicals obtained outside the value chain.

6.2 Yield and productivity potential on industrial scale

Simulated results between *Y. lipolytica* and *E. coli* show that stronger catabolic carbon repression and inhibition of acetate are assumed to cause more variation in the uptake ratio around the reactor, negatively affecting the yields. When the glucose feeding rate increases, the disproportion increases notably in both cases. This causes the problem seen in Figure 5.5 where a higher glucose feeding is required to overcome the toxicity of acetate at the bottom, but then the high glucose concentrations at the top will repress acetate uptake.

The largest factor for the heterogeneity of dissolved oxygen seems to come from the specific uptake rates, which is why *Y. lipolytica* simulation has a high amount of oxygen available at the bottom. With lower specific uptake rates, much higher substrate concentrations are required to match the growth distribution with the feeding rate. The effect of the uptake rates is also supported by the results of the productivity simulations, where *C. oleaginosus* showed more fluctuations between the top and bottom of the reactor than ADP1. Previous modeling results suggest that the oxygen profiles for single-substrate systems would have more heterogeneity compared to those of *E. coli* obtained here (Losoi et al. 2024; Losoi et al. 2022). Based on this knowledge, it can be said that CCR does not at least increase the heterogeneity of the dissolved oxygen.

C. oleaginosus simulations lead to higher volumetric productivities than ADP1 due to two reasons. First of all, wild-type *C. oleaginosus* accumulates much more lipids than the wild-type ADP1. Another reason is that higher total biomass was required for the simulation for the solver to converge. This means that with 30 g L^{-1} biomass *C. oleaginosus* can not reach the steady state. The reason is the lower uptake rates, so near-zero substrate concentrations are not enough to keep the average uptakes at levels that would deplete all the fed substrates.

The difference between the heterogeneities for the volumetric productivities in the ADP1 simulation can be explained by the feeding rates and the NADPH requirement. As the fed glucose is 1:4 of the total substrates, it is efficient enough to fulfil the 0.24 g glucose g^{-1} substrate requirement in all parts of the reactor for the palmitic acid production. Therefore, acetate is the limiting substrate everywhere. For cetyl alcohol and pentadecane, 0.26 g glucose g^{-1} substrate is required, but the feeding rate was kept the same. This leads to acetate being the limiting substrate at the top of the reactor and glucose at the bottom, which causes the larger drop in productivity. The shift in the limiting substrate also explains why the difference between the productivities of cetyl alcohol and pentadecane is so insignificant, unlike the yields in Table 5.2. Whereas the yield of product per unit of acetate consumed is more similar between palmitic acid and cetyl alcohol than between cetyl alcohol and pentadecane, for the yield of product per unit of glucose consumed it is the opposite.

For *C. oleaginosus* there are no similar patterns noticeable throughout the reactor as for ADP1, even though the limiting substrate changes in the case of cetyl alcohol and pentadecane production. Similarly to the *Y. lipolytica* simulation, the ideal glucose ratio was reached first at the bottom. Due to this reason, cetyl alcohol productivity is closer to the palmitic acid production at the lower parts, where acetate is still the limiting substrate. Significantly lower uptake rates compared to ADP1 also cause the change in productivities at the bottom of the reactor to be very modest. Because flow rates dominate reaction rates, substrate concentrations at the bottom are so low that the change in uptake rates is not significant. The total uptake of all the compartments still has to satisfy the steady state. The low uptake rates are also likely the cause for the spike occuring in the *Y. lipolytica* and *C. oleaginosus* simulations. The rates drop below the threshold values more easily, which causes the changes to appear less smooth as a result of the alternation between the uptake rate classes and the environmental rates.

Simulations of ADP1 and *C. oleaginosus* effectively capture the heterogeneity within the reactors during the production of long-chain fatty acids, alcohols, and alkanes. There is still a lack of information that affects the results. First, the affinity constants were assumed to be the same as for *E. coli*. In addition to that, inhibition by acetate was dismissed because of low concentrations. In reality, some toxic effects would be noticeable close to the feeding points. Now, it remains unclear whether the slightly higher acetate tolerance of *C. oleaginosus* offers an advantage over the lower acetate concentrations required by ADP1, which compensates with higher uptake rates.

6.3 Compatibility of the selected strains and future insights

MCA was a suitable method to recognize clusters with desired attributes because the literature review to compile the table was done based on information gathered from a large pool of relevant and recent publications. However, as an exploratory method and with a small sample size, no statistical significance was proved, and any correlations between the attributes should not be used to make assumptions about other microbes. To obtain a completely unbiased screening, a systematic review would also be required. For various microbes and investigating six different attributes, the scope would, however, be too large to include all the relevant studies. The use of flux balance analysis in the screening was mainly to validate the input from the literature. From the screening *E. coli* and *C. kluyveri* stand out as outliers by not expressing the desired attributes. Batch experiments support these findings in the case of *E. coli* which exhibited strong diauxia and low growth rates in acetate in LB medium. Excluding *C. kluyveri* from further laboratory work was justified due to its reported inability to utilize acetate as the sole substrate, which was supported by the flux balance analysis. *Y. lipolytica* was also left out of the batch experiments, although based on the literature survey and MCA, it meets most of the criteria for being a suitable

host. However, the most important criterion was the conversion of acetate to the product, and the alternative yeast species *C. oleaginosus* has shown much higher lipid yields. Due to the similarity between the species, only *C. oleaginosus* was chosen.

The batch experiments narrowed the selection down to three potential candidates: *P. putida*, ADP1 and *C. oleaginosus*. Because the goal of this study was to investigate the potential of converting SCFAs to long-chain products, *P. putida* can also be excluded. The selection between ADP1 and *C. oleaginosus* then comes down to the scale of the production and the operation mode. *C. oleaginosus* has naturally much higher yields, and in pure acetate cultures under ideal conditions, higher titers are expected in batch cultivations. If the lipid productivity is to be maximized by providing a co-substrate in large-scale fed-batches or continuous stirred tanks, heterogeneity does not allow the efficient yields of *C. oleaginosus* to be fully utilized. In these cases, ADP1 with higher uptake rates is a better choice.

Although all batch experiments, excluding *E. coli*, were performed using wild-type strains, genetic engineering is necessary for feasible large-scale processes. To direct acetate mainly towards the carbon skeleton of the products during co-feeding, deletion of genes encoding glyoxylate cycle enzymes is needed. In ADP1 this has been done by blocking the isocitrate lyase, which already leads to a lot higher WE contents and productivities (Luo et al. 2020; S. Santala, V. Santala, et al. 2021). For *C. oleaginosus* the genetic engineering studies focus mainly on enhancing the acetyl-CoA generation. However, in *Y. lipolytica* the deletion of *ICL1* and *ICL1* have improved the itanoic acid production from glucose (J. Fu et al. 2024). This indicates that modifying central metabolism is possible without completely disrupting the growth in oleaginous yeasts. The effects this has on the lipid accumulation when growing on acetate have not been studied.

Another major obstacle is to prevent the degradation of free fatty acids, alcohols, and alkanes. One option is to block the beta oxidation. If the goal is to produce free fatty acids, deleting the genes that encode fatty acid-CoA ligase blocks the first step of the beta oxidation (Q. Liu et al. 2011). As alkanes and alcohols are produced from acyl-CoA, acyl-CoA dehydrogenases that catalyze the conversion of acyl-CoA to enoyl-CoA should be the target for the deletion. In ADP1, these enzymes have not yet been established. In yeasts, the beta oxidation occurs in peroxisomes, and is catalyzed by acyl-CoA oxidases, multifunctional beta-oxidation protein, and 3-ketoacyl-CoA thiolase (Ma et al. 2024; Mlícková et al. 2004). Acyl-CoA oxidases catalyze the dehydrogenation to enoyl-CoA and could be a target location for the deletion, if acyl-CoA derivatives are the desired products (Kasaragod et al. 2017). To accumulate free fatty acids, fatty acyl-CoA synthetases and cytosolic acyl-CoA synthase can be targeted (Soong et al. 2019). Many of the genes that contribute to beta oxidation have been identified in conventional yeasts like *S. cerevisiae* or even in *Y. lipolytica* but *C. oleaginous* requires more screening.

7. CONCLUSIONS

Short-chain fatty acids are abundant as by-products of various industrial processes and can be used as sustainable and cost-effective raw materials for the production of high-value products. The purpose of this study was to identify potential microbial hosts for the valorization of industrial feeds rich in short-chain fatty acids and to evaluate the feasibility of the conversion process on a large scale.

For the screening, eight industrially relevant microbes were selected. Six different attributes were evaluated through a narrative literature review, and the combined effect was examined with multiple correspondence analysis. The theoretical potential of the utilization of the acetate was studied with flux balance analysis. The screening revealed that most microbes can tolerate high concentrations of acetate and some amounts of inhibitors found in industrial streams. A large set of genetic tools and models is also available for the majority of the microbes, but only *A. baylyi* ADP1 and the yeast species *Y. lipolytica* and *C. oleaginosus* accumulate storage compounds with long-chain fatty acids.

The prominent microbial hosts based on the screening were cultivated in small-scale LB cultures. *C. necator*, which has been shown to grow in defined media, did not grow at all, and *C. glutamicum* was able to consume only a fraction of the available acetate. *C. oleaginosus* reached the highest biomass with a low specific acetate uptake rate of 0.14 h^{-1}. ADP1 and *P. putida* achieved slightly lower biomass but had higher specific acetate uptake rates, 0.33 h^{-1} and 0.43 h^{-1}, respectively. Although LB is an undefined medium and does not allow a precise determination of carbon yields from acetate alone, it serves as a useful tool to identify microbes that tolerate pH fluctuations and do not require a strictly defined nutrient composition to grow.

The scalability of the co-feeding of glucose and acetate for effective productivity was studied via numerical simulations. The simulations were performed on reactors divided into smaller compartments with population balance models. The effects of carbon catabolic repression and inhibition were studied on *E. coli* and *Y. lipolytica*. The productivities of palmitic acid, cetyl alcohol, and pentadecane were studied on ADP1 and *C. oleaginosus*.

Simulations revealed that for *E. coli* the disproportion of the ideal substrate uptake ratio in the reactor increased 28% and 41% when the glucose feeding rate was increased from 0.75 to 1.0 and 1.25 g L^{-1} h^{-1}, respectively. In *Y. lipolytica* simulations changing

the glucose feeding rate in similar increments, the disproportion of the ideal substrate uptake ratio was increased by 10% and 27%. These results suggest that carbon catabolic repression is a major disadvantage in large-scale reactors when trying to optimize the production with co-feeding, even when concentrations are kept low, like in the fed-batch cultures. For the heterogeneity of the total consumption and dissolved oxygen concentration, stronger carbon catabolic repression and acetate inhibition do not seem to have negative effects. Instead, lower uptake rates cause heterogeneity and the dissolved oxygen concentration for *Y. lipolytica* at the bottom of the reactor was 37% higher than at the top, whereas for *E. coli* the increase was only 9%.

In ADP1 simulations, the volumetric productivity of palmitic acid at the bottom of the reactor decreased 11% compared to the values at the top. The volumetric productivities of cetyl alcohol and pentadecane decreased by 20%. The results highlight that in the absence of significant substrate inhibition, uniform productivity can be achieved on a large scale when the glucose feeding rate remains above the threshold required for the optimal uptake ratio. In contrast, if the limiting substrate varies within the reactor, a higher level of heterogeneity in productivity is likely to occur. For *C. oleaginosus* the productivities of palmitic acid and pentadecane decreased 24% and for cetyl alcohol 22%. This means that the low specific uptake rates cause so much heterogeneity of substrates between the top and bottom of the reactor that even sufficient glucose feeding rates result in a lot of fluctuations in productivity.

Based on the cultivations and the literature screening *A. baylyi* ADP1 and *C. oleaginosus* both meet the objective stated in this thesis of converting short-chain fatty acids from industrial streams into long-chain fatty acids, alcohols, and alkanes. *C. oleaginosus* with higher lipid accumulation gains an advantage in pure acetate batch cultures, while ADP1 with a higher uptake rate and available genetic tools to direct the acetate into fatty acid synthesis is more suitable to be used in co-feeding processes. Neither of the species naturally accumulates the desired products as such, but instead as TAGs and WEs. Therefore, genetic engineering to block the degradation of free fatty acids and acyl-CoAs is still necessary. Because the cultivations were performed in complex media, the question of the precise acetate utilization rates still needs verification in the defined media. To further investigate the conversion to products, lipid analysis would also be required. From the simulation results, it can be concluded that acetate could serve as a co-substrate on a large scale, although achieving homogeneous productivity would require adjustment of the feeding strategy. As the co-feeding of acetate and glucose has not been studied on a large scale, more experimental data are required to address the reliability of the simulations. Since unstructured kinetics still include multiple variables, the importance of single factors such as carbon catabolic repression should be further studied. The model-based design of experiments could be suitable to identify which factors and factor combinations are significant.

REFERENCES

Abdi, Hervé and Dominique Valentin (2007). “Multiple correspondence analysis”. *Encyclopedia of measurement and statistics* 2.4, pp. 651–657.

Abdi, Hervé and Lynne J Williams (2010). “Principal component analysis”. *Wiley interdisciplinary reviews: computational statistics* 2.4, pp. 433–459.

Almeida, João RM et al. (2009). “Metabolic effects of furaldehydes and impacts on biotechnological processes”. *Applied microbiology and biotechnology* 82, pp. 625–638.

Alvarez, Hector M et al. (1997). “Accumulation of storage lipids in species of *Rhodococcus* and *Nocardia* and effect of inhibitors and polyethylene glycol”. *Lipid/Fett* 99.7, pp. 239–246.

Amer, Abdelrahman and Younggy Kim (2023). “Minimizing the lag phase of *Cupriavidus necator* growth under autotrophic, heterotrophic, and mixotrophic conditions”. *Applied and Environmental Microbiology* 89.2, e02007–22.

Arteaga, José Eduardo et al. (2021). “Furfural biotransformation in *Acinetobacter baylyi* ADP1 and *Acinetobacter schindleri* ACE”. *Biotechnology Letters* 43, pp. 1043–1050.

Baei, Sharifzadeh M et al. (2011). “Growth kinetic parameters and biosynthesis of polyhydroxybutyrate in *Cupriavidus necator* DSMZ 545 on selected substrates”. *Chemical Industry and Chemical Engineering Quarterly* 17.1, pp. 1–8.

Bansal-Mutalik, Ritu and Hiroshi Nikaido (2011). “Quantitative lipid composition of cell envelopes of *Corynebacterium glutamicum* elucidated through reverse micelle extraction”. *Proceedings of the National Academy of Sciences* 108.37, pp. 15360–15365.

Barney, Brett M et al. (2012). “Differences in substrate specificities of five bacterial wax ester synthases”. *Applied and Environmental Microbiology* 78.16, pp. 5734–5745.

Batlle-Vilanova, Pau et al. (2017). “Microbial electrosynthesis of butyrate from carbon dioxide: Production and extraction”. *Bioelectrochemistry* 117, pp. 57–64.

Béligon, Vanessa et al. (2015). “Improvement and modeling of culture parameters to enhance biomass and lipid production by the oleaginous yeast *Cryptococcus curvatus* grown on acetate”. *Bioresource technology* 192, pp. 582–591.

Beopoulos, Athanasios et al. (2009). “*Yarrowia lipolytica* as a model for bio-oil production”. *Progress in lipid research* 48.6, pp. 375–387.

Bloch, Konrad (1971). “15 β-hydroxydecanoyl thioester dehydrase”. *The enzymes*. Vol. 5. Elsevier, pp. 441–464.

Börner, Rosa Aragão (2016). “Isolation and cultivation of anaerobes”. *Anaerobes in biotechnology*, pp. 35–53.

Brock, Matthias and Wolfgang Buckel (2004). “On the mechanism of action of the antifungal agent propionate: Propionyl-CoA inhibits glucose metabolism in *Aspergillus nidulans*”. *European Journal of Biochemistry* 271.15, pp. 3227–3241.

Cai, Fanfan et al. (2023). “Biosynthesis of poly (3-hydroxybutyrate-co-3-hydroxvalerate) from volatile fatty acids by *Cupriavidus necator*”. *Journal of Basic Microbiology* 63.2, pp. 128–139.

Candry, Pieter et al. (2018). “A novel high-throughput method for kinetic characterisation of anaerobic bioproduction strains, applied to *Clostridium kluyveri*”. *Scientific reports* 8.1, p. 9724.

Carlson, CURTIS A et al. (1983). “*Pseudomonas stutzeri* and related species undergo natural transformation”. *Journal of Bacteriology* 153.1, pp. 93–99.

Cecilia, Daniele la et al. (2019). “Biochemical modeling of microbial memory effects and catabolite repression on soil organic carbon compounds”. *Soil Biology and Biochemistry* 128, pp. 1–12.

Chen, Cheng et al. (2015). “Metabolic engineering of *Corynebacterium glutamicum* ATCC13869 for L-valine production”. *Metabolic engineering* 29, pp. 66–75.

Chen, Lin et al. (2021). “Increased lipid production in *Yarrowia lipolytica* from acetate through metabolic engineering and cosubstrate fermentation”. *ACS synthetic biology* 10.11, pp. 3129–3138.

Chew, Shu Yih et al. (2019). “The glyoxylate cycle and alternative carbon metabolism as metabolic adaptation strategies of *Candida glabrata*: perspectives from *Candida albicans* and *Saccharomyces cerevisiae*”. *Journal of biomedical science* 26, pp. 1–10.

Choi, So Young et al. (2020). “Microbial polyhydroxyalkanoates and nonnatural polyesters”. *Advanced Materials* 32.35, p. 1907138.

Christophe, G et al. (2012). “Production of oils from acetic acid by the oleaginous yeast *Cryptococcus curvatus*”. *Applied biochemistry and biotechnology* 167, pp. 1270–1279.

Clark, David P et al. (1983). “. beta.-Hydroxydecanoyl thioester dehydrase does not catalyze a rate-limiting step in *Escherichia coli* unsaturated fatty acid synthesis”. *Biochemistry* 22.25, pp. 5897–5902.

Cremonez, Paulo André et al. (2021). “Two-Stage anaerobic digestion in agroindustrial waste treatment: A review”. *Journal of Environmental Management* 281, p. 111854.

Cronan, John E and Jacob Thomas (2009). “Bacterial fatty acid synthesis and its relationships with polyketide synthetic pathways”. *Methods in enzymology* 459, pp. 395–433.

Cronan Jr, John E and Grover L Waldrop (2002). “Multi-subunit acetyl-CoA carboxylases”. *Progress in lipid research* 41.5, pp. 407–435.

Cui, YQ et al. (1996). “Compartment mixing model for stirred reactors with multiple impellers”. *Chemical engineering research & design* 74.2, pp. 261–271.

David, Aditi et al. (2020). “Acetate production from cafeteria wastes and corn stover using a thermophilic anaerobic consortium: a prelude study for the use of acetate for the production of value-added products”. *Microorganisms* 8.3, p. 353.

DeLisa, Matthew et al. (2017). *Bioprocess engineering: basic concepts*. Pearson.

Dessì, Paolo et al. (2021). “Microbial electrosynthesis: towards sustainable biorefineries for production of green chemicals from CO_2 emissions”. *Biotechnology Advances* 46, p. 107675.

Díez, Mario P et al. (2024). “Valorization of process water from hydrothermal carbonization of food waste by dark fermentation”. *International Journal of Hydrogen Energy* 89, pp. 1383–1393.

Dolan, Stephen K et al. (2018). “Loving the poison: the methylcitrate cycle and bacterial pathogenesis”. *Microbiology* 164.3, pp. 251–259.

Dubey, Mukesh K et al. (2013). “Role of the methylcitrate cycle in growth, antagonism and induction of systemic defence responses in the fungal biocontrol agent *Trichoderma atroviride*”. *Microbiology* 159.Pt_12, pp. 2492–2500.

Duman-Özdamar, Zeynep Efsun et al. (2025). “Model-driven engineering of *Cutaneotrichosporon oleaginosus* ATCC 20509 for improved microbial oil production”. *Bioresource Technology*, p. 132142.

Durot, Maxime et al. (2008). “Iterative reconstruction of a global metabolic model of *Acinetobacter baylyi* ADP1 using high-throughput growth phenotype and gene essentiality data”. *BMC systems biology* 2, pp. 1–23.

Ebrahim, Ali et al. (2013). “COBRApy: constraints-based reconstruction and analysis for python”. *BMC systems biology* 7, pp. 1–6.

Enjalbert, Brice et al. (2015). “Acetate exposure determines the diauxic behavior of *Escherichia coli* during the glucose-acetate transition”. *Journal of bacteriology* 197.19, pp. 3173–3181.

Fakas, Stylianos (2017). “Lipid biosynthesis in yeasts: A comparison of the lipid biosynthetic pathway between the model nonoleaginous yeast *Saccharomyces cerevisiae* and the model oleaginous yeast *Yarrowia lipolytica*”. *Engineering in Life Sciences* 17.3, pp. 292–302.

Fast, Alan G et al. (2015). “Acetogenic mixotrophy: novel options for yield improvement in biofuels and biochemicals production”. *Current Opinion in Biotechnology* 33, pp. 60–72.

Feierabend, Martina et al. (2021). “High-quality genome-scale reconstruction of *Corynebacterium glutamicum* ATCC 13032”. *Frontiers in microbiology* 12, p. 750206.

Fereidouni, Mohammad et al. (2011). “The effect of carbon source supplementation on the production of poly (3-hydroxybutyrate-co-3-hydroxyvalerate) by *Cupriavidus necator*”. *Biotechnology and applied biochemistry* 58.3, pp. 203–211.

Fithian, William and Julie Josse (2017). “Multiple correspondence analysis and the multilogit bilinear model”. *Journal of multivariate analysis* 157, pp. 87–102.

Fu, Jing et al. (2024). “Reprogramming *Yarrowia lipolytica* metabolism for efficient synthesis of itaconic acid from flask to semipilot scale”. *Science Advances* 10.32, eadn0414.

Fukuda, Nobuo (2023). “Apparent diameter and cell density of yeast strains with different ploidy”. *Scientific Reports* 13.1, p. 1513.

Gao, Ruiling et al. (2020). “Enhanced lipid production by *Yarrowia lipolytica* cultured with synthetic and waste-derived high-content volatile fatty acids under alkaline conditions”. *Biotechnology for Biofuels* 13, pp. 1–16.

Garces Daza, Fernando et al. (2023). “An optimized reverse β-oxidation pathway to produce selected medium-chain fatty acids in *Saccharomyces cerevisiae*”. *Biotechnology for Biofuels and Bioproducts* 16.1, p. 71.

Garcia-Gonzalez, Linsey and Heleen De Wever (2018). “Acetic acid as an indirect sink of CO2 for the synthesis of polyhydroxyalkanoates (PHA): comparison with PHA production processes directly using CO2 as feedstock”. *Applied Sciences* 8.9, p. 1416.

Garcia-Ochoa, Felix and Emilio Gomez (2009). “Bioreactor scale-up and oxygen transfer rate in microbial processes: an overview”. *Biotechnology advances* 27.2, pp. 153–176.

Gayen, Kalyan and KV Venkatesh (2007). “A phenomenological model to represent the kinetics of growth by *Corynebacterium glutamicum* for lysine production”. *Journal of Industrial Microbiology and Biotechnology* 34.5, pp. 363–372.

Giannattasio, Sergio et al. (2013). “Molecular mechanisms of *Saccharomyces cerevisiae* stress adaptation and programmed cell death in response to acetic acid”. *Frontiers in microbiology* 4, p. 33.

Gildemyn, Sylvia et al. (2017). “Upgrading syngas fermentation effluent using *Clostridium kluyveri* in a continuous fermentation”. *Biotechnology for biofuels* 10, pp. 1–15.

Goes Job, Maria Eduarda et al. (2025). “Investigating Associations Between Prognostic Factors in Gliomas: Unsupervised Multiple Correspondence Analysis”. *JMIR Bioinformatics and Biotechnology* 6, e65645.

Gong, Zhiwei et al. (2015). “Efficient conversion of acetate into lipids by the oleaginous yeast *Cryptococcus curvatus*”. *Biotechnology for biofuels* 8, pp. 1–9.

Gu, Pengfei et al. (2024). “Application of Acetate as a Substrate for the Production of Value-Added Chemicals in *Escherichia coli*”. *Microorganisms* 12.2, p. 309.

Haile, Adane et al. (2021). “Pulp and paper mill wastes: utilizations and prospects for high value-added biomaterials”. *Bioresources and Bioprocessing* 8, pp. 1–22.

Hamaguchi, Marcelo et al. (2012). “Alternative technologies for biofuels production in kraft pulp mills—potential and prospects”. *Energies* 5.7, pp. 2288–2309.

Harris, Charles R. et al. (Sept. 2020). “Array programming with NumPy”. *Nature* 585.7825, pp. 357–362. DOI: 10.1038/s41586-020-2649-2. URL: https://doi.org/10.1038/s41586-020-2649-2.

Hoshan, Linda et al. (2019). “Effective bioreactor pH control using only sparging gases”. *Biotechnology Progress* 35.1, e2743.

Hosmer, Jennifer et al. (2023). “Bacterial acetate metabolism and its influence on human epithelia”. *Emerging topics in life sciences* 8.1, pp. 1–13.

Hu, Peng et al. (2016). “Integrated bioprocess for conversion of gaseous substrates to liquids”. *Proceedings of the National Academy of Sciences* 113.14, pp. 3773–3778.

Huang, Zhicheng et al. (2023). “The methylcitrate cycle and its crosstalk with the glyoxylate cycle and tricarboxylic acid cycle in pathogenic fungi”. *Molecules* 28.18, p. 6667.

Hunter, J. D. (2007). “Matplotlib: A 2D graphics environment”. *Computing in Science & Engineering* 9.3, pp. 90–95. DOI: 10.1109/MCSE.2007.55.

Ikeda, Masato et al. (2017). “In vivo roles of fatty acid biosynthesis enzymes in biosynthesis of biotin and α-lipoic acid in *Corynebacterium glutamicum*”. *Applied and Environmental Microbiology* 83.19, e01322–17.

Jackowski, Suzanne and CO Rock (1987). “Acetoacetyl-acyl carrier protein synthase, a potential regulator of fatty acid biosynthesis in bacteria.” *Journal of Biological Chemistry* 262.16, pp. 7927–7931.

Jahan, Nusrat et al. (2016). “Development of an accurate kinetic model for the central carbon metabolism of *Escherichia coli*”. *Microbial cell factories* 15, pp. 1–19.

Jawed, K et al. (2022). *Establishing mixotrophic growth of Cupriavidus necator H16 on CO2 and volatile fatty acids. Fermentation 8 (3)*.

Kalscheuer, Rainer and Alexander Steinbüchel (2003). “A novel bifunctional wax ester synthase/acyl-CoA: diacylglycerol acyltransferase mediates wax ester and triacylglycerol biosynthesis in *Acinetobacter calcoaceticus* ADP1”. *Journal of Biological Chemistry* 278.10, pp. 8075–8082.

Kannisto, Matti et al. (2014). “Metabolic engineering of *Acinetobacter baylyi* ADP1 for improved growth on gluconate and glucose”. *Applied and environmental microbiology* 80.22, pp. 7021–7027.

Kannisto, Matti S et al. (2015). “Metabolic engineering of *Acinetobacter baylyi* ADP1 for removal of *Clostridium butyricum* growth inhibitors produced from lignocellulosic hydrolysates”. *Biotechnology for Biofuels* 8, pp. 1–10.

Kasaragod, Prasad et al. (2017). “Structural enzymology comparisons of multifunctional enzyme, type-1 (MFE 1): the flexibility of its dehydrogenase part”. *FEBS Open bio* 7.12, pp. 1830–1842.

Kavšček, Martin et al. (2015). “Optimization of lipid production with a genome-scale model of *Yarrowia lipolytica*”. *BMC systems biology* 9, pp. 1–13.

Kedia, Gopal et al. (2014). “Evaluation of feeding regimes to enhance PHA production using acetic and butyric acids by a pure culture of *Cupriavidus necator*”. *Biotechnology and bioprocess engineering* 19, pp. 989–995.

Kerkhoven, Eduard J et al. (2016). “Regulation of amino-acid metabolism controls flux to lipid accumulation in *Yarrowia lipolytica*”. *NPJ systems biology and applications* 2.1, pp. 1–7.

Khangar, Nutan Vijay and Kirtee Kiran Kamalja (2017). “Multiple Correspondence Analysis and its applications”. *Electronic Journal of Applied Statistical Analysis* 10.2, pp. 432–462.

Kiefer, Dirk et al. (2022). “High-level recombinant protein production with *Corynebacterium glutamicum* using acetate as carbon source”. *Microbial biotechnology* 15.11, pp. 2744–2757.

Koh, Hyun Gi et al. (2024). “Toward rapid and efficient utilization of nonconventional substrates by nonconventional yeast strains”. *Current Opinion in Biotechnology* 85, p. 103059.

Koivuranta, Kari et al. (2018). “Enhanced triacylglycerol production with genetically modified *Trichosporon oleaginosus*”. *Frontiers in microbiology* 9, p. 1337.

Komiyama, Yoko and Sumio Maeda (2020). “Natural transformation in *Escherichia coli*”. *Horizontal Gene Transfer: Methods and Protocols*, pp. 179–187.

Konzock, Oliver et al. (2021). “Tolerance of *Yarrowia lipolytica* to inhibitors commonly found in lignocellulosic hydrolysates”. *BMC microbiology* 21, pp. 1–10.

Kotte, Oliver et al. (2014). “Phenotypic bistability in *Escherichia coli’s* central carbon metabolism”. *Molecular systems biology* 10.7, p. 736.

Kovanda, Lauren et al. (2019). “In vitro antimicrobial activities of organic acids and their derivatives on several species of gram-negative and gram-positive bacteria”. *Molecules* 24.20, p. 3770.

Kremling, Andreas et al. (2018). “An ensemble of mathematical models showing diauxic growth behaviour”. *BMC systems biology* 12, pp. 1–16.

Lai, Chiou-Yan and John E Cronan (2004). “Isolation and characterization of β-ketoacyl-acyl carrier protein reductase (fabG) mutants of *Escherichia coli* and *Salmonella enterica* serovar Typhimurium”. *Journal of bacteriology* 186.6, pp. 1869–1878.

Lê, Sébastien et al. (2008). “FactoMineR: A Package for Multivariate Analysis”. *Journal of Statistical Software* 25.1, pp. 1–18. DOI: 10.18637/jss.v025.i01.

Lee, Hyeonsik et al. (2022). “Engineering acetogenic bacteria for efficient one-carbon utilization”. *Frontiers in Microbiology* 13, p. 865168.

Lee, Min Hee et al. (2019). “Assessing the pentose phosphate pathway using [2, 3-13C2] glucose”. *NMR in Biomedicine* 32.6, e4096.

Lee, Sun Mi et al. (2022). “Enhanced tolerance of *Cupriavidus necator* NCIMB 11599 to lignocellulosic derived inhibitors by inserting NAD salvage pathway genes”. *Bioprocess and Biosystems Engineering* 45.10, pp. 1719–1729.

Leitão, Renato Carrhá et al. (2006). “The effects of operational and environmental variations on anaerobic wastewater treatment systems: A review”. *Bioresource technology* 97.9, pp. 1105–1118.

Lennen, Rebecca M and Brian F Pfleger (2012). “Engineering *Escherichia coli* to synthesize free fatty acids”. *Trends in biotechnology* 30.12, pp. 659–667.

Liu, Aiqiu et al. (2013). “Fatty alcohol production in engineered *E. coli* expressing *Marinobacter* fatty acyl-CoA reductases”. *Applied microbiology and biotechnology* 97, pp. 7061–7071.

Liu, Jiao et al. (2017). “Development of a CRISPR/Cas9 genome editing toolbox for *Corynebacterium glutamicum*”. *Microbial cell factories* 16, pp. 1–17.

Liu, Qian et al. (2011). “Biosynthesis of poly (3-hydroxydecanoate) and 3-hydroxydodecanoate dominating polyhydroxyalkanoates by β-oxidation pathway inhibited *Pseudomonas putida*”. *Metabolic Engineering* 13.1, pp. 11–17.

Liu, Zhenquan et al. (2020). “Application of different types of CRISPR/Cas-based systems in bacteria”. *Microbial cell factories* 19, pp. 1–14.

Lobanova, Juliya S et al. (2022). “Genome engineering of the *Corynebacterium glutamicum* chromosome by the Extended Dual-In/Out strategy”. *Journal of microbiological methods* 200, p. 106555.

Losoi, Pauli et al. (2022). “Substantial gradient mitigation in simulated large-scale bioreactors by optimally placed multiple feed points”. *Biotechnology and Bioengineering* 119.12, pp. 3549–3566.

– (2024). “Modeling large-scale bioreactors with diffusion equations. Part II: Characterizing substrate, oxygen, temperature, carbon dioxide, and pH profiles”. *Biotechnology and Bioengineering* 121.3, pp. 1102–1117.

Luo, Jin et al. (2020). “Wax ester production in nitrogen-rich conditions by metabolically engineered *Acinetobacter baylyi* ADP1”. *Metabolic Engineering Communications* 10, e00128.

Ma, Yongshuo et al. (2024). “Engineering peroxisomal biosynthetic pathways for maximization of triterpene production in *Yarrowia lipolytica*”. *Proceedings of the National Academy of Sciences* 121.5, e2314798121.

Magnuson, Kelly et al. (1992). “Cloning and nucleotide sequence of the fabD gene encoding malonyl coenzyme A-acyl carrier protein transacylase of *Escherichia coli*”. *FEBS letters* 299.3, pp. 262–266.

Marsh, E Neil G and Matthew W Waugh (2013). *Aldehyde decarbonylases: enigmatic enzymes of hydrocarbon biosynthesis*.

Mendoza Martinez, Clara Lisseth et al. (2021). “Hydrothermal carbonization of chemical and biological pulp mill sludges”. *Energies* 14.18, p. 5693.

Meng, Xin et al. (2011). “Increasing fatty acid production in *E. coli* by simulating the lipid accumulation of oleaginous microorganisms”. *Journal of Industrial Microbiology and Biotechnology* 38.8, pp. 919–925.

Mills, Tirzah Y et al. (2009). “Cellulosic hydrolysate toxicity and tolerance mechanisms in *Escherichia coli*”. *Biotechnology for biofuels* 2, pp. 1–11.

Mlícková, Katerina et al. (2004). “Lipid accumulation, lipid body formation, and acyl coenzyme A oxidases of the yeast *Yarrowia lipolytica*”. *Applied and environmental microbiology* 70.7, pp. 3918–3924.

Monk, Jonathan et al. (2014). “Optimizing genome-scale network reconstructions”. *Nature biotechnology* 32.5, pp. 447–452.

Morchain, Jérôme et al. (2013). “Coupling of biokinetic and population balance models to account for biological heterogeneity in bioreactors”. *AIChE Journal* 59.2, pp. 369–379.

– (2014). “A coupled population balance model and CFD approach for the simulation of mixing issues in lab-scale and industrial bioreactors”. *AIChE Journal* 60.1, pp. 27–40.

Muñoz-Elías, Ernesto J et al. (2006). “Role of the methylcitrate cycle in *Mycobacterium tuberculosis* metabolism, intracellular growth, and virulence”. *Molecular microbiology* 60.5, pp. 1109–1122.

Mutyala, Sakuntala et al. (2023). “Citrate Synthase Overexpression of *Pseudomonas putida* Increases Succinate Production from Acetate in Microaerobic Cultivation”. *ACS omega* 8.29, pp. 26231–26242.

Narayanan, Venkatachalam et al. (2017). “Increased lignocellulosic inhibitor tolerance of *Saccharomyces cerevisiae* cell populations in early stationary phase”. *Biotechnology for biofuels* 10.1, p. 114.

Narisetty, Vivek et al. (2022). “Development of hypertolerant strain of *Yarrowia lipolytica* accumulating succinic acid using high levels of acetate”. *ACS Sustainable Chemistry & Engineering* 10.33, pp. 10858–10869.

Niu, Jinhui et al. (2022). “Construction and analysis of an enzyme-constrained metabolic model of *Corynebacterium glutamicum*”. *Biomolecules* 12.10, p. 1499.

Nogales, Juan et al. (2020). “High-quality genome-scale metabolic modelling of *Pseudomonas putida* highlights its broad metabolic capabilities”. *Environmental microbiology* 22.1, pp. 255–269.

Nomura, Takashi et al. (2024). “Microwave Effect in Hydrolysis of Levoglucosan with a Solid Acid Catalyst for Pyrolysis-Based Cellulose Saccharification”. *ChemistryOpen*, e202300311.

Ochoa-Estopier, Abril and Stéphane E Guillouet (2014). “D-stat culture for studying the metabolic shifts from oxidative metabolism to lipid accumulation and citric acid production in *Yarrowia lipolytica*”. *Journal of biotechnology* 170, pp. 35–41.

Oehlenschläger, Katharina et al. (2024). “New insights into the influence of pre-culture on robust solvent production of *C. acetobutylicum*”. *Applied Microbiology and Biotechnology* 108.1, p. 143.

Otten, Jonathan K et al. (2022). “The potential of caproate (hexanoate) production using *Clostridium kluyveri* syntrophic cocultures with *Clostridium acetobutylicum* or *Clostridium saccharolyticum*”. *Frontiers in Bioengineering and Biotechnology* 10, p. 965614.

Parera Olm, Ivette and Diana Z Sousa (2023). “Upgrading dilute ethanol to odd-chain carboxylic acids by a synthetic co-culture of *Anaerotignum neopropionicum* and *Clostridium kluyveri*”. *Biotechnology for Biofuels and Bioproducts* 16.1, p. 83.

Park, Jong Myoung et al. (2011). “Genome-scale reconstruction and in silico analysis of the *Ralstonia eutropha* H16 for polyhydroxyalkanoate synthesis, lithoautotrophic growth, and 2-methyl citric acid production”. *BMC systems biology* 5, pp. 1–11.

Park, Junyoung O et al. (2019). “Synergistic substrate cofeeding stimulates reductive metabolism”. *Nature Metabolism* 1.6, pp. 643–651.

Park, Young-kyoung et al. (2020). “De novo biosynthesis of odd-chain fatty acids in *Yarrowia lipolytica* enabled by modular pathway engineering”. *Frontiers in bioengineering and biotechnology* 7, p. 484.

Pearcy, Nicole et al. (2022). “A genome-scale metabolic model of *Cupriavidus necator* H16 integrated with TraDIS and transcriptomic data reveals metabolic insights for biotechnological applications”. *PLoS computational biology* 18.5, e1010106.

Pedrino, Matheus et al. (2025). “Upgrading *Pseudomonas* sp. toward Tolerance to a Synthetic Biomass Hydrolysate Enriched with Furfural and 5-Hydroxymethylfurfural”. *ACS Omega*.

Pereira, Ana S et al. (2021). “Factors affecting microbial lipids production by *Yarrowia lipolytica* strains from volatile fatty acids: Effect of co-substrates, operation mode and oxygen”. *Journal of Biotechnology* 331, pp. 37–47.

Pham, Nhung et al. (2021). “Genome-scale metabolic modeling underscores the potential of *Cutaneotrichosporon oleaginosus* ATCC 20509 as a cell factory for biofuel production”. *Biotechnology for biofuels* 14, pp. 1–17.

Pigou, Maxime and Jérôme Morchain (2015). “Investigating the interactions between physical and biological heterogeneities in bioreactors using compartment, population balance and metabolic models”. *Chemical Engineering Science* 126, pp. 267–282.

Pinhal, Stéphane et al. (2019). “Acetate metabolism and the inhibition of bacterial growth by acetate”. *Journal of bacteriology* 201.13, pp. 10–1128.

Polat, Ece et al. (2025). “Recovery of volatile fatty acids from anaerobic fermentation broth of baker’s yeast industry effluent by liquid- liquid extraction”. *Journal of Industrial and Engineering Chemistry* 141, pp. 431–440.

Raes, Sanne MT et al. (2017). “Continuous long-term bioelectrochemical chain elongation to butyrate”. *ChemElectroChem* 4.2, pp. 386–395.

Ragsdale, Stephen W and Elizabeth Pierce (2008). “Acetogenesis and the Wood–Ljungdahl pathway of CO2 fixation”. *Biochimica et Biophysica Acta (BBA)-Proteins and Proteomics* 1784.12, pp. 1873–1898.

Rawlings, Merriann and John E Cronan Jr (1992). “The gene encoding *Escherichia coli* acyl carrier protein lies within a cluster of fatty acid biosynthetic genes.” *Journal of Biological Chemistry* 267.9, pp. 5751–5754.

Reddy, M Venkateswar et al. (2018). “Medium-chain fatty acids (MCFA) production through anaerobic fermentation using *Clostridium kluyveri*: effect of ethanol and acetate”. *Applied biochemistry and biotechnology* 185, pp. 594–605.

Reed, Jennifer L et al. (2003). “An expanded genome-scale model of *Escherichia coli* K-12 (i JR904 GSM/GPR)”. *Genome biology* 4, pp. 1–12.

Robak, M et al. (2002). “Study of acetate utilization and citrate secretion by *Yarrowia lipolytica* yeast”. *Zeszyty Naukowe Akademii Rolniczej we Wroclawiu. Rozprawy (Poland)* 442192.

Robles-Rodríguez, Carlos E et al. (2018). “Modeling and optimization of lipid accumulation by *Yarrowia lipolytica* from glucose under nitrogen depletion conditions”. *Biotechnology and bioengineering* 115.5, pp. 1137–1151.

Robles-Rodríguez, Carlos Eduardo et al. (2015). “Dynamical metabolic modelling for lipid accumulation by *Yarrowia lipolytica* growing on glucose”. *2015 23rd Mediterranean Conference on Control and Automation (MED)*. IEEE, pp. 815–820.

Roden, Eric E and Qusheng Jin (2011). “Thermodynamics of microbial growth coupled to metabolism of glucose, ethanol, short-chain organic acids, and hydrogen”. *Applied and environmental microbiology* 77.5, pp. 1907–1909.

Sagong, Hye-Young et al. (2018). “Structural insights into polyhydroxyalkanoates biosynthesis”. *Trends in biochemical sciences* 43.10, pp. 790–805.

Salcedo-Vite, Karina et al. (2019). “*Acinetobacter baylyi* ADP1 growth performance and lipid accumulation on different carbon sources”. *Applied microbiology and biotechnology* 103, pp. 6217–6229.

Sandoval-Espinola, Walter J et al. (2015). “Inoculum optimization of *Clostridium beijerinckii* for reproducible growth”. *FEMS microbiology letters* 362.19, fnv164.

Santala, Suvi, Elena Efimova, et al. (2014). “Rewiring the wax ester production pathway of *Acinetobacter baylyi* ADP1”. *ACS Synthetic Biology* 3.3, pp. 145–151.

Santala, Suvi and Ville Santala (2021). “*Acinetobacter baylyi* ADP1—naturally competent for synthetic biology”. *Essays in Biochemistry* 65.2, pp. 309–318.

Santala, Suvi, Ville Santala, et al. (2021). “Partitioning metabolism between growth and product synthesis for coordinated production of wax esters in *Acinetobacter baylyi ADP1*”. *Biotechnology and Bioengineering* 118.6, pp. 2283–2292.

Schirmer, Andreas et al. (2010). “Microbial biosynthesis of alkanes”. *Science* 329.5991, pp. 559–562.

Schmollack, Marc et al. (2022). “Metabolic engineering of *Corynebacterium glutamicum* for acetate-based itaconic acid production”. *Biotechnology for Biofuels and Bioproducts* 15.1, p. 139.

Schuchmann, Kai and Volker Müller (2014). “Autotrophy at the thermodynamic limit of life: a model for energy conservation in acetogenic bacteria”. *Nature Reviews Microbiology* 12.12, pp. 809–821.

Schwartz, Cory and Ian Wheeldon (2018). “CRISPR-Cas9-mediated genome editing and transcriptional control in *Yarrowia lipolytica*”. *Synthetic Biology: Methods and Protocols*, pp. 327–345.

Senneca, O et al. (2020). “Thermal treatment of lignin, cellulose and hemicellulose in nitrogen and carbon dioxide”. *Fuel* 271, p. 117656.

Seo, Yeong hwan et al. (2013). “Cultivation and lipid production of yeast *Cryptococcus curvatus* using pretreated waste active sludge supernatant”. *Bioresource technology* 135, pp. 304–308.

Shuler, Michael L (1992). “Bioprocess enzineering.” *Prentice-Hall*, pp. 412–420.

Sievert, Carson (2020). *Interactive Web-Based Data Visualization with R, plotly, and shiny*. URL: https://plotly-r.com.

Soong, Ya-Hue Valerie et al. (2019). “Cellular and metabolic engineering of oleaginous yeast *Yarrowia lipolytica* for bioconversion of hydrophobic substrates into high-value products”. *Engineering in Life Sciences* 19.6, pp. 423–443.

Sourial, Nadia et al. (2010). “Correspondence analysis is a useful tool to uncover the relationships among categorical variables”. *Journal of clinical epidemiology* 63.6, pp. 638–646.

Stahl, Andreas et al. (2001). “Fatty acid transport proteins: a current view of a growing family”. *Trends in Endocrinology & Metabolism* 12.6, pp. 266–273.

Steen, Eric J et al. (2010). “Microbial production of fatty-acid-derived fuels and chemicals from plant biomass”. *Nature* 463.7280, pp. 559–562.

Stellner, Nikolaus I et al. (2023). “Expanding the genetic toolbox for *Cutaneotrichosporon oleaginosus* employing newly identified promoters and a novel antibiotic resistance marker”. *BMC biotechnology* 23.1, p. 40.

Stöveken, Tim et al. (2005). “The wax ester synthase/acyl coenzyme A: diacylglycerol acyltransferase from *Acinetobacter* sp. strain ADP1: characterization of a novel type of acyltransferase”. *Journal of bacteriology* 187.4, pp. 1369–1376.

Sui, Xinyue et al. (2024). “Phenolic compounds induce ferroptosis-like death by promoting hydroxyl radical generation in the Fenton reaction”. *Communications Biology* 7.1, p. 199.

Tai, Mitchell and Gregory Stephanopoulos (2013). “Engineering the push and pull of lipid biosynthesis in oleaginous yeast *Yarrowia lipolytica* for biofuel production”. *Metabolic engineering* 15, pp. 1–9.

Takeno, Seiki et al. (2013). “Development of fatty acid-producing *Corynebacterium glutamicum* strains”. *Applied and environmental microbiology* 79.21, pp. 6776–6783.

Tampio, Elina A et al. (2019). “Volatile fatty acids (VFAs) and methane from food waste and cow slurry: Comparison of biogas and VFA fermentation processes”. *Gcb Bioenergy* 11.1, pp. 72–84.

Teixeira, Paulo Gonçalves et al. (2017). “Quantitative in vivo evaluation of the reverse β-oxidation pathway for fatty acid production in *Saccharomyces cerevisiae*”. *bioRxiv*, p. 201616.

Tokic, Milenko et al. (2020). “Large-scale kinetic metabolic models of *Pseudomonas putida* KT2440 for consistent design of metabolic engineering strategies”. *Biotechnology for biofuels* 13, pp. 1–19.

Van Rossum, Harmen M et al. (2016). “Engineering cytosolic acetyl-coenzyme A supply in *Saccharomyces cerevisiae*: pathway stoichiometry, free-energy conservation and redox-cofactor balancing”. *Metabolic engineering* 36, pp. 99–115.

Vassilev, Igor et al. (2024). “Comparing the performance of fluidized and fixed granular activated carbon beds as cathodes for microbial electrosynthesis of carboxylates from CO2”. *Bioresource Technology*, p. 130896.

Verduyn, Cornelis (1992). “Physiology of yeasts in relation to biomass yields”. *Quantitative aspects of growth and metabolism of microorganisms*, pp. 325–353.

Vicente, Diogo et al. (2023). “The role of bacterial polyhydroalkanoate (PHA) in a sustainable future: A review on the biological diversity”. *International Journal of Environmental Research and Public Health* 20.4, p. 2959.

Virtanen, Pauli et al. (2020). “SciPy 1.0: Fundamental Algorithms for Scientific Computing in Python”. *Nature Methods* 17, pp. 261–272. DOI: 10.1038/s41592-019-0686-2.

Von Stockar, U and J-S Liu (1999). “Does microbial life always feed on negative entropy? Thermodynamic analysis of microbial growth”. *Biochimica et Biophysica Acta (BBA)-Bioenergetics* 1412.3, pp. 191–211.

Vrábel, P et al. (1999). “Compartment model approach: Mixing in large scale aerated reactors with multiple impellers”. *Chemical Engineering Research and Design* 77.4, pp. 291–302.

Vrábel, Peter et al. (2000). “Mixing in large-scale vessels stirred with multiple radial or radial and axial up-pumping impellers: modelling and measurements”. *Chemical Engineering Science* 55.23, pp. 5881–5896.

Wältermann, Marc et al. (2000). “*Rhodococcus opacus* strain PD630 as a new source of high-value single-cell oil? Isolation and characterization of triacylglycerols and other storage lipids”. *Microbiology* 146.5, pp. 1143–1149.

Wang, Wei et al. (2014). “Connecting lignin-degradation pathway with pre-treatment inhibitor sensitivity of *Cupriavidus necator*”. *Frontiers in microbiology* 5, p. 247.

Wang, Xia et al. (2018). “Tolerance improvement of *Corynebacterium glutamicum* on lignocellulose derived inhibitors by adaptive evolution”. *Applied microbiology and biotechnology* 102, pp. 377–388.

Wang, Xuan et al. (2013). “Engineering furfural tolerance in *Escherichia coli* improves the fermentation of lignocellulosic sugars into renewable chemicals”. *Proceedings of the National Academy of Sciences* 110.10, pp. 4021–4026.

Wang, Zhijiao et al. (2024). “Establishing CRISPRi for programmable gene repression and genome evolution in *Cupriavidus necator*”. *ACS Synthetic Biology* 13.3, pp. 851–861.

Weaver, Daniel S et al. (2014). “A genome-scale metabolic flux model of *Escherichia coli* K–12 derived from the EcoCyc database”. *BMC systems biology* 8, pp. 1–24.

Weldon, Michael and Christian Euler (2025). “Physiology-informed use of *Cupriavidus necator* in biomanufacturing: a review of advances and challenges”. *Microbial Cell Factories* 24.1, p. 30.

Wendisch, Volker F et al. (2000). “Quantitative determination of metabolic fluxes during coutilization of two carbon sources: comparative analyses with *Corynebacterium glutamicum* during growth on acetate and/or glucose”. *Journal of Bacteriology* 182.11, pp. 3088–3096.

White, Stephen W et al. (2005). “The structural biology of type II fatty acid biosynthesis”. *Annu. Rev. Biochem.* 74.1, pp. 791–831.

Wirth, Nicolas T et al. (2022). “A synthetic C2 auxotroph of *Pseudomonas putida* for evolutionary engineering of alternative sugar catabolic routes”. *Metabolic Engineering* 74, pp. 83–97.

Woerner, M et al. (2022). “HYDROTHERMAL LIQUEFACTION OF BLACK LIQUOR”. *Biofuels, bioproducts and biorefining* 9.6, pp. 630–638.

Wolf, Natalie et al. (2020). “Molecular basis of growth inhibition by acetate of an adenylate cyclase-deficient mutant of *Corynebacterium glutamicum*”. *Frontiers in microbiology* 11, p. 87.

Xu, Bo et al. (1999). “Modeling of overflow metabolism in batch and fed-batch cultures of *Escherichia coli*”. *Biotechnology progress* 15.1, pp. 81–90.

Xu, Jingyang et al. (2017). “Application of metabolic controls for the maximization of lipid production in semicontinuous fermentation”. *Proceedings of the National Academy of Sciences* 114.27, E5308–E5316.

Yang, Songyuan et al. (2019). “Production of medium chain length polyhydroxyalkanoate from acetate by engineered *Pseudomonas putida* KT2440”. *Journal of Industrial Microbiology and Biotechnology* 46.6, pp. 793–800.

Yao, Hui et al. (2025). “Selective butyrate production from CO2 and methanol in microbial electrosynthesis-influence of pH”. *Bioelectrochemistry*, p. 109000.

Yu, Ai-Qun et al. (2016). “Genetic engineering of an unconventional yeast for renewable biofuel and biochemical production”. *Journal of Visualized Experiments: JoVE* 115, p. 54371.

Yu, Xiaochen et al. (2014). “Effect of lignocellulose degradation products on microbial biomass and lipid production by the oleaginous yeast *Cryptococcus curvatus*”. *Process Biochemistry* 49.3, pp. 457–465.

Zhang, Anlong et al. (2015). “Anaerobic Digestion for Use in the Pulp and Paper Industry and Other Sectors: An Introductory Mini-Review.” *BioResources* 10.4.

Zhang, Yu et al. (2017). “A new genome-scale metabolic model of *Corynebacterium glutamicum* and its application”. *Biotechnology for biofuels* 10, pp. 1–16.

Zhou, Wenting et al. (2019). “Phosphate removal combined with acetate supplementation enhances lipid production from water hyacinth by *Cutaneotrichosporon oleaginosum*”. *Biotechnology for Biofuels* 12, pp. 1–11.

Zou, Wei et al. (2018). “Genome-scale metabolic reconstruction and analysis for *Clostridium kluyveri*”. *Genome* 61.8, pp. 605–613.

APPENDIX A: SUPPLEMENTARY DATA

A.1 Stoichiometry analysis

A.1.1 Product yields

Calculating the theoretical maximum productions largely follows the procedure introduced by Xu et al. (2017). However, glucose is now added as a co-substrate, and palmitic acid or its derivative is the end product.

The overall equation for the process is

$$8\mathrm{Acetyl-CoA} + 7\mathrm{ATP} + 14\mathrm{NADPH} \rightarrow \mathrm{C_{16}H_{32}O_2} + 6\mathrm{H_2O}, \tag{A.1}$$

where acetyl-CoA and ATP are provided by acetate, and NADPH is provided by glucose. Converting glucose into glucose-6-phosphate requires ATP, and if G6P is fully oxidized during oxPPP, the total equation is

$$\mathrm{C_6H_{12}O_6} + \mathrm{ATP} \rightarrow 12\mathrm{NADPH} + 6\mathrm{CO_2}. \tag{A.2}$$

To obtain acetyl-CoA from acetic acid, two molecules of ATP are used

$$\mathrm{CH_3COO^-} + \mathrm{CoA} + 2\mathrm{ATP} \rightarrow \mathrm{Acetyl-CoA}. \tag{A.3}$$

The TCA cycle from acetyl-CoA leads to the following cofactors

$$\mathrm{Acetyl-CoA} \rightarrow 3\mathrm{NADH} + \mathrm{FADH_2} + \mathrm{GTP} + 2\mathrm{CO_2}\,. \tag{A.4}$$

ATP yields are assumed to be 2.5 per NADH, 1.5 per $FADH_2$, and 1 per GTP. Half of a molecular oxygen is required to carry 2 electrons, so the Equation A.4 can be simplified to

$$\mathrm{Acetyl-CoA} + 2\mathrm{O_2} \rightarrow 10\mathrm{ATP} + 2\mathrm{CO_2} + 2\mathrm{H_2O}\,. \tag{A.5}$$

Multiplying A.1 by 12, A.2 by 14, A.3 by a and A.5 by b, summing all the equations and

setting the intermediates ATP and acetyl-CoA to 0, the following system of two equations can be solved

$$\begin{cases} 14 + 2a - 10b + 84 = 0 \\ -a + b - 96 = 0 \end{cases} \tag{A.6}$$

. This results in *a* = 132.25 and *b* = 36.25. If now the total equation is divided by 12 to obtain 1 mol of palmitic acid, we get

$$11.04\mathrm{CH_3COOH} + 1.17\mathrm{C_6H_{12}O_6} + 6.04\mathrm{O_2} \rightarrow \mathrm{C_{16}H_{32}O_2} + 13.04\mathrm{CO_2} + 13.04\mathrm{H_2O}. \tag{A.7}$$

For cetyl alcohol yield, the conversion from palmitic acid uses two reduction steps requiring 2 more NADPH (A. Liu et al. 2013), and the Equation A.1 can be replaced with

$$8\mathrm{Acetyl-CoA} + 8\mathrm{ATP} + 16\mathrm{NADPH} \rightarrow \mathrm{C_{16}H_{34}O} + 7\mathrm{H_2O}. \tag{A.8}$$

To convert palmitic acid into pentadecane, one reduction step and decarbonylation step are needed (Schirmer et al. 2010), and the A.1 is replaced with

$$8\mathrm{Acetyl-CoA} + 8\mathrm{ATP} + 16\mathrm{NADPH} + 0.5\mathrm{O_2} \rightarrow \mathrm{C_{15}H_{32}} + 8\mathrm{H_2O} + \mathrm{CO}. \tag{A.9}$$

The rest of the calculations are performed exactly like in the case of palmitic acid.

A.1.2 Biomass yields

Non-lipid biomass yields were calculated similarly to Hu et al. (2016), but glucose was introduced as a co-substrate. The average bacterial and yeast biomass compositions obtained from literature were $CH_{1.66}O_{0.41}N_{0.21}$ and $CH_{1.65}O_{0.54}N_{0.14}$, respectively (Von Stockar et al. 1999). Here, only the derivation of the equation for the bacterial biomass is shown.

The approximation for biomass yield of 3.14 g DCW per available electron was used (Shuler 1992). For glucose, there are 24 available electrons, and for acetate ,8 so multiplying these by 3.14 and dividing by the molecular mass of non-lipid biomass, we get

$$\mathrm{CH_3COOH} \rightarrow 0.9608\mathrm{CH_{1.66}O_{0.41}N_{0.21}} + 1.0392\mathrm{CO_2}, \tag{A.10}$$

$$\mathrm{C_6H_{12}O_6} \rightarrow 2.885\mathrm{CH_{1.66}O_{0.41}N_{0.21}} + 3.115\mathrm{CO_2}. \tag{A.11}$$

The carbon dioxide is calculated by subtracting the carbon in biomass from the available carbon. The ATP usage was assumed to be 105 mmol $\mathrm{g}^{-1}\,\mathrm{DCW}$ (Verduyn 1992), so the equations with energy expenditures are

$$\mathrm{CH_3COOH} + 2.635\mathrm{ATP} \rightarrow 0.9608\mathrm{CH_{1.66}O_{0.41}N_{0.21}} + 1.0392\mathrm{CO_2}, \tag{A.12}$$

$$\mathrm{C_6H_{12}O_6} + 7.913\mathrm{ATP} \rightarrow 2.885\mathrm{CH_{1.66}O_{0.41}N_{0.21}} + 3.115\mathrm{CO_2}. \tag{A.13}$$

As the energy is assumed to be supplied by acetate, the ATP is produced via equations A.3 and A.5. Therefore, the equations are now

$$2.3185\mathrm{CH_3COOH} \rightarrow 0.9608\mathrm{CH_{1.66}O_{0.41}N_{0.21}} + 1.698\mathrm{CO_2}, \tag{A.14}$$

$$1.0\mathrm{C_6H_{12}O_6} + 0.9813\mathrm{CH_3COOH} \rightarrow 2.885\mathrm{CH_{1.66}O_{0.41}N_{0.21}} + 5.0775\mathrm{CO_2}. \tag{A.15}$$

Multiplying A.14 by $(11.04 - 1.17 \cdot 0.981)/2.3185$ and A.15 by 1.17 to get the ratio in Equation 4.13 and summing, the formula for non-lipid biomass yield is obtained

$$11.04\mathrm{CH_3COOH} + 1.17\mathrm{C_6H_{12}O_6} \rightarrow 10.52\mathrm{CH_{1.66}O_{0.41}N_{0.21}} + 18.58\mathrm{CO_2}. \tag{A.16}$$

A.2 Supporting figures and tables

1. Table A.1 compiles the lipid compositions achieved by wil-type microbes in acetate cultures.
2. Figure A.1 visualizes the variables of MCA in the first and second dimensions.
3. Figure A.2 visualizes the variables of MCA in the first and third dimensions.
4. Figure A.3 shows the growth of *P. putida*, *C. glutamicum* and *C. oleaginosus* during the first 15 hours of the cultivation.

Table A.1. *Approximation of the maximum lipid content and proportion of the long-chain fatty acid residues of all of the FAs in the wild-type microbes when grown on acetate. C. kluyveri produces extracellular medium-chain fatty acids and does not accumulate them in typical storage compounds.*

Microbe	Lipids (%DCW)	Long-Chain FA (%)	Sources
E. coli	0	0	(Meng et al. 2011)
A. baylyi ADP1	10	>95	(M. S. Kannisto et al. 2015; Barney et al. 2012)
P. putida	20	0	(Yang et al. 2019)
C. oleaginosus	73	>95	(Gong et al. 2015)
C. necator H16	72	0	(Garcia-Gonzalez et al. 2018)
Y. lipolytica	12	>98	(Gong et al. 2015; Beopoulos et al. 2009)
C. glutamicum	1.3	>80	(Bansal-Mutalik et al. 2011)
C. kluyveri	0	0	(Gildemyn et al. 2017)

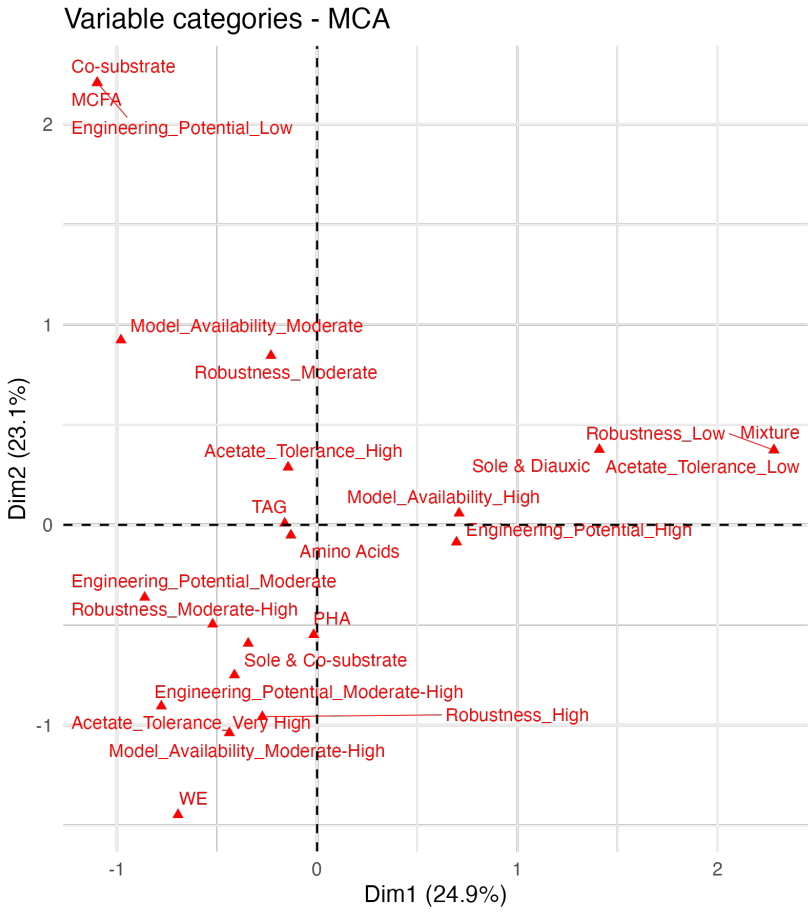

Figure A.1. *All the variables plotted against the first and second dimension of the MCA. The closer the variables are to each other, the more likely they are to be correlated and found in similar microbes.*

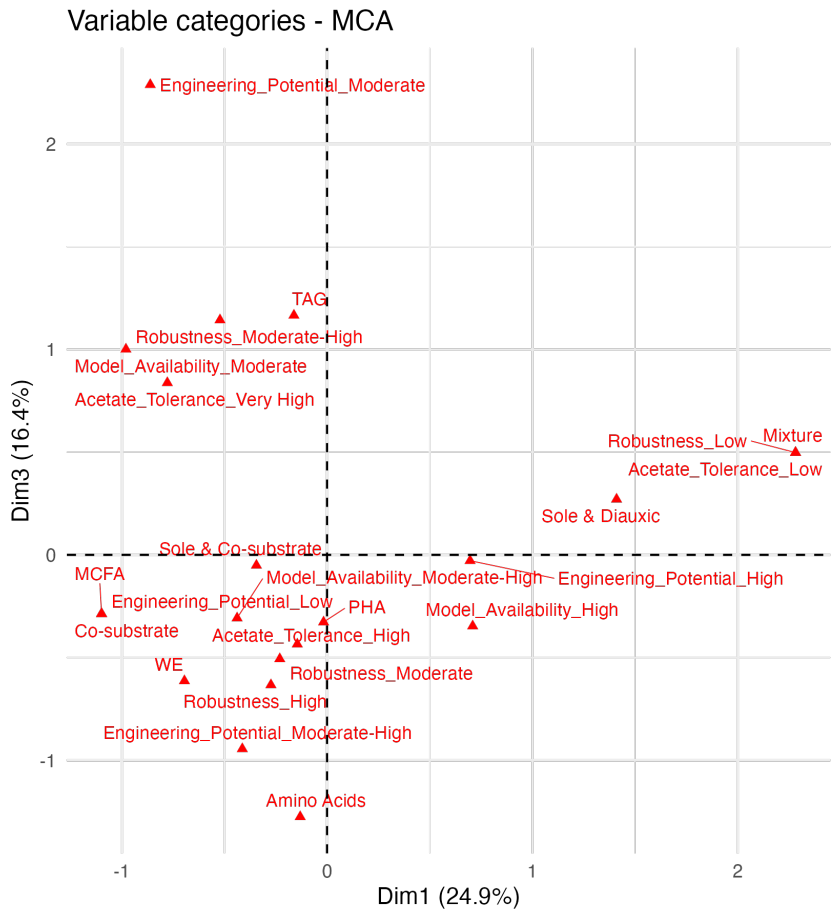

Figure A.2. *All the variables plotted against the first and third dimension of the MCA. The closer the variables are to each other, the more likely they are to be correlated and found in similar microbes.*

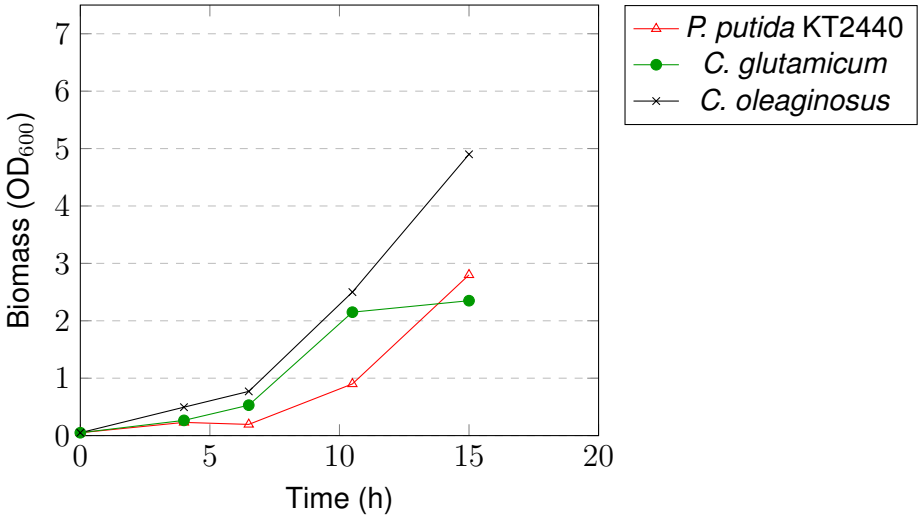

Figure A.3. *Biomass production in batch cultivations for the first 15 h. LB-media supplemented with 100 mM sodium acetate was used. The OD_{600} data is calculated as the average from two parallel replicates.*